THE
PHYSICAL REVIEW

A journal of experimental and theoretical physics established by E. L. Nichols in 1893

SECOND SERIES, VOL. 72, NO. 5 SEPTEMBER 1, 1947

Multiple Scattering of Electrons in the Gas of a Wilson Cloud Chamber

LYLE W. SMITH AND P. GERALD KRUGER
University of Illinois, Urbana, Illinois

(Received April 30, 1947)

The deviation from linearity of straight electron tracks appearing in a cloud chamber has been measured and found to be in agreement with that predicted by the theory of multiple scattering insofar as the energy of the electrons is known. The method described could be easily modified to give a more valuable and exact check on the theory of multiple scattering.

1. INTRODUCTION

SOME earlier reports[1,2] have suggested the presence of a new penetrating radiation, presumably a low mass neutral particle which decays at rest. There was some cloud-chamber evidence[3] that this assumption was correct. In order to evaluate the cloud-chamber data it was necessary to determine to what extent multiple scattering in the gas of the cloud chamber and turbulent motion of the gas affected the determination of electron energy. The effect of multiple scattering on curvature measurements has been discussed by Williams[4] and Bethe.[5]

2. EXPERIMENTAL ARRANGEMENT

In order to obtain data on multiple scattering in a gas, the cloud chamber was operated under conditions which were the same as those which prevailed when data on the supposed decay electrons were taken, except that there was no magnetic field. The cloud chamber contained air at atmospheric pressure and three aluminum foils 0.80 mm thick, spaced 5 cm apart. The chamber was surrounded by a ring, 19 cm thick and 21 cm high made of lead blocks, and was placed about four meters from the target of the cyclotron and almost in a direct line with the deuteron beam striking the target. The cyclotron was completely enclosed by water tanks of 120-cm thickness, and the tanks on the side between the target and the cloud chamber contained a saturated solution of boric acid.

In order to get an approximation to the energy of the electrons which produce the straight tracks which were measured, only those tracks were used which penetrated one or more of the aluminum foils. Since the minimum energy at which this can occur is known roughly, and the energy spectrum of electrons in the chamber under these conditions is known from data[6] taken with a magnetic field, one can assign an average energy to these tracks. The average kinetic energy will be assumed to be 1.5 Mev.

The actual quantity which was measured on the straight tracks was their deviation from

[1] G. K. Groetzinger, P. G. Kruger, and Lloyd Smith, Phys. Rev. **67**, 52 (1945).
[2] G. K. Groetzinger and Lloyd Smith, Phys. Rev. **68**, 55 (1945).
[3] P. G. Kruger and Lyle W. Smith, Phys. Rev. **68**, 104 (1945).
[4] E. J. Williams, Phys. Rev. **59**, 460 (1940).
[5] H. A. Bethe, Phys. Rev. **70**, 821 (1946).
[6] P. Gerald Kruger and Lyle W. Smith, Phys. Rev. **72**, 360 (1947).

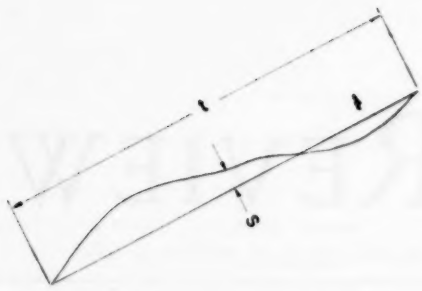

FIG. 1. Exaggerated shape of scattered track. S and t represent the quantities measured.

linearity. To do this the same measuring engine was used which was used to measure track curvature in the case when a magnetic field was present. The measured quantity was the perpendicular distance between the midpoint of the track and a straight line connecting the two ends. This is similar to the measurement of a sagitta of an arc in the case of curvature measurements. The following further criteria were used in selecting tracks for measurement.

(1) All sections of the track must lie in the same plane, and this plane must lie within 10° of the median plane of the cloud chamber.

(2) All sections of the track must be of the same age and density of ionization.

(3) There can be no obvious single scattering over the region of the track which is measured. The minimum angle at which single scattering can be detected is estimated to be 0.1 radian.

(4) Adjacent sections of the track, when extended, must meet in the foil.

Pictures of the tracks were taken with a stereoscopic mirror system and reprojected through the same camera and mirror system onto a ground glass screen for measurement. Because of the way in which the measurements were made the results will give the projection of the scattering angle on a plane, not necessarily the median plane of the cloud chamber.

In general, the track may have any sort of shape between its end points as is shown greatly exaggerated in Fig. 1. The quantities which are measured experimentally are t and S.

Rossi and Greisen[7] have given a formula, attributable to Fermi, which expresses the distribution of S as a function of the length of the track and the multiple scattering angle θ. By θ we shall always mean the projection of the scattering angle on a plane. This distribution of S is

$$P(S)dS=\frac{24}{\pi t^2\langle\theta^2\rangle_{Av}}\exp\left(-\frac{24S^2}{t^2\langle\theta^2\rangle_{Av}}\right)ds, \quad (1)$$

so that

$$\langle\theta^2\rangle_{Av}=\frac{48\langle S^2\rangle_{Av}}{t^2}=\frac{24\pi\langle S\rangle^2_{Av}}{t^2}, \quad (2)$$

is the relation which we shall use to compare our results with the theory.

The mean square average angle of scattering in a length of track t is[4,5]

$$\langle\theta^2\rangle_{Av}=\frac{4\pi e^4Z^2Nt}{(mc^2)^2}\frac{(W/mc^2)^2}{[(W/mc^2)^2-1]^2}\ln\frac{\theta_{max}}{\theta_{min}}, \quad (3)$$

where Z is the atomic number, N the number of atoms per cm³ of the scattering substance, and W is the total energy of the particle. θ_{min} is determined by screening and is given by

$$\theta_{min}=\frac{e^2Z^{\frac{1}{3}}}{hc}\frac{(W/mc^2)^2}{(W/mc^2)^2-1}. \quad (4)$$

We shall take θ_{max} as the minimum angle (assumed to be 0.1 radian) which can be recognized as single scattering in the gas of the cloud chamber. Since from (3) we have $\langle\theta^2\rangle_{Av}\sim t$, and we know from (1) that $\langle S\rangle^2_{Av}/t^2\sim\langle\theta^2\rangle_{Av}$, we shall expect the relation $\langle S\rangle_{Av}\sim t^{\frac{1}{2}}$ to obtain for the various lengths of tracks which were measured. Table I gives the results of the measurements where C and $\langle S\rangle_{Av}$ are the length of track and average deviation from linearity, respectively. Columns 4 and 5 give the experimental and theoretical values of the mean square scattering angle, respectively. The experimental value of $(2\pi^{-1}\langle S^2\rangle_{Av})^{\frac{1}{2}}$ is included in the

TABLE I. Results of measurements on straight tracks. The first column gives the length of the straight track in cm over which the average deviation $\langle S\rangle_{Av}$ has been measured. $(2\pi^{-1}\langle S^2\rangle_{Av})$ gives the experimental value for this quantity. $\langle\theta^2\rangle_{Av}^{exp}$ and $\langle\theta^2\rangle_{Av}^{theo}$ give the experimental and theoretical values of the mean square scattering angle. The last column gives the number of tracks on which measurements were made over the lengths given in column one.

t(cm)	$\langle S\rangle_{Av}$(cm)	$(2\pi^{-1}\langle S^2\rangle_{Av})^{\frac{1}{2}}$	$\langle\theta^2\rangle_{Av}^{exp}$	$\langle\theta^2\rangle_{Av}^{theo}$	No. of tracks
3	0.0155	0.0156	20.2×10^{-4}	19.4×10^{-4}	163
4	0.0231	0.0234	25.2×10^{-4}	25.4×10^{-4}	107
5	0.0311	0.0288	30.5×10^{-4}	32.4×10^{-4}	44

[7] B. Rossi and K. Greisen, Rev. Mod. Phys. **13**, 268 (1941).

table as an indication of the consistency of the measurements, since if the distribution of S is gaussian this quantity should be equal to $\langle S \rangle_{Av}$.

Because of the fact that we know only an approximate value for W, i.e., 2 Mev, and that there is certainly some range of energies represented by the measured tracks, exact agreement with the theory cannot be expected. For instance, if W is taken to be 3 Mev, the theoretical results will be lowered by approximately a factor of two.

Figure 2 shows the experimental relationship between $\langle S \rangle_{Av}$ and $t^{\frac{3}{2}}$. Since this plot is a straight line we conclude that all of the measured deviations from linearity are due to multiple scattering and that any turbulence of the gas in the cloud chamber is negligible under these conditions. This is in agreement with the fact that no turbulence is observed visually in the cloud chamber.

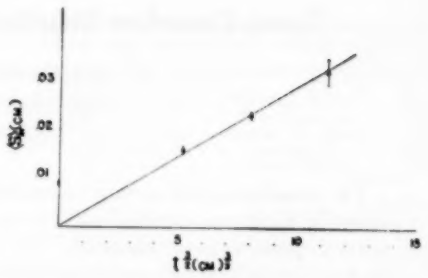

FIG. 2. Experimental relation between $\langle S \rangle_{Av}$ and $t^{\frac{3}{2}}$.

3. CONCLUSIONS

The distortion of straight electron tracks in a Wilson cloud chamber has been measured and found to be due to multiple scattering, within experimental error, the effect of turbulent motion of the gas not being observed. The magnitude of the multiple scattering is in agreement with the theory insofar as the energy of the electron is known.

It is obvious that the above method may be modified by injecting electrons of a known energy into a cloud chamber, e.g., from a Van de Graaff generator. This modification could give a more valuable and exact check on the theory of multiple scattering which at present has its only experimental confirmation in the scattering of electrons by thin foils. When a foil is used as the scattering substances certain rather arbitrary criteria[8] must be applied to insure that no large angle scattering masks the multiple scattering. Contributions due to large angle scattering can be completely avoided if the path of the electron can be observed over the whole region in which the scattering is measured.

[8] G. Wentzel, Ann. d. Physik **69**, 333 (1922).

Cloud-Chamber Search for a Low Mass Neutral Particle

P. GERALD KRUGER AND LYLE W. SMITH
University of Illinois, Urbana, Illinois

(Received April 30, 1947)

The possibility that certain anomalous electron tracks in a cloud chamber may be due to decay of a low mass neutral particle has been examined, and it is concluded that such tracks are not caused by decay electrons. This conclusion is necessary because of the failure to observe such tracks in 5000 pictures when hydrogen gas was used in the cloud chamber instead of air.

IN order to check the results of two previous investigations[1,2] on the possible existence of a new low mass neutral particle, a Wilson cloud chamber containing three aluminum foils has been used as a detector in a search for decay electrons which might be emitted by such a particle. The arrangement of the cloud chamber is described elsewhere.[3] By observing the loss of an electron passing through a foil it is possible to determine the direction of motion of the electron. Thus, if an electron and a positron start from a common point and proceed collinearly in opposite directions, as would be the case if a neutral particle at rest decayed into a positive and negative electron, a decrease in energy in both directions should be observed provided they penetrate one or more foils each. In any case the common point of origin is not determinable exactly but should lie somewhere between or in one of the two foils which have been penetrated. If any such events occur, one must carefully evaluate the extent to which multiple scattering and chance affect their identification. Several such events have been observed, and it is the purpose of this note to describe how the validity of these tracks was checked.

Tracks chosen for measurement (1) penetrated two or more foils and (2) satisfied other criteria.[3] The majority of such tracks selected are electrons which apparently lose energy at each successive foil penetration. However, some anomalous tracks occur whose central portion exhibits a smaller curvature than either end portion. Also, some tracks were observed whose central portion was of larger curvature than the end portions. In addition to tracks which were selected according to the above criteria, all $\pm$ electron pairs produced by γ-rays occurring in the chamber were measured. As a check on the chance coincidence of independent tracks, tracks were selected which penetrated one foil and ended on another, and which penetrated no foil and ended on one.

Several independent determinations of the radius of curvature of each track were made with a measuring engine which determined the chord and sagitta of the arc of track.

Several experimental arrangements were used.

(1) Cloud chamber filled with one atmosphere of air and shielded by lead.[3] Tungsten target in the cyclotron (1800 pictures).

(2) Cloud chamber filled with one atmosphere of air and shielded by lead. Copper target in the cyclotron (2600 pictures).

(3) Cloud chamber filled with one atmosphere of air with reduced lead shielding. Copper target in the cyclotron (1940 pictures).

(4) Cloud chamber filled with one atmosphere of hydrogen and shielded by lead. Copper target in the cyclotron (5000 pictures).

In all cases the cyclotron target was bombarded with 10-Mev deuterons. When reduced lead shielding was used around the cloud chamber, the cyclotron beam was held to approximately $\frac{1}{5}$ of its value when maximum lead shielding was used. With arrangement (4) the cyclotron beam was approximately 20 percent larger than for arrangement (2).

Table I gives the results of measurement on electron tracks which have penetrated two or more foils. Column 1 gives the track number, columns 2 and 4 the measured energies of the end portions in Mev, and column 3 the measured energy of the center portion in Mev. In the case of anomalous tracks the calculated[3] root mean

[1] G. K. Groetzinger, P. G. Kruger, and Lloyd Smith, Phys. Rev. **67**, 52 (1945).
[2] G. K. Groetzinger and Lloyd Smith, Phys. Rev. **68**, 55 (1945).
[3] Lyle W. Smith and P. Gerald Kruger, Phys. Rev. **72**, 357 (1947).

square deviations due to multiple scattering are given by the bracketed quantities.

The greater number of the anomalous tracks can be explained by supposing them to be electrons, one or more portions of which suffer multiple scattering several times larger than the root mean square scattering. This in some cases is quite improbable but nevertheless possible. The number of such tracks which could be caused by chance can be easily estimated. The total area of the foils is 9800 mm², and we assume the "area of confusion" on the foils to be 3 mm²; then, knowing the number of fractional parts of tracks which appear in the cloud chamber, one can arrive at the probabilities for chance coincidence for the arrangements (1), (2), and (3) to be 1/11,200, 1/7050, and 1/1030 per picture, respectively. The calculation for arrangement (3) was checked by looking for "S-shaped" tracks which satisfied all the criteria. One such track was observed in 940 pictures.

The possibility that the anomalous tracks are due to decay electrons is indicated by the internal consistency of the measured energy of their central portions and by the fact that when lead shielding was removed from around the cloud chamber the number of electrons per picture increased by a factor of 3.8 while the anomalous tracks with larger energy center portions remained approximately constant. Since under these conditions the deuteron beam current was about $\frac{1}{3}$ of that in arrangements (1) and (2), this should have resulted in a 19-fold increase in anomalous tracks if they had been produced by gamma-rays. However, when hydrogen was put in the cloud chamber no anomalous tracks were observed. The probability for this occurring is approximately 0.05 if the average ratio of anomalous tracks to electrons is the same here as for arrangements (2) and (3). The decrease in the number of electron tracks observed in this case is in agreement with the measured decrease in sensitive time of the cloud chamber when filled with hydrogen.

Pair production by gamma-rays in a foil could give rise to the anomalous tracks in their energy range only if one of the pair were scattered through a large angle in the foil. Also, if the anomalous tracks were caused by such pair production, their frequency of occurrence should have increased markedly when the lead shielding around the cloud chamber was decreased.

It must be concluded that the evidence is contrary to the assumption that the anomalous tracks are caused by the decay of a neutral particle.

TABLE I. Results of measurements on tracks from electrons which have penetrated two or more foils.

Track number	Electron energy from measurements on one end portion of track (Mev)	Electron energy from measurements on center portion of track (Mev)	Electron energy from measurements on last end portion of track (Mev)
	Arrangement 1		
10–1	2.3 ±0.2(0.2)	3.4 ±0.1(0.3)	2.3 ±0.1(0.2)
13–1	1.8 ±0.2(0.1)	3.0 ±0.1(0.1)	2.4 ±0.2(0.2)
17–2	3.0 ±0.2(0.2)	3.4 ±0.1(0.1)	2.0 ±0.2(0.2)
13–2	2.7 ±0.3	2.2 ±0.3	1.9 ±0.4
15–2	2.9 ±0.3	2.5 ±0.2	2.3 ±0.1
17–0	1.6 ±0.1	1.1 ±0.1	0.7 ±0.1
19–1	6.8 ±0.6	4.9 ±0.5	3.1 ±0.7
23–4	1.9 ±0.1	1.6 ±0.1	1.0 ±0.1
18–1	4.4 ±0.2	3.9 ±0.4	3.7 ±0.2
	Arrangement 2		
34–3	1.19 ±0.04(0.1)	2.19 ±0.33(0.2)	0.47 ±0.05(0.04)
34–4	0.08 ±0.02(0.005)	2.32 ±0.17(0.2)	2.10 ±0.10(0.2)
35–2	2.29 ±0.09(0.1)	2.39 ±0.09(0.2)	1.91 ±0.09(0.1)
35–3	0.47 ±0.07(0.1)	2.03 ±0.08(0.2)	0.80 ±0.07(0.01)
47–5	2.03 ±0.12(0.2)	2.32 ±0.17(0.2)	1.95 ±0.16(0.1)
50–1	2.69 ±0.22(0.2)	3.13 ±0.18(0.2)	2.52 ±0.2(0.1)
24–1	3.0 ±0.2(0.1)	1.75 ±0.05(0.1)	2.1 ±0.2(0.1)
37–2	2.0 ±0.2(0.2)	1.40 ±0.05(0.1)	1.50 ±0.02(0.1)
26–3	4.3 ±0.5	2.9 ±0.2	2.8 ±0.1
27–1	3.3 ±0.3	2.3 ±0.2	2.1 ±0.2
30–1	3.0 ±0.1	1.8 ±0.1	0.46 ±0.05
31–3	10.4 ±1.0	7.4 ±0.5	3.2 ±0.3
34–4	2.3 ±0.2	2.1 ±0.2	0.40 ±0.05
35–1	1.7 ±0.2	1.4 ±0.2	1.2 ±0.1
39–1	1.7 ±0.1	1.10 ±0.05	0.88 ±0.04
48–2	2.4 ±0.2	1.8 ±0.2	0.50 ±0.05
	Arrangement 3		
53–6	1.71 ±0.03(0.1)	2.15 ±0.13(0.2)	1.67 ±0.03(0.2)
55–15	1.50 ±0.05(0.1)	1.70 ±0.04(0.1)	1.34 ±0.05(0.1)
55–7	3.7 ±0.2(0.2)	2.0 ±0.1(0.2)	2.2 ±0.1(0.2)
55–8	5.5 ±0.5(0.6)	3.3 ±0.2(0.3)	3.4 ±0.2(0.3)
53–3	2.0 ±0.2	1.5 ±0.1	0.99 ±0.05
53–5	3.9 ±0.4	3.0 ±0.3	2.0 ±0.1
54–3	1.7 ±0.1	1.5 ±0.1	0.72 ±0.05
55–3	2.8 ±0.2	1.9 ±0.2	1.6 ±0.1
55–9	2.1 ±0.2	1.5 ±0.1	1.10 ±0.03
55–10	3.5 ±0.2	2.6 ±0.2	2.1 ±0.1
56–7	2.8 ±0.3	2.0 ±0.3	1.9 ±0.1
56–10	2.9 ±0.1	2.0 ±0.1	1.30 ±0.05
56–12	2.3 ±0.1	2.1 ±0.2	0.87 ±0.03
58–6	3.3 ±0.2	2.2 ±0.2	1.7 ±0.2
58–13	4.3 ±0.2	3.5 ±0.4	2.9 ±0.3
	Arrangement 4		
86–3	2.0 ±0.1	1.55 ±0.05	0.3 ±0.1
91–1	1.6 ±0.1	1.0 ±0.1	0.3 ±0.1
91–2	1.7 ±0.1	1.2 ±0.1	0.20 ±0.05
102–1	5.5 ±1.5	2.2 ±0.2	1.3 ±0.05
107–1	3.5 ±0.5	2.4 ±0.2	1.8 ±0.1

On the Slow Neutron Absorption Resonances in Iodine

WM. B. JONES, JR.
Cornell University, Ithaca, New York

(Received May 3, 1947)

The 12-channel slow neutron velocity spectrometer at Cornell University is described. Reported here is a measurement with this spectrometer of the neutron cross section of iodine over an energy range extending from 0.0026 to 1000 ev. Below 3 ev, the iodine cross section was found to obey the 1/v absorption law. The total cross section at thermal energy ($kT=0.025$ ev) was found to be 10.3×10^{-24} cm²/atom. The scattering cross section, found by extrapolating to zero time of flight the straight line which best fitted the data on a cross-section *vs.* time-of-flight graph, is 3.6×10^{-24} cm²/atom. A single resonance was observed at 20.3 ev. A region containing at least three resonances was observed between 25 and 50 ev. An indication of a resonance or group of resonances was found near 85 ev. An attempt was made to match a symmetrical type Breit-Wigner formula to the observed data at the 20.3 ev resonance. The constants chosen in this manner for the resonance are: $E_r=20.3\pm0.5$ ev, $\sigma_0=80\times10^{-24}$ cm²/atom with $\sigma_0>40\times10^{-24}$ cm²/atom, and $\Gamma=0.45$ ev with $\Gamma<0.8$ ev. Consideration of the activities for three thicknesses of the absorber for this resonance showed that the absorbers were thick and that $\sigma_0\Gamma^2=15\times10^{-24}$ ev² cm²/atom, neglecting the Doppler effect. In the neutron energy region between 25 and 50 ev, the relation between the activity and the absorber thicknesses used showed that the absorbers were thick for the resonances in this region. From the curve of activity as a function of thickness, it was found that $\Sigma_r(\sigma_{0r}\Gamma_r^2)^{\frac{1}{2}}=32.5\times10^{-12}$ ev-cm/atom$^{\frac{1}{2}}$ for these resonances, neglecting the Doppler effect. An attempt at fitting two resonances of about equal strength to the data proved to be impossible, and it was concluded that there are three or more resonances in this region. Consideration of the maximum widths of these resonances, that account for the absorption, indicated that the widths were less than 1 or 2 ev. This conclusion is reached regardless of the relation of the level widths to the Doppler width. Therefore, it is believed that there are no resonances for neutron energies between 0 and 70 ev which are so wide as to be incompatible with the present theory of nuclei. Since iodine has only one stable isotope, the resonances observed are for one type nucleus. It would be valuable to know exactly the number of resonances for a wide range of neutron energies; however, the apparatus used in the present experiment does not have sufficient resolution to resolve resonances with a spacing as small as 7 ev at 40-ev energy.

1. INTRODUCTION

THE slow neutron cross section of iodine has been investigated by a number of workers. The earliest measurements were made by indirect methods. Because the resonance absorption in iodine occurs for rather high neutron energies, it has not been possible to determine very accurately by indirect methods the character of the cross section as a function of energy. However, the results of experiments by indirect methods[1] indicated that the resonance-level widths in most nuclei were a few tenths of an electron volt but that the iodine resonance-absorption width was about 15 ev. It was concluded from these experiments that either there is an unusually wide absorption resonance in iodine or there are perhaps several absorption resonances of about equal strengths and with small spacings.

It is much more compatible with theoretical ideas and with much of the experimental data on resonances in various nuclei to attribute the resonance absorption of neutrons by iodine to several closely spaced resonances rather than to one wide resonance. Recently, some experiments of a survey nature with a slow neutron velocity spectrometer[2] indicated that there is one weak absorption resonance in iodine of normal width at 20.6 ev and a region of strong absorption extending from 30 to 45 ev. The wide region of absorption was interpreted as resulting from two absorption resonances, because the measured absorption as a function of energy was not of the shape usually observed for a single resonance. However, even under the assumption of two resonances for this region, one cannot come to the conclusion that the levels are of widths expected from the theory.

In view of the doubt as to the nature of the slow neutron absorption properties of iodine, a more detailed investigation of iodine with a slow neutron velocity spectrometer was indicated. In addition, iodine has only one stable isotope, and

[1] H. A. Bethe, Rev. Mod. Phys. **9**, 134 (1937).

[2] C. S. Wu, L. J. Rainwater, and W. W. Havens, Phys. Rev. **71**, 175 (1947).

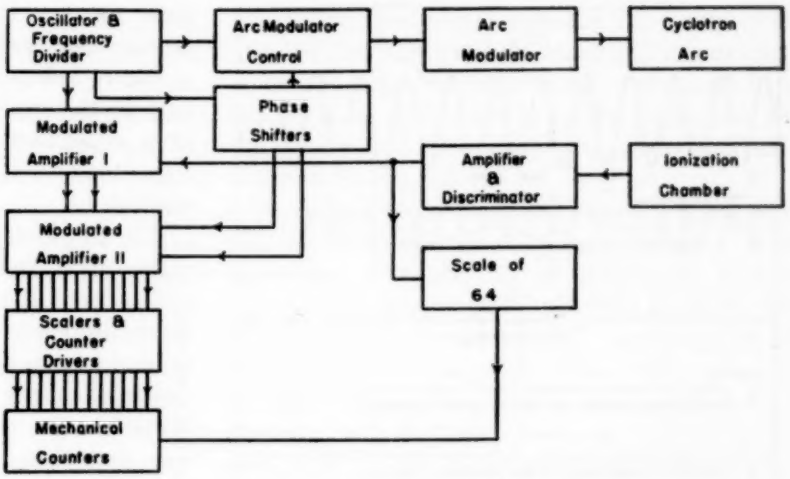

FIG. 1. Block diagram of timing apparatus.

if several resonances were found, information would be obtained on the energy levels in a single nucleus. The experiment to be described here is a study of the neutron cross section of iodine with a slow neutron velocity spectrometer.

2. APPARATUS

The time-of-flight method and an apparatus used for time-of-flight measurements have been described earlier.[3] The apparatus of Baker and Bacher[3] has been improved and expanded by Bacher, Baker, and McDaniel[4] and by McDaniel.[5] The timing equipment used in the present experiment is, with minor improvements the same as that used, but not described, by McDaniel in the measurement of the slow neutron cross section of indium.[5]

The timing equipment of the apparatus is composed of electrical circuits which will turn on the ion source of the cyclotron for a chosen, definite period of time and accurately modulate pulse amplifiers. The cyclotron ion source is an arc type source and will be referred to as the arc. The modulated amplifiers are connected so that certain pulses from the linear amplifier used with the BF_3 ionization chamber are selected. Each modulated pulse amplifier will amplify only those pulses originating from neutrons detected by the BF_3 chamber within a time-of-flight interval determined essentially by the on-time of the arc, the on-time of the pulse amplifier, and the time separation of these on-times. There are 12 of these modulated pulse amplifiers so that the intensity of the neutron beam in 12 time-of-flight intervals may be measured simultaneously. The cycle of turning on the arc and turning on the modulated amplifiers is repeated at a frequency which is as high as possible without having neutrons produced in one cycle detected in the succeeding cycles.

Figure 1 is a block diagram of the timing equipment. The arrows on the lines connecting the blocks indicate the directions in which the signals proceed between the components of the equipment. In order to simplify the diagram, the cathode-ray oscilloscope and its associated linear sweep circuit, which comprise an important component of the equipment, are not shown. The oscilloscope sweep circuit is so arranged that the sweep may be triggered accurately in any phase with respect to the timing wave which determines the repetition frequency for the equipment. The sweep speed may be adjusted continuously from a speed of 5 μs for a sweep across the screen of the 5-inch cathode-ray tube to a speed of 0.02 second for a sweep across the screen. The sweep speed was calibrated frequently by comparison with the time standard of the equipment. Tap switches are connected so that the vertical deflection plate of the cathode-ray tube may be conveniently connected to any one of the 35 points of the equipment

[3] C. P. Baker and R. F. Bacher, Phys. Rev. **59**, 332 (1941).
[4] R. F. Bacher, C. P. Baker, and B. D. McDaniel, Phys. Rev. **69**, 443 (1946).
[5] B. D. McDaniel, Phys. Rev. **70**, 832 (1946).

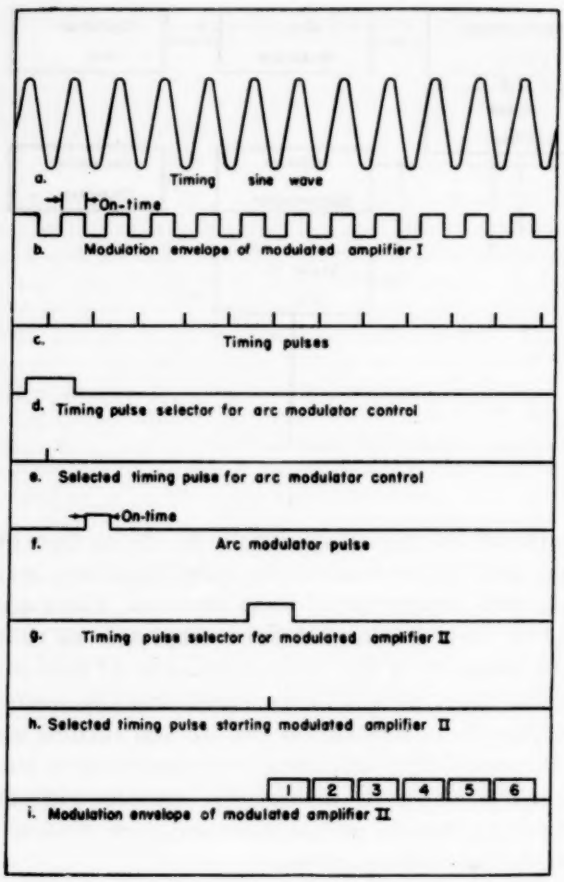
a. Timing sine wave
On-time
b. Modulation envelope of modulated amplifier I
c. Timing pulses
d. Timing pulse selector for arc modulator control
e. Selected timing pulse for arc modulator control
On-time
f. Arc modulator pulse
g. Timing pulse selector for modulated amplifier II
h. Selected timing pulse starting modulated amplifier II
1 2 3 4 5 6
i. Modulation envelope of modulated amplifier II

FIG. 2. Timing diagram for timing apparatus.

where there are wave forms which should be viewed in the adjustment and checking of the operation of the equipment.

The time standard is a 100 kc/sec. (± 0.02 percent) crystal oscillator. A six-stage frequency divider is employed to obtain the timing waves of the desired frequencies for determining the on-time of the modulated amplifiers, the time separation of the arc on-time and the on-time of the modulated amplifiers, and the repetition frequency. The timing wave which determines the on-time of the modulated amplifiers has a period twice as long as the on-time. This timing wave will be referred to as the fast timing wave. The detector on-times used in this experiment were 5, 10, 50, and 250 μs corresponding to fast timing wave frequencies of 100, 50, 10, and 2 kc/sec., respectively. The uncertainty in the detector on-times is less than 0.15 μs for the 5 μs on-time and less than 1.5 percent of the on-time for the longer on-times. The repetition periods used were 300, 320, 400, and 5000 μs.

Figure 2 shows a timing diagram for the operation of the timing equipment during a portion of a repetition period. Reference is made to Figs. 1 and 2 in outlining the operation of the equipment.

The BF_3 ionization chamber gives an electrical pulse upon the detection of a neutron. The pulses from the chamber are amplified by the linear amplifier, and an amplitude discriminator is used to pass only the neutron pulses which are larger than the thermal noise pulses from the amplifier. The rise time of the amplifier is slightly less than 2 μs; this is somewhat greater than the collection time for the electrons in the ionization chamber. The neutron pulses from the discriminator are sent through a pulse shaper which makes all pulses passed by the discriminator of the same size and duration. From the pulse shaper the pulses are sent to a scale-of-64 circuit driving a mechanical counter so that all detected neutrons are counted. From the pulse shaper, the pulses are also sent into the modulated amplifier *I* which separates the pulses into two sets of timed groups. One set of timed groups is composed of those pulses resulting from neutrons detected in time intervals equal in length to one-half the period of the fast timing wave, and these intervals are separated by a time equal to one-half the period of the fast timing wave. The other set of timed groups of pulses are those not included in the first set of time groups. Figure 2a shows the fast timing wave and Fig. 2b the modulation envelope determining one set of the timed pulse groups.

The low frequency timing wave is sent into phase shifters and from the phase shifters are obtained three pulses which may be adjusted so as to have any desired duration and to start at any desired phase with respect to the low frequency timing wave. Coincidences between these pulses occurring at the repetition frequency and pulses derived from the fast timing wave (shown in Fig. 2c) are used to trigger the arc modulator control and the two sets of 6 modulated amplifiers of modulated amplifier *II*. Thus the accuracy of all the timing is determined by the fast timing wave.

A selected timing pulse which triggers the arc

modulator control is shown in Fig. 2e. This pulse initiates a linear time sweep in the arc modulator control so the arc may be turned on at a phase which is continuously adjustable over a time interval of about twice the length of a fast timing wave period. This linear time sweep is also used to determine the on-time of the arc. The arc on-time is always made equal to the detector on-time. Figure 2f shows a typical phasing for the arc modulator pulse.

The grouped neutron pulses from modulated amplifier *I* are sent into modulated amplifier *II* where certain groups of the pulses are selected to be recorded by the mechanical counters. The selector pulse (Fig. 2g), which selects the fast timing pulse (Fig. 2h) to start one of the chain of 6 amplifiers of modulated amplifier *II*, may be phased to start the modulation chain with any one of the timing pulses. A chain of the modulated amplifier *II* selects six successive groups of pulses of one set of the grouped neutron pulses from modulated amplifier *I*. Thus the neutron pulses appearing in these six time intervals may be recorded on mechanical counters. The other chain of modulated amplifier *II* selects any six successive groups of pulses of the other set of grouped neutron pulses from modulated amplifier *I*. Figure 2i shows the modulation envelopes of the amplifiers of one chain. Thus, there are twelve time intervals in which detected neutrons are counted. These twelve time intervals are referred to as the detector channels. The double modulation scheme insures stability and uniformity in the detector channel on-times.

Since the resolving time of the mechanical counters and their driving circuits is relatively large (about 1/30 sec.), it is necessary to use scaling circuits so that no appreciable number of neutron counts will be missed by the recording devices. A scale-of-64 circuit is used with the recorder of the total neutrons detected. A scale-of-4 is used with each of the recorders of the twelve timed intervals.

The neutron source used was the Cornell cyclotron. Deuterons produced by the arc are accelerated in the cyclotron, are brought out of the accelerating region of the cyclotron, and allowed to fall upon a Be target, thus producing neutrons by the (d,n) reaction. The peak deuteron current falling upon the target during the experimental runs was between the limits of 80 and 150 micro amperes. The target is almost completely surrounded with water, contained in a copper tank, which serves as the moderator for the neutrons. A diagram of the moderator tank is shown in Fig. 3a.

A diagram of the neutron beam collimator and the neutron detector is shown in Fig. 4. The collimator is made up of concentric hollow cylinders of paraffin and B_2O_3 with an especially thick hollow cylinder of B_2O_3 surrounding the BF_3 ionization chamber. This collimation is necessary so that the neutron source will be well defined; i.e., so that neutrons scattered by materials in the cyclotron room will not be scattered into the BF_3 chamber. The collimator is sufficiently effective so that a fast neutron background is detectable only at energies above 100 ev. The BF_3 ionization chamber used as the neutron detector is very similar in construction to the chamber described by Baker and Bacher.[3] The ionization chamber has an effective length of 15 cm and is filled with BF_3 of high purity to

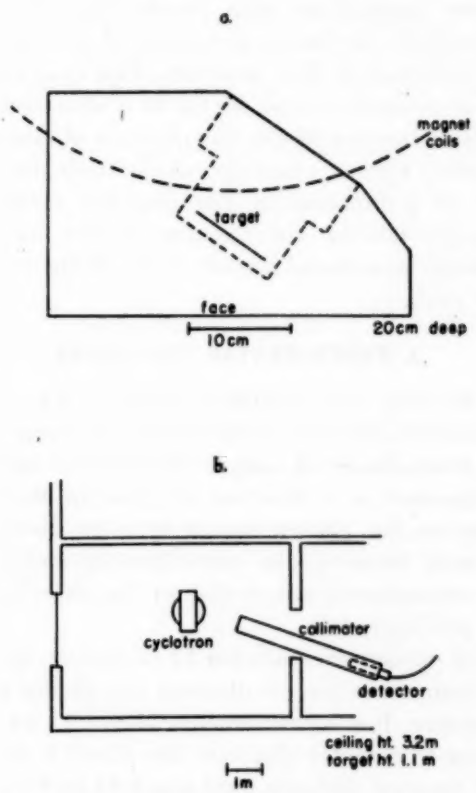

FIG. 3. (a) Moderator tank arrangement, (b) room plan.

a pressure of 2 atmospheres. The chamber collecting potential used is of the order of 3 kv. Figure 3b is a diagram showing the relative positions of neutron source, collimator, and detector.

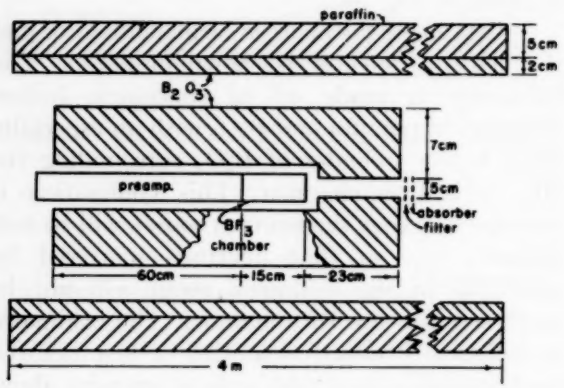

FIG. 4. The neutron beam collimator and neutron detector.

A monitor for the neutron source was used. The monitor neutron detector is a parallel plate ionization chamber in which one plate is coated with uranium. The chamber is filled to a pressure of one atmosphere with argon. This chamber depends on the fission properties of uranium for the detection of slow neutrons. This type chamber is convenient and useful as a slow neutron monitor because of the flat plateaus obtained in counting rate as a function of discriminator bias and as a function of the chamber collecting voltage. During the experiment the monitor chamber was placed directly beneath the moderator tank.

3. EXPERIMENTAL PROCEDURE

The total cross section of iodine as a function of neutron energy was determined by measuring the transmission of samples of iodine of uniform thicknesses as a function of time of flight of neutrons for chosen source-detector distances. In most respects, the procedure for measuring the transmission was similar to that described in the references.[3,4]

For measurements below 12-ev neutron energy, the source-to-detector distance was chosen to be 3 meters. For measurements above 12 ev, the source-to-detector distance was about 6 meters. The greatest distance used was 6.84 meters, and the exact value of the distance in each of the high energy runs was determined by the neutron filter which is described below. The distance was measured from the effective position of the source to the effective position of the detector.

The repetition period of the timing equipment was chosen so that neutrons produced in one cycle would not be detected in succeeding cycles. For each repetition period used, it was shown that no significant fraction of the neutrons produced in one cycle was detected in succeeding cycles. This was done by testing with a repetition period much longer than that to be used in the experimental run. With this long repetition period, the detector channels were set to measure the neutron intensities at times of flight equal to the times of flight for recycled neutrons for the repetition period and times of flight of interest for the experimental run. For measurements at neutron energies below 0.6 ev, a repetition period of 5000 μs was used with the source-detector distance of 3 meters. In the energy range 0.6 ev to 10 ev, a thick Cd (0.9 g/cm^2) filter was used which absorbs low energy neutrons, and this allowed a repetition period of 400 μs to be used at the 3-meter source-detector distance without neutron recycling difficulty. Since the average source intensity is proportional to the repetition frequency, *ceteris paribus*, the Cd filter is used to advantage in increasing the channel counting rates. At energies higher than 10 ev, a filter of very thick Cd (3 to 5 g/cm^2) and 1.0 g/cm^2 of In was used. An In absorber of 1.0 g/cm^2 thickness absorbs more than 99 percent of the neutrons with time of flight between 56 and 66 μs/m. If the source-detector distance, d, the repetition period, T_r, and τ_2, a time-of-flight between 56 and 66 μs/m, are chosen for a time-of-flight measurement, τ_1 so that $\tau_1=\tau_2-T_r/d$, the recycled neutrons of the first preceding cycle can be removed by a 1.0 g/cm^2 In filter. If recycled neutrons for the other preceding cycles can be removed with another material, such as Cd, an In filter can be used to advantage in making the repetition period short. Such a filter was found feasible for the high energy measurements.

Corrections must be made for the various time lags in the apparatus in order to obtain the exact timing of the neutron time-of-flight intervals from the timing of the various modulation

envelopes observed on the oscilloscope. One correction is the time lag obtained from the fast neutron time distribution function measured with the apparatus. This function will be referred to as the FN-function, and the method of obtaining it is explained below. The FN-function gives the sum of the time lags of the apparatus involved in neutron production and detection. Another correction is the mean time of the neutrons in the moderator. A third type of timing correction is the effect of the variation of the neutron source intensity with energy. This correction is small if the intensity variation is small within the resolution width of the apparatus. The resolution was always made sufficiently good so that this correction was negligible.

To obtain the FN-function, the BF_3 chamber is replaced by a similarly constructed butane filled chamber. Such a chamber detects fast neutrons by detecting the recoil protons. The FN-function is obtained by measuring the fraction of the total neutrons detected which are counted in a detector channel as a function of the time delay of the channel, with respect to the arc modulator pulse. For this measurement, the water is removed from the moderator tank. Not only does the FN-function indicate the time lag, but also the sharpness of the arc modulation and detection of the neutrons by the equipment. The ideal shape of this function is that of an isosceles triangle with a base twice as long as the on-time. Figure 5 shows a typical FN-function obtained with an on-time of 5 μs. The dotted curve shows the ideal shape of the function. The "tailing" of this function on either side is caused, for the most part, by the finite rise time of the linear amplifier and the straggling in the acceleration of the deuterons in the cyclotron. Thus, for all on-times, the "tailing" is about of the same duration and the FN-function is, therefore, more nearly triangularly shaped for longer on-times. The time lag is taken as the delay of the centroid of this function with respect to the center of the arc modulator pulse. The FN-function was taken at some time during each set of observations, and the delay was always found to be within 0.15 μs of 7.4 μs for the 5 μs on-time and very nearly 7.5 μs for the other on-times used.

For energies above 0.7 ev, the mean time of the neutrons in the moderator is taken as the mean deceleration time, assuming the protons in the water are not bound. For example, this time is 1.5 μs for 1-ev neutrons. At energies below 0.04 ev, the mean time of the neutrons in the moderator is taken as the decay time constant

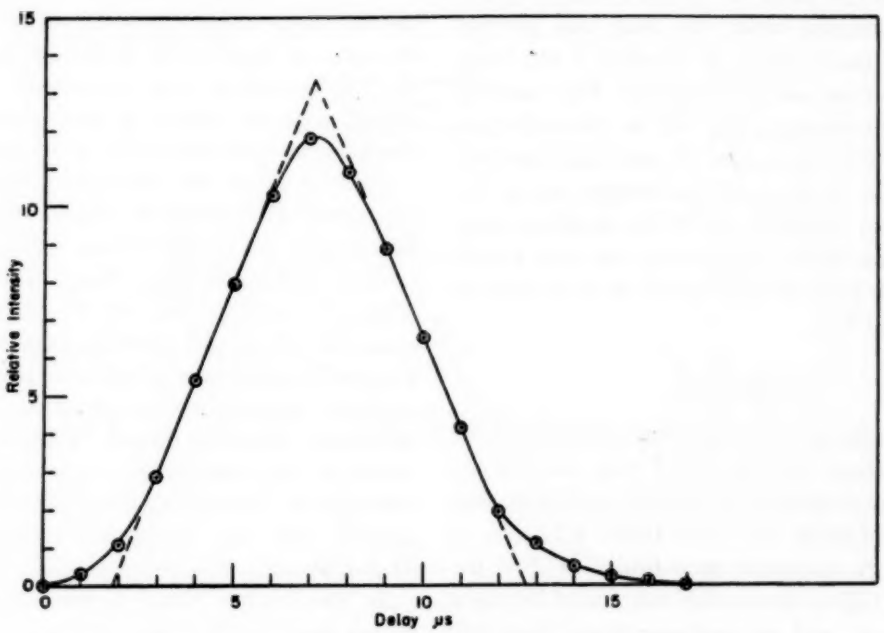

FIG. 5. FN-function or observed time distribution of fast neutrons for 5 μs on-time.

TABLE I. Important features of the experimental conditions.

Run No.	On-time μs	Distance m	Repetition period μs	Source modifier or filter	Absorber thickness g/cm²	Time of flight μs/m	Energy ev
1	250	3	5000	Tray	16.7	490–1420	0.0026–0.0216
2	50	2.97	5000	Tray	31.0	290–477	0.023–0.063
3	50	3	5000	Tray	31.0	98–274	0.0695–0.542
4	10	3	400	0.9 g/cm² Cd	31.0	64–101	0.51–1.28
5	10	3	400	0.9 g/cm² Cd	31.0	23.8–60.6	1.42–9.2
6	5	6.84	300	5 g/cm² Cd 1 g/cm² In	16.2	12.8–20.85	12–31.9
7	5	6.32	300	5 g/cm² Cd 1 g/cm² In	5.96	9.09–17.8	16.5–63.3
8	5	6.32	300	5 g/cm² Cd 1 g/cm² In	2.5	9.09–17.8	16.5–63.3
9	5	6.6	320	5 g/cm² Cd 1 g/cm² In	9.78	5.66–14.0	26.6–164
10	5	6.04	320	3.4 g/cm² Cd 1 g/cm² In	16.2	2.07–11.2	41.6–1200

of the time distribution of neutrons emerging from the moderator. Using water alone as the moderator gave a value for the mean time of 85 μs. Therefore, for measurements in the low energy region, the moderator was modified by placing a sheet of thick Cd directly on the face of the moderator tank to remove the low energy neutrons emerging from the tank and placing adjacent to this a sheet of paraffin 2 cm thick to regenerate low energy neutrons. This paraffin and Cd sheet combination will be referred to as the "tray." The mean time of neutrons emerging from the tray is 30 μs. In the energy region between 0.04 ev and 0.7 ev, it was assumed that the mean time of the neutrons in the tray varied linearly with time of flight from 30 μs at 0.04 ev to 1.8 μs at 0.7 ev.

4. RESULTS

The transmission by several thicknesses of iodine absorbers was measured over the energy interval from 0.0026 ev to 1000 ev, corresponding to a time-of-flight interval from 2.2 μs/m to 1400 μs/m. A resonance was found at 20.3 ev. A region of high cross section was found between 29 and 46 ev, and an analysis shows that this region must contain at least 3 resonances of about equal strength. Indications of resonances at higher energies were found.

The iodine used for the absorbers was resublimed iodine crystals with a minimum purity of 99.985 percent. Brass containers were used for the iodine and a "blank" of brass of the same thickness as the sum of the thicknesses of the two faces of the containers was interposed in the neutron beam when counts were being taken with no absorber. The containers were packed tightly with the iodine in such a way that each absorber was believed to be of uniform thickness.

Table I gives the important features of the experimental conditions under which the data were taken. All the data were corrected for background and time lags. Each separate run is assigned a run number for the purpose of reference. On all graphs showing experimental data, a legend is given which indicates the run number, on-time, source-detector distance, and absorber thickness. Thus the legend "1-250-3m 31 g/cm²" refers to run number one in which the on-time was 250 μs, the source-detector distance was 3 meters, and the absorber thickness used was 31 g/cm².

In the energy range below 10 ev, measurements were made with a resolution which was sufficiently high to detect possible resonances.

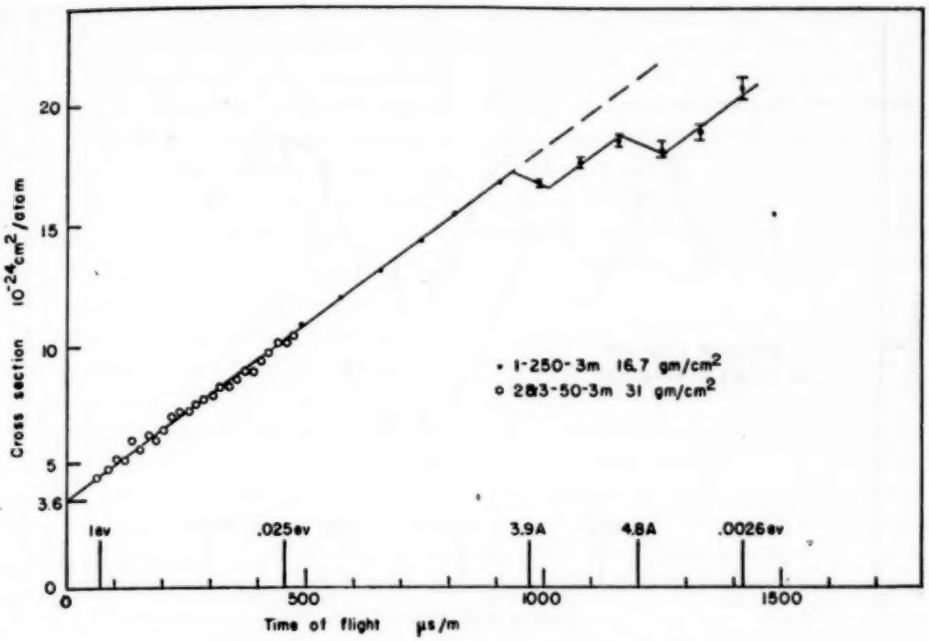

FIG. 6. Low energy neutron cross section of iodine.

Sufficient accuracy was obtained so that the 1/v law would be tested. Figure 6 shows a cross-section plot for times of flight greater than 90 μs/m. The statistical probable errors in the points are indicated by the lengths of the vertical lines through the points, or for those points with no vertical line the probable error is no greater than the diameter of the point. No correction for the effect of the apparatus resolution function on the transmission was made. No such correc-

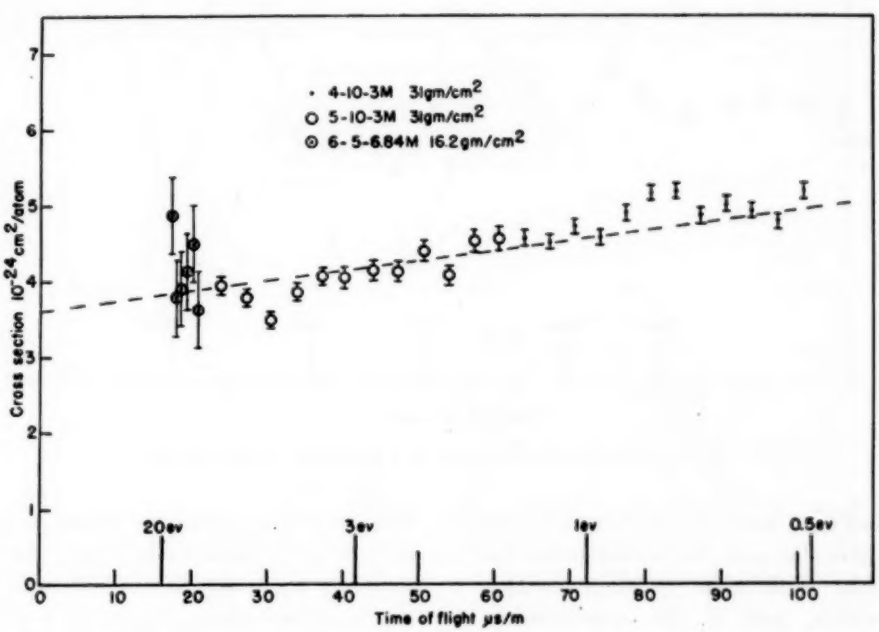

FIG. 7. Neutron cross section of I in the 0.5 to 15-ev region. The dotted line is the best straight line fit for the low energy data.

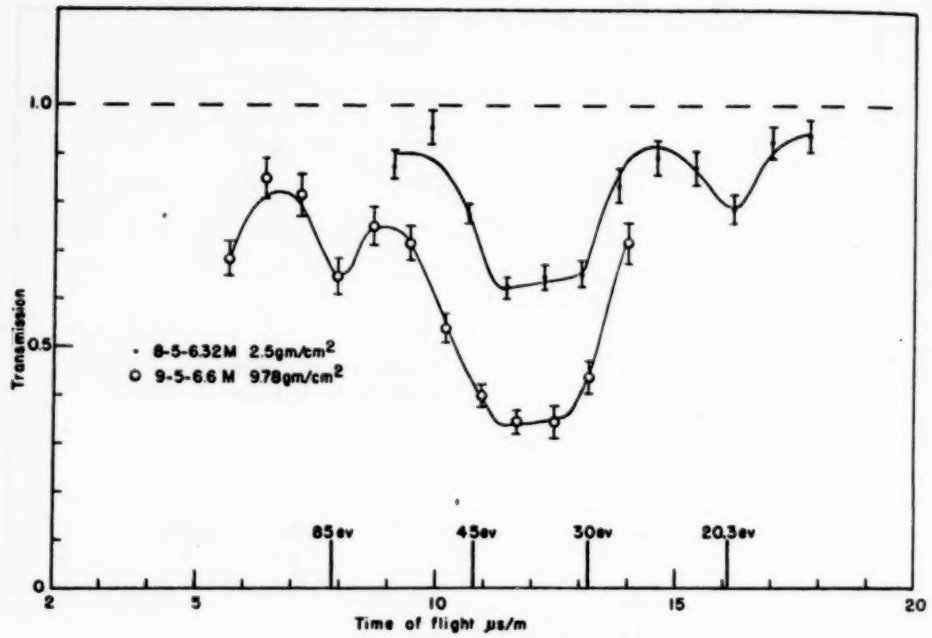

FIG. 8. Observed transmission of I absorbers at high energy.

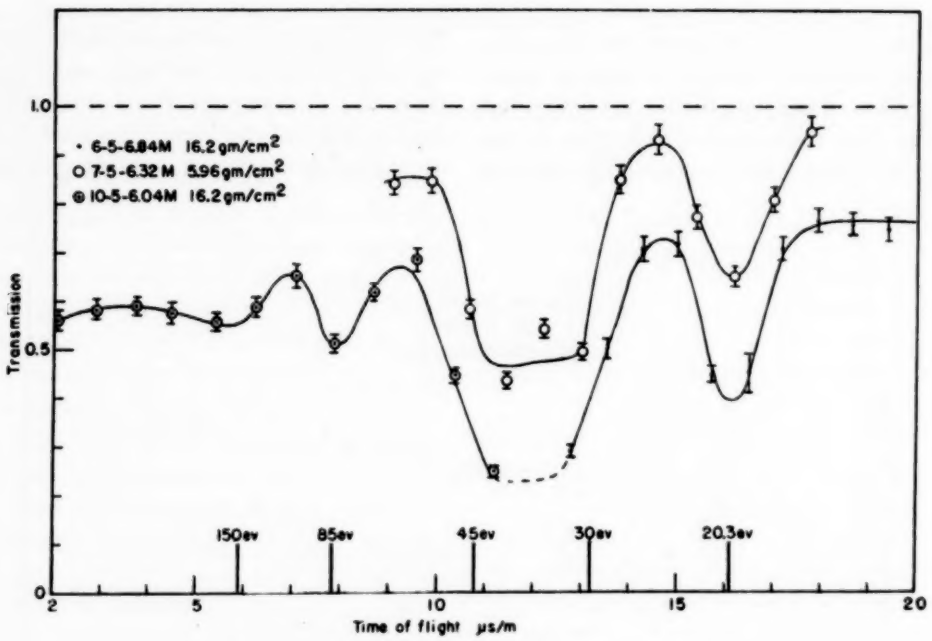

FIG. 9. Observed transmission of I absorbers at high energy.

tion is necessary, at least for the most interesting part of the curve, because the transmission varies nearly linearly with time of flight within a resolution width, and if the transmission is linear with time of flight, the measured transmission is equal to the actual transmission. Breaks in the curve are noted at times of flight of 970 μs/m and 1200 μs/m, corresponding to neutron wave-lengths of 3.9 and 4.8A, respectively, which were interpreted as the effect of the crystalline structure of iodine on the scattering cross section. Except for the crystalline

effects, the points lie very nearly on a straight line, thus verifying the 1/v absorption law. The equation for the best straight line through the points, excluding the crystalline effects, is given by $\sigma=(3.6+0.0146t)\times10^{-24}$ cm²/atom, where t is the time of flight in μs/m and σ is the cross section. This is the same as $\sigma=(3.6+1.06E^{-\frac{1}{2}})\times10^{-24}$ cm²/atom, where E is the energy in ev. The error in the slope of this curve is believed to be no more than 4 percent. The intercept of this curve is taken as the scattering cross section at the energies above 0.5 ev. At energy kT (0.025 ev), $\sigma=10.3\times10^{-24}$ cm²/atom.

Figure 7 shows the time-of-flight region between the low energy resonance and 100 μs/m. Again, no correction has been made for the effect of the resolution function on the cross section. The statistical errors are shown in the usual manner. The dotted straight line has the same slope and intercept as the straight line which best fits the data shown in Fig. 6.

Figures 8 and 9 show the measured transmission as a function of time of flight for the data taken above 14 ev. Data were taken with several thicknesses of absorber in order to determine the character of the resonances indicated in these figures. The curves through the points serve to indicate the probable shape of the transmission curve as seen by the spectrometer. The curves indicate that there is a single absorption resonance near 16 μs/m. The flat region of low transmission of the curves between 11 and 12 μs/m contains a number of unresolved resonances. At 8 μs/m there is an indication of another resonance or group of resonances. At higher energies, there are indications of other resonances.

In a region where the transmission varies nonlinearly by a large amount within a resolution width of the apparatus, it is expected that large corrections have to be made in the data to obtain the true transmission of the absorber. With the best resolution used with the present apparatus there are large variations in the cross section of iodine within a resolution width, in the region of the resonances. The variation in the transmission can be reduced by making the absorber thin, but it is very difficult to obtain a good indication of the cross section from the measured transmission of a very thin absorber. One can obtain some information on the character of the cross section by measuring the transmission for several thicknesses of the absorber as was done in the region of the resonances.

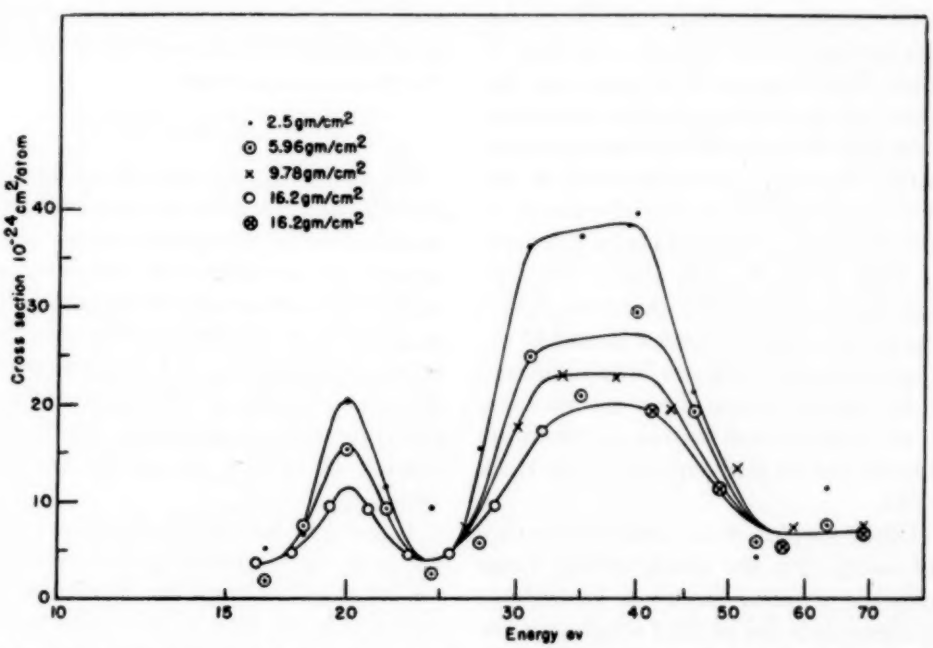

FIG. 10. Cross section of I in the region of the main resonances calculated from the formula $T=\exp(-\sigma n)$, with no correction for apparatus resolution.

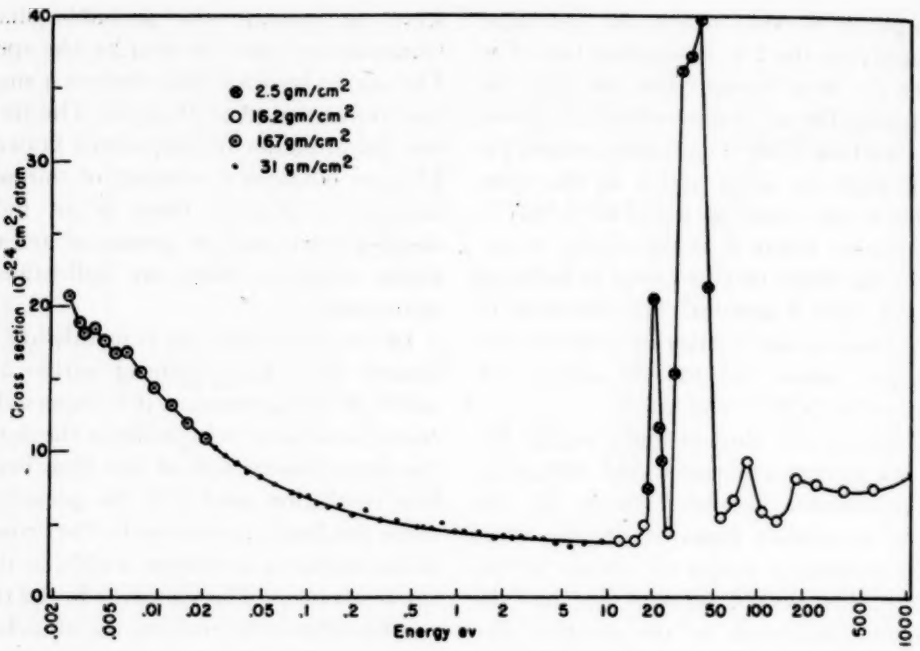

FIG. 11. Cross section of I as a function of neutron energy for the energy region studied. No correction has been made for apparatus resolution.

Figure 10 demonstrates the effect of changing the absorber thickness in transmission measurements. The cross section was obtained from the observed transmission in the formula $T=\exp(-\sigma n)$, where T is the transmission and n is the absorber thickness in atoms/cm². The cross section thus obtained is plotted as a function of the logarithm of the energy. It is noted that the apparent cross section increases with decreasing absorber thickness in the region of the resonances, as is expected. Thus the best indication of the cross section in the region of the resonances is given by the thinnest absorber. One fact demonstrated by this graph is that there are large variations in the cross section within a resolution width in the energy region between 30 and 45 ev, where the spectrometer indicates little variation. Of course, in regions where there are no large variations of cross section within a resolution width, the cross section is given best by the thick absorber data.

Figure 11 shows a plot of the cross section as a function of energy for the whole energy range investigated, the abscissa having a logarithmic scale. Only those data are plotted which give the best representation of the cross section in the regions where data were taken for several thicknesses of absorber. However, it must be remembered that in the region of the resonances the best measured values of the cross section are subject to large corrections because of the finite resolution width. Using a logarithmic energy scale shows the data in such a way that the resolution width is the same order of magnitude over the whole energy range.

5. DISCUSSION

For the most part, this discussion is concerned with the treatment of the data in the region of the resonances. In the region below 15-ev neutron energy the variations in the cross section are sufficiently slow (except for the crystalline effects) so there is no significant difference between the actual transmission and the observed transmission of an absorber. In the region of the resonances the corrections required in the observed transmission to obtain the actual transmission are very large.

Baker and Bacher[3] have given a treatment of the problem of obtaining the transmission curve for an absorber from the transmission observed with a slow neutron velocity spectrometer. They demonstrate that it is rather difficult to proceed directly from the observed transmission to the

actual transmission of an absorber. A much simpler procedure is to assume a certain transmission, find the effect of the resolution of the apparatus on the assumed transmission, and compare this result with the observed transmission. This process is repeated until a good comparison with the experimentally determined transmission is found. In the region of a resonance, the transmission assumed is that obtained from the Breit-Wigner single-level formula[6] with a correction for the Doppler effect, and the parameters in the formula are adjusted for the best correspondence to the observed data.

The resolution function is the sensitivity of the apparatus, for any one channel, as a function of the neutron time of flight. If the resolution function were determined solely by the on-times, its shape would be that of an isosceles triangle with the base of the triangle twice the on-time. However, several other factors influence the shape of the resolution function. The combined effect of the on-time of the arc and detector channels, the straggling in the arrival of deuterons at the Be target, and the uncertainty in the time of detection caused by the finite rise time of the linear amplifier is shown by the FN-function. A typical FN-function is shown in Fig. 5 for an on-time of 5 μs. It is seen that by far the largest contribution to the spread of the FN-function is the on-time.

Contributions to the spreading of the resolution not measured by the FN-function are the uncertainty of the time spent by the neutrons in the moderator, the uncertainty in the source position, and the uncertainty in the position of the detection of the neutrons in the BF_3 chamber. Under the conditions of interest here, i.e., for neutron energies greater than 15 ev and distances of flight greater than six meters, only the last of these three contributions is of significance. The neutrons are almost equally likely to be captured at any point along the 15-cm length of the BF_3 chamber. The time required for a 20-ev neutron to traverse 15 cm is 2.4 μs. The uncertainty in the source position is less than one centimeter, and this is small compared with 15 cm. The uncertainty in the time of the neutrons in the moderator is a few tenths of a microsecond, and this is small compared with the time for a neutron to traverse the chamber length. Therefore, the resolution function is determined essentially by the FN-function and the simple step-function representing the sensitivity of the apparatus as a function of distance.

Figure 12a shows the apparatus resolution function for an on-time of 5 μs, a source-detector distance of 6.5 meters, and for 20-ev neutrons. In making comparisons between the Breit-Wigner formula and the data, it is convenient to use a step-function approximation for the resolution function. Figure 12b shows the step-function approximation used for the resolution function shown in Fig. 12a. The step-function is made symmetrical with respect to the line corresponding to zero time. Also, the second moment of the step-function taken at zero time is made equal to the second moment of the resolution function taken with respect to the vertical line through its centroid.

A symmetrical form of the Breit-Wigner single-

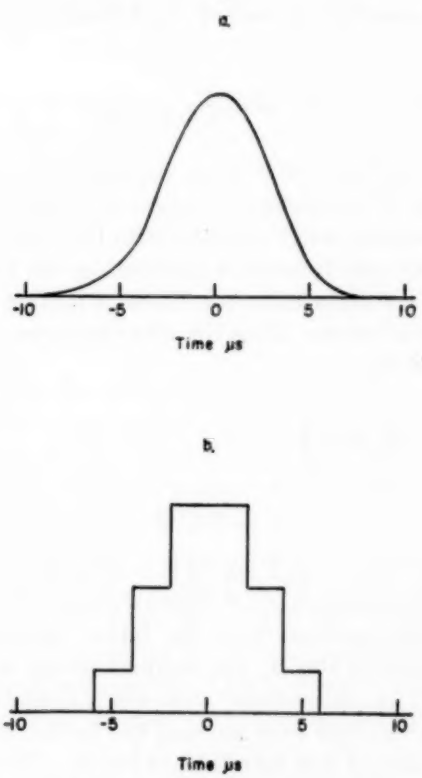

FIG. 12(a). Apparatus resolution function for 5 μs on-time, 20-ev neutrons, and 6.5-m distance of flight. (b). Step-function approximation for resolution function above.

[6] H. Feshbach, D. C. Peaslee, and V. F. Weisskopf, Phys. Rev. 71, 145 (1947).

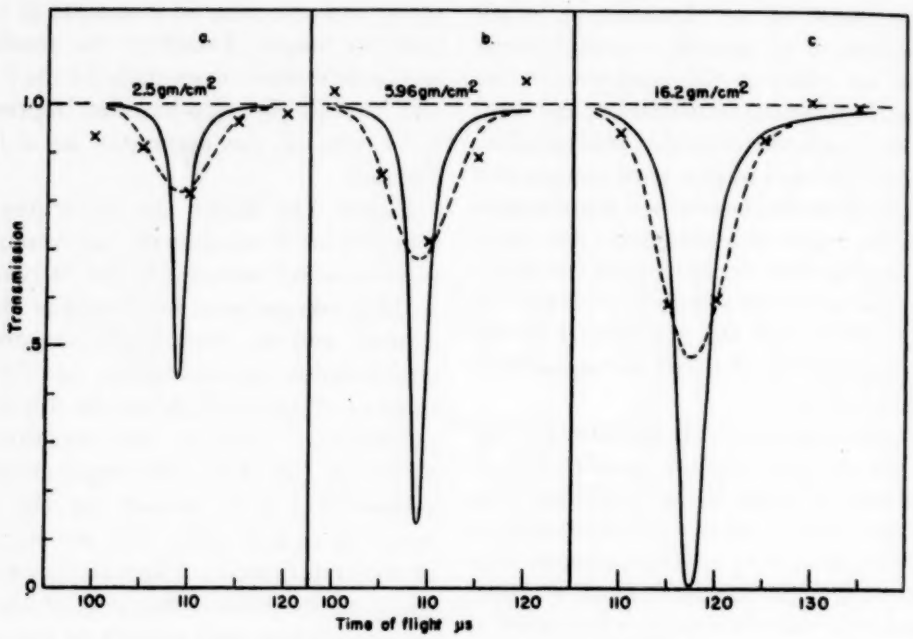

FIG. 13. Comparison of the Breit-Wigner formula with experimental points for three thicknesses of absorber used for the 20.3-ev resonance.

level formula was used of the following form:

$$\sigma_a(E)=\frac{\sigma_0\Gamma^2}{\Gamma^2+4(E-E_r)^2},$$

where σ_a = neutron cross section, E = neutron energy, E_r = resonance energy, σ_0 = cross section at resonance, and Γ = level width. The cross section given by this formula is modified by the Doppler effect resulting from the thermal motion of the absorber atoms. Thus the effective cross section is given by

$$\sigma(E)=(1/\pi^{\frac{1}{2}}\Delta)\int_{-\infty}^{\infty}\sigma_a(E')\times\exp[-(E-E')^2/\Delta^2]dE',$$

where $\Delta = 2(E_rE_{th}m/M)^{\frac{1}{2}}$ = Doppler width, m = neutron mass, E_{th} = thermal energy, M = mass of target nucleus. Since the Debye temperature for iodine is 106°K, the thermal energy is taken as kT, in accordance with the calculation by Lamb,[7] to take into account the lattice binding. The value of Δ is then 0.13 ev for $E_r = 20$ ev.

The low energy resonance is now considered. In order to make a comparison between a theoretical curve and an observed transmission, the observed transmission curve must be corrected for the scattering cross section. The value of the cross section obtained by extrapolating the curve which gives the best fit in the 1/v region, to zero time of flight, is used as the scattering cross section. Thus the observed transmission in the region of the resonance was divided by the transmission corresponding to a scattering cross section of 3.6×10^{-24} cm²/atom. Values are chosen for the parameters of the Breit-Wigner formula to give σ_a. From σ_a, σ is then determined. For each absorber thickness, σ was used to determine the transmission as a function of time of flight for the source-detector distance used in taking the data under consideration. The step-function approximation to the resolution function is then used to obtain the transmission curve due to absorption that would be observed for a cross section given by the Breit-Wigner formula with the chosen parameters. Such transmission curves were compared with the observed curves and parameters adjusted until the best correspondence was obtained.

Figure 13a, b, and c shows the transmission curves obtained from the theory with a particular

[7] W. E. Lamb, Phys. Rev. 55, 190 (1939).

set of parameters which gives the best correspondence to the observed data for the three absorber thicknesses used on the low energy resonance. The solid curves are the transmissions given by the theory, the dotted curves are these transmissions after being put through the resolution function, and the crosses show the experimental data corrected for the scattering cross section. The values of the parameters giving this correspondence are $E_r=20.3$ ev, $\sigma_0=80\times10^{-24}$ cm²/atom, $\Gamma=0.45$ ev. The error in E_r is about 0.5 ev. Because of the magnitude of the experimental errors, the values of σ_0 and Γ may be varied over quite a wide range, with correspondence between the theory and experiment within the experimental error. Also, because of the Doppler effect, no minimum value of Γ or maximum value of σ_0 can be given. The maximum value of Γ and minimum value of σ_0, which give a theoretical curve which could be said to correspond to the experimental points, are 0.8 ev and 40×10^{-24} cm²/atom, respectively.

Another method of analysis which is useful yields information on the values of the parameters in the Breit-Wigner formula, and is largely independent of the resolution of the apparatus. The method has to do with the behavior of the activity integral for a resonance as a function of absorber thickness. The activity, I, for a resonance and a particular absorber thickness is given by

$$I=\int(1-T)dy,$$

where T is the transmission of the absorber as a function of time of flight t, and $dy=dt/t_r$, where t_r is the time of flight corresponding to the E_r for the resonance. The limits of the integral are taken as values of t on either side of the resonance where $T\approx1$. For a given absorber thickness the value of I is the same for any resolution that is used to measure T if the resolution is sufficiently good to separate the resonance in question from other resonances.

If the symmetrical form of the Breit-Wigner formula is used, then

$$I=\int_{-\infty}^{\infty}\left[1-\exp\left(-\frac{n\sigma_0\Gamma^2}{\Gamma^2+4(E-E_r)^2}\right)\right]dy.$$

If $n\sigma_0$ is sufficiently small so that the exponential term in the integrand may be approximated by the first two terms of a power series, then

$$I=\pi n\Gamma\sigma_0/4E_r.$$

No error is made in this equation by neglecting the Doppler effect. Thus the activity is proportional to the absorber thickness for thin absorbers.

If $n\sigma_0\gg1$, little error is made by assuming $\Gamma^2\ll(E-E_r)^2$ in computing the activity using the Breit-Wigner formula. Making this approximation, one obtains

$$I=(\pi n\Gamma^2\sigma_0)^{\frac{1}{2}}/2E_r.$$

Thus for thick absorbers, the activity is proportional to the square root of the absorber thickness.

If the apparatus resolution is so wide that levels cannot be resolved, if $n\sigma_0\gg1$ for each level, and if the separation of the levels is large compared with the level widths (as must be the case for the Breit-Wigner formula to hold).

$$I=(n\pi)^{\frac{1}{2}}\sum_r(\sigma_{0r}\Gamma_r^2/4E_r^2)^{\frac{1}{2}},$$

where r denotes parameters characterizing the rth level, and the sum is taken over the unresolved group. Again, for thick absorbers, the activity is proportional to the square root of the absorber thickness. The Doppler effect introduces an error in all these formulas for I for thick absorbers. However, if $\Delta\ll\Gamma_r$ for the resonances or if the absorber is sufficiently thick, the error is negligible.

In Fig. 14a is shown a plot of activity calculated from the experimental curves (corrected for scattering cross section) as a function of the square root of the absorber thickness for the low energy resonance. With the possible exception of the point for the thinnest absorber, these points fall very nearly on a straight line. From the slope of this curve, one finds that $\sigma_0\Gamma^2=15\times10^{-24}$ ev² cm²/atom, assuming no error to be introduced by the Doppler effect. This is in agreement with the value of 17×10^{-24} ev² cm²/atom, by use of the values of σ_0 and Γ obtained from the curve-fitting method described above. The Doppler effect is neglected because an analysis taking into account this effect is difficult, and the data are

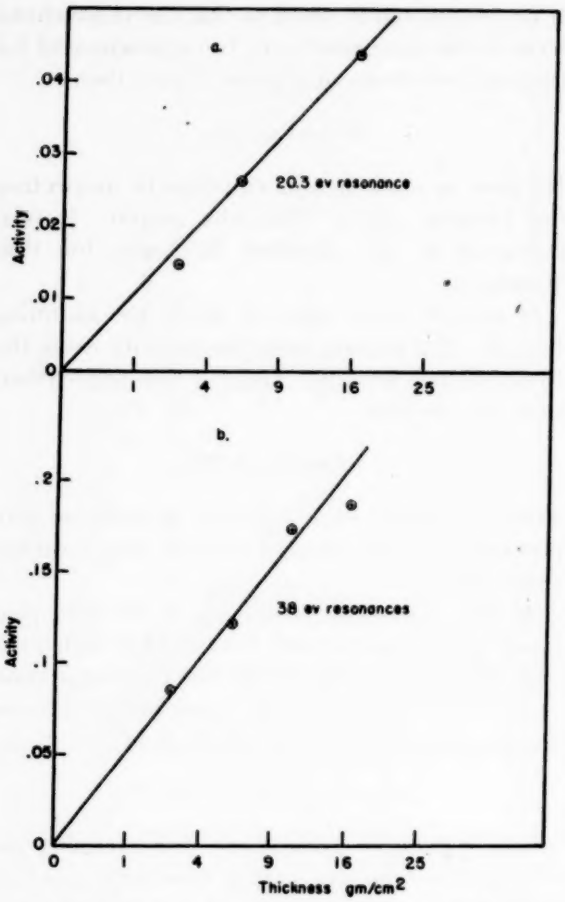

FIG. 14. Activity *vs.* square root of absorber thickness.

not sufficiently accurate to warrant this refinement of the analysis.

The energy region 25 to 50 ev is now considered. If the cross section were constant between 30 and 40 ev, the apparatus resolution is sufficiently good so that the measured transmission would be an exponential function of the thickness. That this is not the case is demonstrated in Fig. 10. Therefore, it may be concluded that the 25- to 50-ev region must contain at least two resonances. By making use of the curve-matching method it was not found possible to fit two resonance curves of about equal $\sigma_0\Gamma^2$ to the data for all thicknesses of absorber used. One sees that this is evidently the case from two considerations. The width of the dips in the transmission curves are about the same for all thicknesses of absorber. This indicates that there must be narrow resonances near the edges of the dip in transmission. However, two narrow resonances near the edges of the dip would not give a flat bottom to the dip for the thick as well as the thin absorbers. Therefore it is concluded that in this energy region there are at least 3 resonances. No attempt was made at curve matching to determine the characteristics of 3 resonances that might fit the data, because there are insufficient data to justify such an attempt. There is no method of deducing from the data the maximum number of resonance levels in this energy region.

Shown in Fig. 14b is a plot of activity for the 25- to 50-ev region as a function of the square root of the absorber thickness. The points fall very nearly on a straight line, indicating that the absorbers are thick for all or most of the resonances in this region. One finds from this curve that $\sum_r (\sigma_{0r}\Gamma_r^2)^{\frac{1}{2}}$ for the resonances is 32.5×10^{-12} ev-cm/atom$^{\frac{1}{2}}$. This value is given under the assumption that 38 ev is near the resonance energy for each resonance and that no error is introduced by the Doppler effect.

The data on the 25- to 50-ev region are now reviewed to determine what evidence exists for believing that the resonances in this region have widths of the order expected from the theory. It is assumed that the Breit-Wigner formula holds for these resonances. This means that the widths of the resonances must be small compared with the spacing. If, for example, it is supposed that there are 3 levels with about 10-ev spacing of about equal strengths, $\sigma_0\Gamma^2=120\times10^{-24}$ ev^2 cm^2/atom for each level. The data indicate that σ_0 for such resonances is large compared with 40×10^{-24} cm^2/atom. Thus, for this possible distribution of levels, the widths are no greater than 1 ev. If it is supposed that there are 3 levels unequally spaced, then the levels nearest each other must be weak and narrow because of their small spacing, and the third level could have $\sigma_0\Gamma^2$ as large as 200×10^{-24} ev^2 cm^2/atom corresponding to a width perhaps as great as 2 ev. Thus, to correspond to the data, no one of the three supposed levels could have a width of more than 1 or 2 ev. If it is supposed that there are four or more resonances within this region, it is evident that the level widths can be no more than 1 or 2 ev. The conclusions drawn above are based on the assumption that $\Gamma\gg\Delta$. On the other hand, the level widths may be about the same as, or smaller than, the Doppler width, $\Delta=0.19$ ev, at

this energy. However, if this is so, then one is led to the same conclusion, namely, that abnormally wide levels are not indicated by the data.

With regard to the energy region above 60 ev, little can be said about the constants of the resonances. It seems evident that there is at least one resonance in the neighborhood of 85 ev. However, the resolution of the apparatus is not sufficiently good at this and higher energies to make it possible to obtain more information than this from the data.

Because of the fact that the iodine resonances occur at rather high energies, it is not expected that the data obtained by indirect methods should compare well with the present data. The recently reported results of Wu, Rainwater, and Havens,[2] using the Columbia neutron spectrometer on iodine, agree with the results obtained here with regard to the energies for the resonance absorption and with regard to the slope and intercept for the best straight-line fit for the data in the low energy region. However, their result for the value for $\sigma_0\Gamma^2$ of about 4×10^{-24} ev^2 cm^2/atom for the 20.3-ev resonance is only $\frac{1}{4}$ the value obtained here. They assume that the 38-ev group of resonances is composed of two levels of equal strengths with $\sigma_0\Gamma^2=135\times10^{-24}$ ev^2 cm^2/atom. In the present experiment it is found that there must be at least three resonances in the 38-ev region. If it is assumed that there are only three resonances of equal strength, the data presented here indicate that $\sigma_0\Gamma^2=115\times10^{-24}$ ev^2 cm^2/atom for each resonance level. Using their data and postulating three levels of equal strength, one obtains $\sigma_0\Gamma^2=60\times10^{-24}$ ev^2 cm^2/atom. There is no apparent reason for these discrepancies unless an error has been made or unless the resolution of their apparatus is not sufficiently good to separate the resonance groups in the particular way they are separated in the present experiment.

The author wishes to express his gratitude to Professor B. D. McDaniel, Dr. C. P. Baker, Professor P. Morrison, and many other members of the Laboratory of Nuclear Studies at Cornell University for many helpful suggestions in carrying out this investigation. Support under contract N6-ORI-91 of the Office of Navy Research is gratefully acknowledged.

Energy Levels in the Nucleus Mn^{56}*

A. B. MARTIN†
*Yale University,** *New Haven, Connecticut*

(Received May 15, 1947)

The energy distribution of the protons emitted in the reaction $Mn^{55}(d,p)Mn^{56}$ has been studied by an absorption method. For excitations up to 4.38 Mev above the ground state of the Mn^{56} nucleus, the protons are found to fall into six distinct energy groups, corresponding to excited states at 1.07, 1.77, 2.48, 3.61, and 4.38 Mev above ground. Results are also presented which indicate that the yields of the individual proton groups vary slowly with deuteron energy, showing no sharp resonance effects. From the Q-value for the most energetic proton group the mass of the nucleus Mn^{55} has been computed to be $54.9634 \pm .0022$ mass units.

INTRODUCTION

A NUMBER of investigators[1] have observed the energy levels in nuclei of low mass number, at excitations up to about 5 Mev, which are exhibited in the process of (d,p), (d,n), (α,p) and other particle emission reactions. The results do not appear to be in agreement with generally accepted theories,[2] which predict a greater density of levels than is observed and, also, that the level density should increase rapidly with excitation and with atomic weight. This experimental method has been applied mainly to the study of elements of low atomic weight, and the energy level spacing observed in these cases is on the average about 1 Mev or somewhat greater; moreover, no uniform trend of level spacing, either with excitation in a particular nucleus or, at a given excitation, with atomic weight, is apparent. It is of interest to extend studies of this type to elements of higher atomic weights to determine if better agreement with theory can be obtained for particle emission reactions of this type, particularly with regard to the theoretical prediction of smaller level spacings in heavier nuclei.

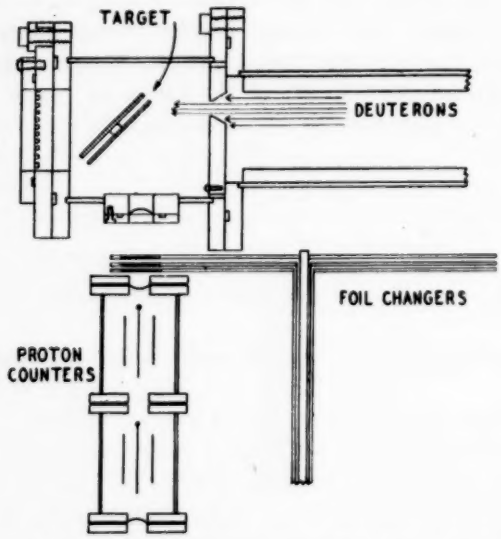

FIG. 1. Sketch of the bombardment chamber, mechanical foil changers and proton counters used in measuring the range of protons emitted in a direction perpendicular to the direction of the deuteron beam. The target is manganese metal (Mn^{55}) evaporated on gold foil.

In the present work, the energy levels in the nucleus Mn^{56} have been determined by measuring the energies of the protons that are emitted when the element Mn^{55} is bombarded with deuterons. These nuclei contain a sufficient number of particles to make the statistical approach of theory at least reasonably valid. The assignment of levels to Mn^{56} is unique since manganese contains only a single isotope.

In addition to the main problem of measuring proton energies, a study has been made of the yields of the individual proton groups as a function of deuteron energy.

* A dissertation presented in partial fulfillment of the requirements for the degree of Doctor of Philosophy in the Graduate School of Yale University.

† Now at Clinton Laboratories, Oak Ridge, Tennessee.

** Assisted by the Office of Naval Research under Contract N6ori-44.

[1] For example, J. D. Cockcroft and W. B. Lewis, Proc. Roy. Soc. **154**, 246 (1936); W. L. Davidson, Jr., Phys. Rev. **56**, 1062 (1939); E. B. M. Murrell and L. C. Smith, Proc. Roy. Soc. **173**, 410 (1939); Ernest Pollard and W. W. Watson, Phys. Rev. **58**, 12 (1940); T. W. Bonner, Proc. Roy. Soc. **174**, 339 (1940); M. G. Holloway and B. L. Moore, Phys. Rev. **58**, 847 (1940).

[2] H. A. Bethe and R. F. Bacher, Rev. Mod. Phys. **8**, 173 (1936); H. A. Bethe, *ibid.* 9, 86 (1937); John Bardeen, Phys. Rev. **51**, (1937).

EXPERIMENTAL ARRANGEMENT

The experimental arrangement used to measure proton range is shown in Fig. 1. The target is mounted in the outer bombardment chamber of the cyclotron and is inclined at an angle of 45° to both the incident beam of deuterons and to the direction of the protons that are to be counted. The geometry of the system is such that only protons emitted at angles of $90\pm4°$ to the direction of the deuteron beam will be detected.

The target material was 99.986 percent pure manganese obtained from Electro Manganese Corporation, Knoxville, Tennessee. Principal impurities were 0.012 percent sulfur as sulfide, 0.001 percent sulfur as sulfate, and less than 0.001 percent iron. Thin targets of uniform thickness were prepared by evaporating the manganese metal on gold foils. The target used to obtain most of the data to be presented here had a thickness of 1.0 cm air equivalent. A second target, having a thickness of 0.2 cm air equivalent also was used to obtain data on the high intensity groups and to study the effect of target thickness on the resolution of the method.

Various thicknesses of aluminum foils are held in position between the target and the proton counters by the mechanical foil changers, shown in Fig. 1, which are operated remotely from the cyclotron control room. Also, a considerable portion of the data was obtained using a gas absorption cell in place of the foil changers. This cell was designed so that one of its end plates could be bolted directly to the exit port of the bombardment chamber and the other end plate could be fastened directly to the face of the first counter, thus eliminating all air spaces in the path of the protons and providing a continuous control over the total absorption. A pressure line made up of one-half inch copper tubing was run from the cyclotron to the control room so that the pressure of air in the cell could be adjusted from the operator's position.

Two proton counters, operating into a coincidence circuit, are used in order to reduce the background count due to the high flux of neutrons in the vicinity of the cyclotron. The counters are operated in the proportional region, and the counting level of the second one is normally set to a comparatively high level in order to peak up the proton groups. The gas used in the counters was tank argon; counter pressures of 10, 20, 40, and 65 cm Hg were employed in the course of this work, the counting level being changed in each case to achieve the highest possible resolution.

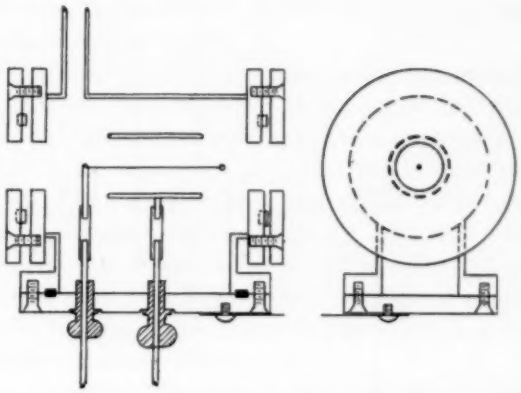

FIG. 2. Detailed drawing of the proton counter. The preamplifier unit is attached directly to the base plate of the brass cylinder enclosing the counter. Aluminum foils, held in place by rubber gasket seals, normally cover the counter ports.

A detailed drawing of the proton counter is shown in Fig. 2. The counter cylinder is of brass and is 3 cm long and 1.9 cm in diameter. The central wire is 10-mil tungsten; a small glass bead encloses the free end. High voltage is applied to the counter cylinder, and a negative pulse is taken from the central wire. A small preamplifier unit is attached to the base plate of each counter case so that the lead from the central wire to the grid of the first amplifier tube is made as short as possible, thus keeping the capacity of the wire to a minimum.

A circuit diagram of the preamplifier unit is shown in Fig. 3. This unit is essentially an impedance transformer, which takes pulses from the counter wire at a high impedance level and has a cathode follower output stage matched to a 75-ohm line. The pulses are then piped over approximately 60 feet of shielded cable to the main amplifier and the remainder of the counting system, which are located in the cyclotron control room. The feedback from the plate of the second tube, through the variable condenser, to the grid of the first, is a capacity neutralization scheme which effectively reduces the capacity of the grid input circuit, enabling a sharp pulse (about 1-microsecond half-width), with a fast rate of rise

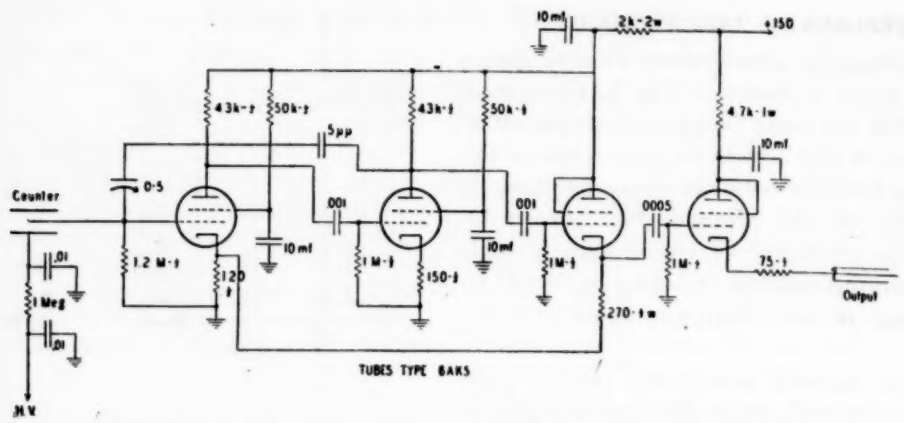

FIG. 3. Circuit diagram of the preamplifier unit. The feedback from tube 2 to tube 1 effectively reduces the capacity of the grid input circuit and sharpens the pulses from the counter. Negative feedback is employed in the cathode circuits to stabilize against voltage fluctuations and tube characteristics.

(0.1 microsecond or less), to be obtained from the counter.

The portion of the counting system at the operator's position consists of two main video amplifiers, a coincidence circuit, a slightly modified Higinbotham scale-of-64 circuit, and the usual mechanical recorders. The main amplifiers have a band pass of about 4 megacycles and a gain of 80 db. The response characteristics favor high frequencies; the low frequency response is made poor intentionally to reduce the effect of microphonics, hum, and similar sources of interference.

The coincidence circuit employs a pentode tube. The output of one of the counters is applied to the control grid of the pentode; the output of the other goes to the screen grid. Both grids are biased beyond cut-off so that the tube will conduct only when positive pulses are applied to the two grids simultaneously. The resolving time of the coincidence circuit is of the order of one to five microseconds. This figure was determined by measuring the number of random coincidences, N_R, occurring in the interval during which N_1 counts were recorded in counter 1 and N_2 counts registered in counter 2, the counters being activated by independent particles. The resolving time τ is then given by $N_R=2\tau N_1 N_2$.

As mentioned above, a number of different gas pressures were used in the counters in the course of these observations, in an effort to attain higher resolution, and at each pressure it was necessary to readjust the counting level in order to obtain the best results; that is, the maximum peaking of the proton groups consistent with a reasonable counting rate. The change in counter "depth" resulting from the use of different counting levels was taken into account by a method similar to that described by Holloway and Moore.[3] A number of calibrations using ThC′ alpha-particles and an analytical study based on proton counting observations were both used to determine this correction term.

The range-energy relation for protons was taken from the curves of Livingston and Bethe.[4]

ENERGY AND HOMOGENEITY OF THE DEUTERON BEAM

It was necessary to determine as accurately as possible the energy of the deuterons from the cyclotron, since the energy of the bombarding particle enters into the calculation of the disintegration energy (the Q-value) of a nuclear reaction. The homogeneity of the deuteron beam is of interest in connection with the resolution of this method of inquiry. Measurements were made on the range of the deuterons by causing the beam to pass through an absorption cell, placed at the target position, and then into a detection chamber. Two types of detectors were used in this study. One was a simple Faraday chamber, in which the amount of beam collected on an insulated probe in vacuo was measured by means

[3] M. G. Holloway and B. L. Moore, Phys. Rev. 58, 847 (1940).

[4] M. Stanley Livingston and H. A. Bethe, Rev. Mod. Phys. 9, 245 (1937).

of a sensitive galvanometer. The other was a standard counter of the type shown in Fig. 2. In order to use such a counter in this application, it was necessary to reduce the beam current to a low value, employ a very small aperture (0.025-cm diameter), and measure the output of the counter by means of a counting rate meter circuit which would record up to 50,000 pulses per second. The results obtained from the use of these two detectors were in good agreement; the averaged data from six separate runs give 3.68 ± 0.05 Mev for the mean energy of the beam. When correction is made for the straggling of the deuterons resulting from their passage through the absorbing material, the half-width of the differential energy curve turns out to be 0.18 ± 0.04 Mev.

A study was made to determine the effect on beam homogeneity of varying certain of the cyclotron parameters, namely, the RF voltage, deflector voltage, gas pressure, and cross section of beam used as determined by the position and separation of the collimator jaws at the entrance to the bombardment chamber. Although a somewhat more homogeneous beam was indicated at low deflector plate voltages, no significant change in beam homogeneity was found for reasonable variations in these parameters.

The number of deuterons striking the target during each proton counting run was measured by a current integrator of the neon discharge type.[5] The unit beam which was used for each counting interval was 3×10^{10} deuterons, which corresponds to a beam current of 0.25 microamperes integrated over a period of approximately 50 seconds.

PROTON GROUPS FROM $Mn^{55}(d,p)Mn^{56}$

Figure 4 shows the results obtained over the range of proton energies from 3.0 to 9.0 Mev. The lower limit to the measurements is set by the range of the deuterons scattered from the target. The proton group ending at about 8 Mev is the end group for the reaction in question. On several occasions attempts were made to find a group of higher energy. The results were in all cases negative; it can be stated that if a group having an energy greater than 8 Mev exists, the yield is less than 5 percent of that of the end group indicated in Fig. 4.

The less prominent groups having energies greater than 4.7 Mev are shown more clearly in Fig. 5, where the scales have been expanded. A total of 21 separate runs were made over this interval of proton range, and all of these have been used for analytic purposes, although only 11 were used to obtain the averaged points shown on this graph. In Fig. 5, the number of counts taken to determine a particular point is given by the ordinate in each case.

The numerical results obtained from these data are shown in Table I. The proton range has in each case been corrected for the effects of the straggling of the protons in the absorbing material, the inhomogeneity of the deuteron energy, and the effective counter depth. The error in the measured proton range caused by finite geometry of the detection system was calculated to be 0.3 percent for the most unfavorable case. The error caused by the finite thickness of the target is also small: 0.1 cm in range for the 30-cm

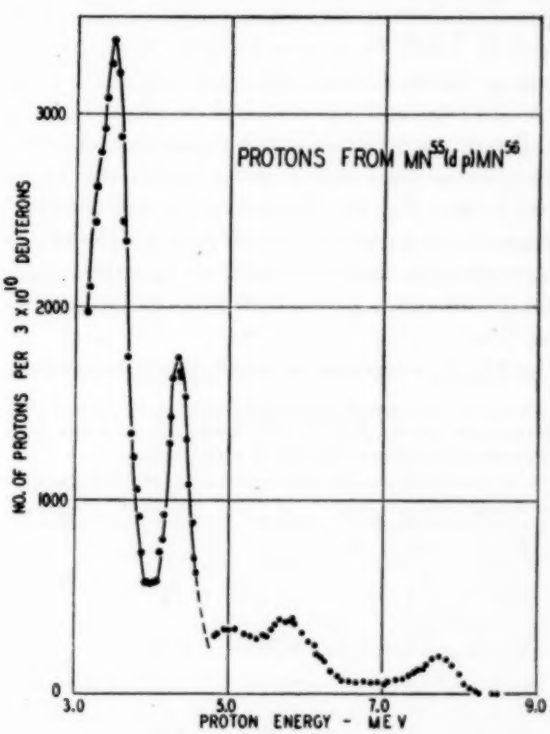

FIG. 4. The yield of protons per unit deuteron beam is plotted against proton energy. Eight runs were made over the energy range from 3.0 to 4.7 Mev; 21 runs were made over the interval from 4.7 to 8.5 Mev.

[5] B. E. Watt, Rev. Sci. Inst. 12, 362 (1941).

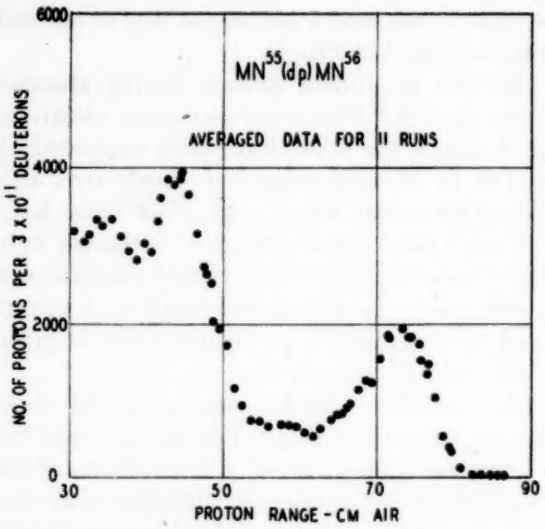

FIG. 5. A plot of the proton yield as a function of proton range, showing the less prominent groups having energies greater than 4.7 Mev. The number of counts taken to determine a particular point is given by the ordinate in each case.

proton group, for example. These last two sources of error have been neglected in computing the disintegration energies for these reactions. The reproducibility of the results obtained is indicated in Table II, where several values for the various disintegration energies, obtained from different runs and different sets of averaged data, are listed. An analysis of the experimental errors which enter into this method yields the figure ± 0.11 Mev for the reliability of the Q-values obtained, and a study of the half-widths of the proton groups observed indicates that the resolution of this method was 0.30 Mev in the present case.

In Fig. 5, a number of small deviations from a smooth curve, suggesting partially resolved groups, are noticeable, for example at ranges of about 34 cm, 41 cm, 44 cm, and 70 cm. None of these small irregularities survived a statistical analysis, however. Moreover, from a series of experiments that were performed to determine the effect of small amounts of the most probable impurities that might be present in the manganese metal or deposited on the surface of the target, it was found that approximately 40 percent of the small deviations were to be associated with proton groups from (d,p) reactions in sulfur and in deuterium. It is concluded, therefore, that these small irregularities are not to be taken as evidence of partially resolved groups from the reaction $Mn^{55}(d,p)Mn^{56}$.

The results of the present work are in general agreement with those of other investigators who have studied heavy particle emission reactions of this general type. The persistence of level spacings of the order of 0.85 Mev in the nucleus Mn^{56} supports the view that the nuclear energy levels exhibited in the process of heavy particle emission reactions are restricted by some selection principle, not yet fully understood, to a small fraction of the number that are theoretically possible. The fact that the level spacing observed for Mn^{56} is somewhat smaller than the spacing found in lighter elements might be regarded as at least qualitative agreement with the prediction of theory that the density of levels should increase at higher atomic weights.

TABLE I. Numerical results for the proton groups from the reaction $Mn^{55}(d,p)Mn^{56}$. The mean proton range, after corrections have been applied, is shown here.

Proton range (cm air)	Proton energy (Mev)	Q (Mev)	Levels (Mev)	Spacing (Mev)
22.9	3.98	0.38	4.38	
				0.77
30.8	4.73	1.15	3.61	
				1.13
44.7	5.85	2.28	2.48	
				0.71
54.4	6.55	2.99	1.77	
				0.70
64.7	7.23	3.69	1.07	
				1.07
82.3	8.29	4.76	0	
			Average spacing	0.85

YIELD OF INDIVIDUAL GROUP AS A FUNCTION OF DEUTERON ENERGY

The energy of the deuterons striking the target was changed by introducing aluminum foils in the path of the beam at the entrance to the bombardment chamber. The deuteron energies attained in this way were 3.68 Mev, 3.33 Mev, and 3.15 Mev. Measurements were then made

TABLE II. Several values for the disintegration energies, obtained from different runs and sets of averaged data.

Excitation	Q-values (Mev)	Best value
Ground	4.75, 4.74, 4.78, 4.79	4.76
First	3.64, 3.72, 3.67, 3.74	3.69
Second	2.96, 2.98, 3.02, 3.03	2.99
Third	2.25, 2.27, 2.28, 2.32	2.28
Fourth	1.14, 1.15, 1.16, 1.17	1.15
Fifth	0.31, 0.38, 0.38, 0.43	0.38

to determine the relative yields from the four most prominent proton groups of the Mn^{56} spectrum, namely, the first, second, fourth, and sixth, in order of increasing proton range. Data similar to those shown in Fig. 4 were obtained at each beam energy, and care was taken to define the peak of each group as accurately as possible.

The results, shown graphically in Fig. 6, suggest that broad resonance phenomena are in operation in the case of groups *A* and *B*, the maximum yield for these groups occurring for a beam energy of about 3.4 Mev. Groups *C* and *D*, however, show no evidence of a resonance process for beam energies between 3.15 and 3.68 Mev. These results are in general agreement with the findings of Bennett, *et al*,[6] who observed that the yield of a single proton group from the reaction $C^{12}(d,p)C^{13}$ was a slowly varying function of the deuteron energy, with no indication of sharp resonance effects.

The dashed curves in Fig. 6 are approximately the envelopes of the proton energy distributions for the two deuteron energies indicated, and correspond to the distribution of proton energies suggested by Volkoff's[7] treatment of the Oppenheimer-Phillips process. It is of interest to note that the present results are not in accord with Volkoff's development: (1) the amplitude of the distribution falls off more rapidly than $E_p^{-\frac{1}{2}}$ for the proton energies obtained in the present work, and (2) the distribution does not exhibit a maximum in the vicinity of

$$E_p = E_D\left[\frac{1+\{1+1.3E_D(1+11.1/Z)\}^{\frac{1}{2}}}{2(1+11.1/Z)}\right] = 4.9\ \text{Mev}.$$

The possibility of a maximum in the distribution at a somewhat lower proton energy (<3.0 Mev) could not be investigated in the present work because it was not possible to count protons effectively in the presence of the comparatively large flux of deuterons scattered from the target.

MASS OF THE NUCLEUS Mn^{55}

If it is assumed that the emission of the proton group of longest range leaves the Mn^{56} nucleus in the ground state, a knowledge of the *Q*-value for this group enables the calculation of the mass of the nucleus Mn^{55}.

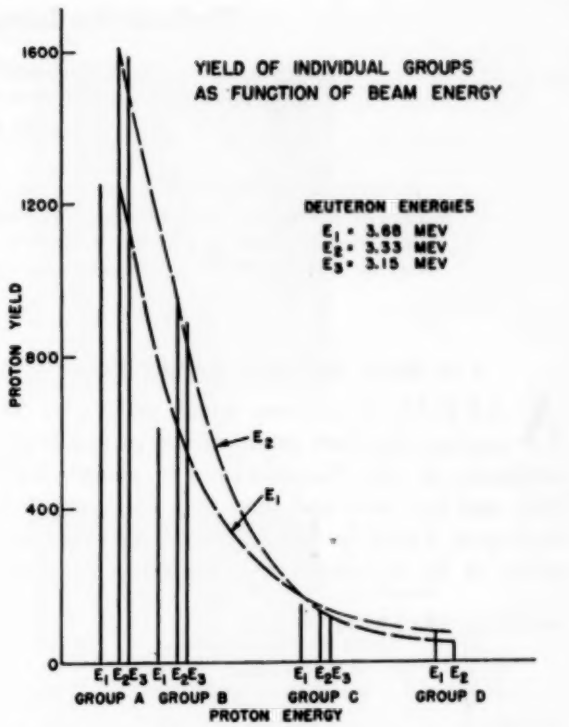

FIG. 6. The relative yields of the four most prominent proton groups from the reaction $Mn^{55}(d,p)Mn^{56}$ for three different deuteron energies.

From Dempster's[8] value for the packing fraction of Fe^{56}, the data of Elliot and Deutsch[9] for the beta- and gamma-rays emitted by Mn^{56}, and the maximum *Q*-value obtained in the present work, the mass of Mn^{55} is found to be 54.9634 ±.0022 mass units. This result agrees, within the limits of error, with the value found by Davidson[10] by the use of the same general method.

ACKNOWLEDGMENTS

It is a pleasure to express appreciation to Professor Ernest Pollard for his constant interest and encouragement during this investigation, and to acknowledge with gratitude the contribution of Professor Howard Schultz, who designed the preamplifier units, main amplifiers, and coincidence circuits used in the counting system. I am also indebted to Professor R. F. Humphreys for many valuable discussions in connection with this problem.

[6] W. E. Bennett, T. W. Bonner, H. T. Richards, and B. E. Watt, Phys. Rev. **59**, 781 (1941).
[7] G. M. Volkoff, Phys. Rev. **57**, 866 (1940).
[8] A. J. Dempster, Phys. Rev. **53**, 64 (1938).
[9] L. G. Elliot and M. Deutsch, Phys. Rev. **64**, 321 (1943).
[10] Wm. L. Davidson, Jr., Phys. Rev. **56**, 1062 (1939).

Radioactive Isotopes of Mo and Tc

J. E. EDWARDS* AND M. L. POOL
Mendenhall Laboratory, Ohio State University, Columbus, Ohio

(Received May 19, 1947)

Evidence is presented which permits the assignment of a 4.3-day Tc activity to Tc^{96}. It decays by K-capture. X-ray photographs of long-period Tc activities show Mo x-rays resulting from K-capture decay of a 52-day Tc activity. Tc x-rays resulting from an isomeric transition involving a 95-day Tc^{97*} activity were also photographed.

I. 67-HOUR Mo^{99} AND 4.3-DAY Tc^{96}

A 4.6-DAY Tc activity which decays by K-capture has been produced[1] by proton bombardment of Mo. Gamma-rays of energy 0.05 Mev and 0.5 Mev and beta-rays of energy 0.6 Mev were found to be associated with the activity. A Tc activity with a period of approximately 2 days was also reported.[2] It was produced by deuteron bombardment of Mo and strong x-rays characteristic of Mo were found.

A 67-hour activity assigned to Mo^{99} has been produced by the reactions Mo(d, p)[2], Mo(n, γ)[2,3], Mo$(n, 2n)$[2,3], Zr(α, n)[4,5] and is found in fission products from U and Th.[5–8] The isotope, with

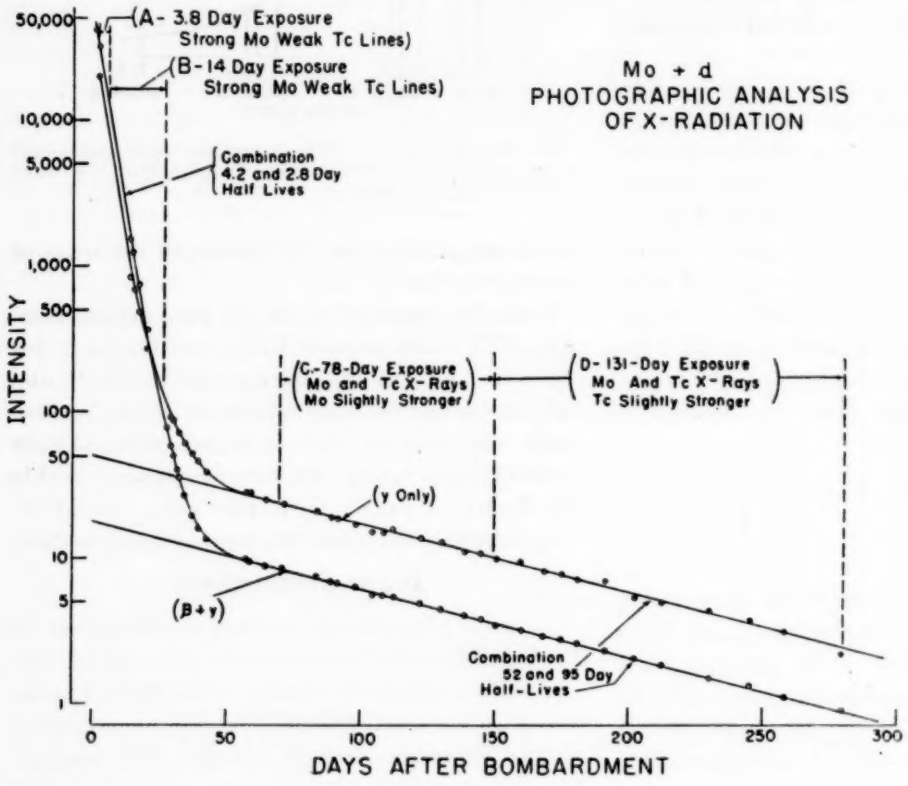

FIG. 1. Decay curves from Mo+d showing procedure of x-ray photography.

* Present address: Ohio University, Athens, Ohio.

[1] D. Ewing, T. Perry, and R. McCreary, Phys. Rev. **55**, 1136 (1939).
[2] G. T. Seaborg and E. Segré, Phys. Rev. **55**, 808 (1939).
[3] R. Sagane, S. Kojima, G. Miyamoto, M. Ikawa, Phys. Rev. **57**, 1180 (1940).
[4] J. E. Edwards and M. L. Pool, Phys. Rev. **69**, 253 (1946).
[5] The plutonium project, "Nuclei formed in fission," Rev. Mod. Phys. **18**, 513 (1946).
[6] Hahn and Strassmann, Naturwiss. **27**, 451 (1939).
[7] Hahn, Strassmann, and Flugge, Naturwiss. **27**, 544 (1939).
[8] Hahn and Strassmann, Naturwiss. **29**, 369 (1941).

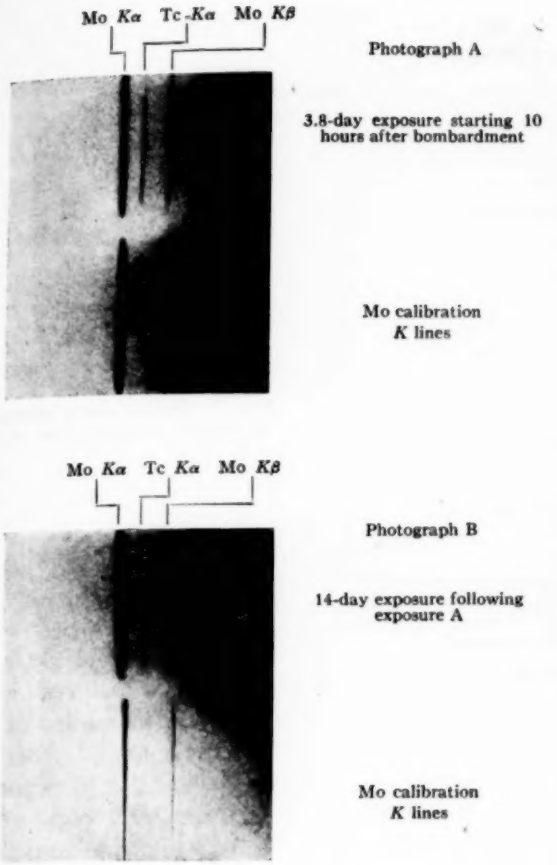

FIG. 2. Photographs of the combination of 4.3-day Tc^{96} and 67-hour Mo^{99}.

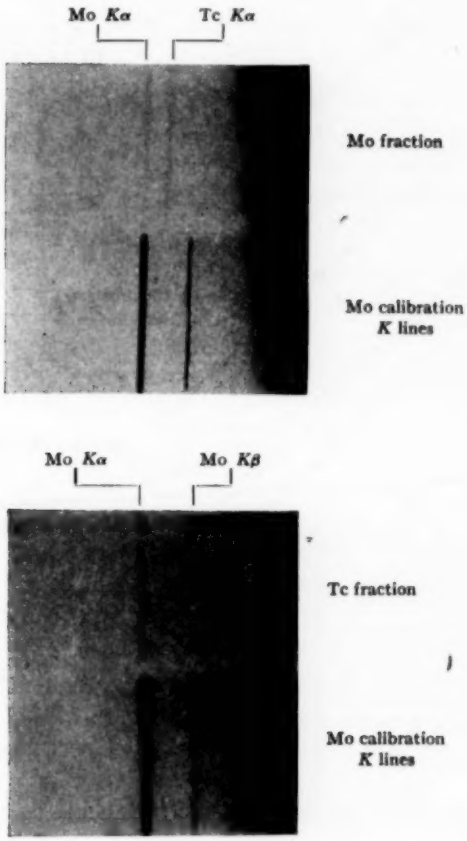

FIG. 3. Exposures of 11 days; chemical fractions from Mo+*d* were used. Exposures started 10 hours after bombardment.

characteristic radiations of 1.5 and 1.2-Mev β-particles and gamma-rays of 0.4, 0.24, and 0.75 Mev, decays to a 6-hour daughter product Tc^{99*}. The 6-hour activity with the emission of 0.136 and 0.18-Mev gamma-rays and conversion electrons drops to the ground state,[5] 4×10^6 year Tc^{99}. The *K* and *L* conversion electrons[9] and x-rays[10] characteristic of Tc have been identified photographically.

4.3-day Tc and 67-hour Mo^{99} activities are both produced by deuteron bombardment of Mo. A study of the x-rays associated with the decay of these isotopes and long-lived Tc isotopes was undertaken using curved mica crystal spectrographs.[11] A deuteron activated Mo sample was photographed for a total of 422 days. Five successive photographs were made. The photographic procedure for the first 4 photographs is shown in Fig. 1. Photographs A and B (Fig. 2) were obtained while the 67-hour Mo^{99} and the 4.3-day Tc were predominant in the activity. Very strong Mo *K* lines and a weak Tc *K* line are found in both photographs. The absence of any marked difference in the relative intensities of the Mo $K\alpha$ and Tc $K\alpha$ lines indicates that the sources of the Mo and Tc x-rays have half-lives of the same order of magnitude.

In order to identify the atomic number of the x-ray sources in photographs A and B, photographs of the Mo and Tc chemical fractions from a deuteron-activated Mo sample were obtained (Fig. 3). The exposures were made in similar spectrographs for 11 days, starting 10 hours after bombardment. The Tc fraction showed strong

[9] D. C. Kalbfell, Phys. Rev. **54**, 543 (1938).
[10] P. H. Abelson, Phys. Rev. **56**, 753 (1939).
[11] J. E. Edwards. M. L. Pool, and F. C. Blake, Phys. Rev. **67**, 150 (1945).

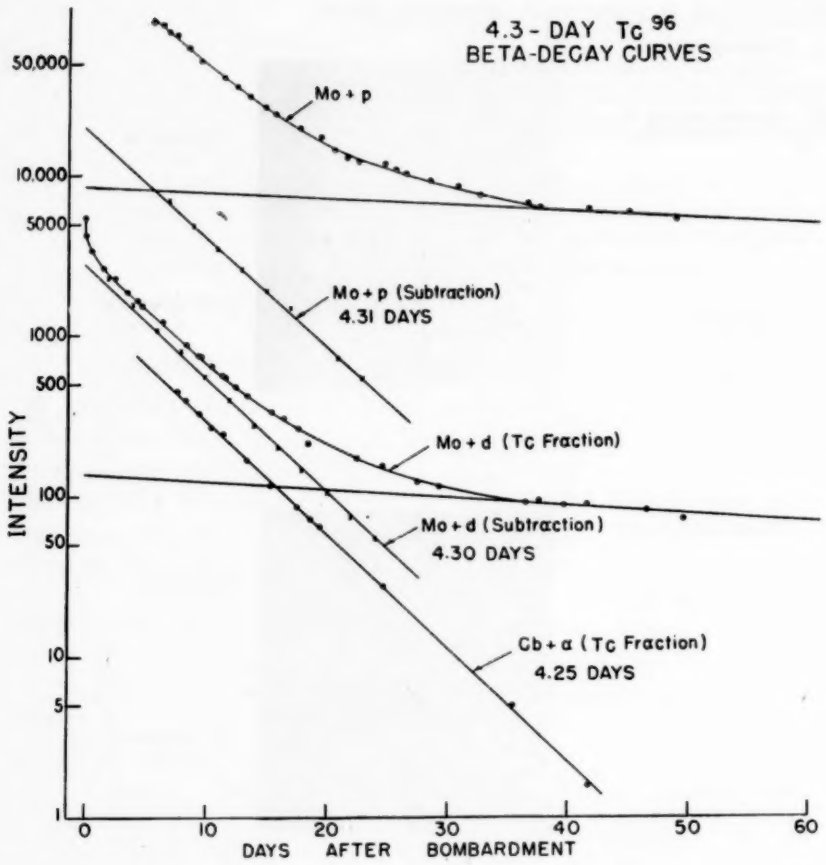

FIG. 4. Decay characteristics of the total radiation from 4.3-day Tc^{96}.

Mo lines while weak Mo and Tc x-rays were found in the Mo fraction. A small amount of Tc in the Mo fraction was responsible for the weak Mo $K\alpha$ line. Additional exposures of the two fractions for 14 days gave no lines from the Mo fraction and a very weak Mo $K\alpha$ line from the Tc fraction. These experiments demonstrate that Mo x-rays are associated with a Tc activity of a

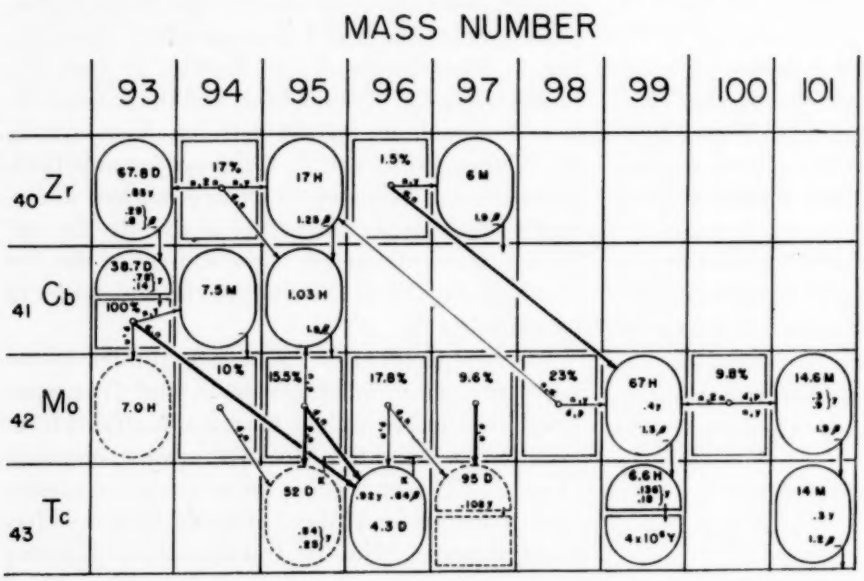

FIG. 5. Section of the atomic chart.

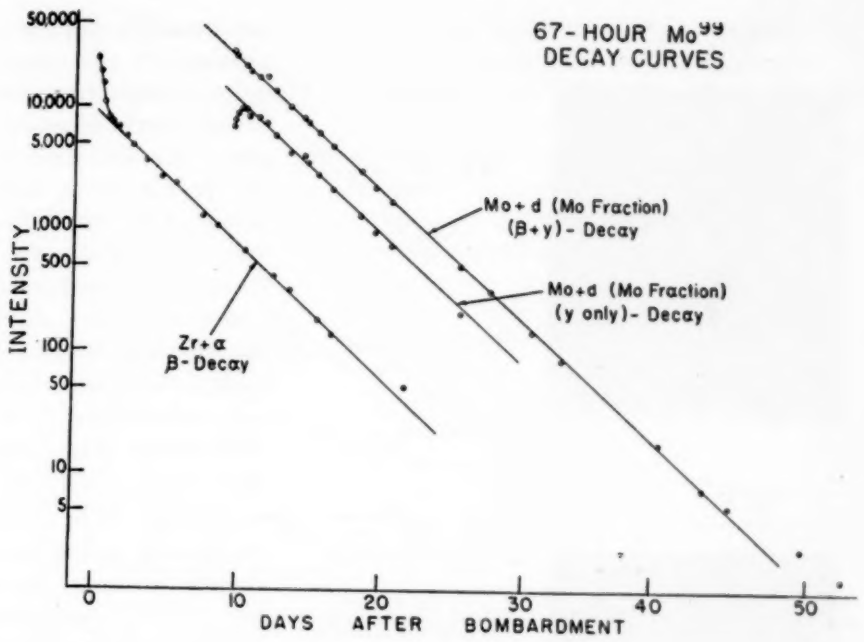

FIG. 6. Decay characteristics of 67-hour Mo^{99}.

few days half-life and Tc x-rays are associated with an Mo activity also of a few days half-life.

Decay characteristics (Fig. 4) and radiation energies of a 4.3-day Tc activity were obtained. The decay characteristics from Mo+p, Mo+d (Tc fraction), and Cb+α (Tc fraction) all show half-lives of nearly 4.3 days. This 4.3-day activity can thus be definitely assigned to Tc^{96}. Long-period activities were also present in the Mo+p and the Mo+d (Tc fraction) samples but no activity longer than 4.3-days half-life was observed in the Cb+α (Tc fraction) sample. By Al and Pb absorption measurements 4.3-day Tc^{96} was found to emit x-rays characteristic of the Mo region, 0.64-Mev charged particles in agreement[1] with other work, and gamma-rays of energy 0.92 Mev. The photographic evidence of Mo x-rays associated with this activity leaves no doubt that it decays mainly by K-electron capture (Fig. 5).

The Tc x-rays (Fig. 3) associated with 67-hour Mo^{99} are due to internal conversion of a gamma-ray as the 6-hour daughter product, Tc^{99*}, drops to the ground state, 4×10^6 year Tc^{99}. Sixty-seven-hour Mo^{99} was produced by deuteron bombardment of Mo and by alpha-bombardment of Zr (Fig. 6). A rise of 6-hour period was observed in the gamma-radiation of the Mo fraction immediately after chemical separation from Tc. Half-life values and radiation energy measurements on Mo^{99} and Tc^{99*} are in agreement with other work.[2,10] No activities of half-life longer than 67 hours were observed in Mo.

II. LONG-PERIOD ACTIVITIES IN Tc

Long-period Tc activities (90 days and 62 days) have been produced by deuteron bombardment[2,12–14] of Mo. The 62-day activity emits x-rays characteristic[2,14] of Mo while radiations from the 90-day activity are thought to be Tc x-rays[14] and conversion electrons.[15] Two converted gamma-rays in the long half-life activities have energies[15] of 0.087 Mev and 0.184 Mev. Evidence of the growth of the 90-day Tc activity from 2.8-day Ru^{97} has been reported,[16,17] permitting its assignment to Tc^{97}.

X-rays associated with long half-life activities after deuteron activation of Mo were photographed according to the procedure shown in Fig. 1. Exposures C and D (Fig. 7) were obtained with a mica crystal curved to a radius of 8 inches. Mo $K\alpha$ and Tc $K\alpha$ lines appear in both the 78-

[12] B. N. Cacciapuoti and E. Segré, Phys. Rev. **52**, 1252 (1937).
[13] B. N. Cacciapuoti, Phys. Rev. **55**, 110 (1939).
[14] A. C. Helmholz, Phys. Rev. **60**, 415 (1941).
[15] D. C. Kalbfell, Phys. Rev. **55**, 422 (1939).
[16] W. H. Sullivan, N. R. Sleight, and E. M. Gladrow, Phys. Rev. **70**, 778 (1946).
[17] E. E. Motta, G. E. Boyd, and A. R. Brosi, Phys. Rev. **71**, 210 (1947).

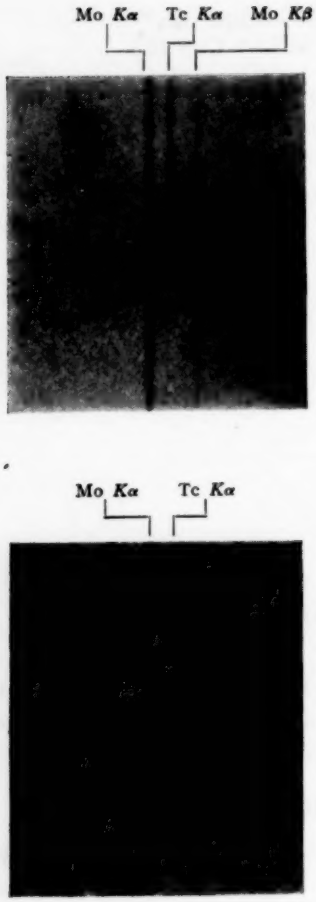

FIG. 7. Photographs of long-period Tc activities.

day exposure and the 131-day exposure with approximately the same intensity. However, it is quite evident from the original films that the Mo $K\alpha$ line in exposure C is slightly stronger than the Tc $K\alpha$ line, while in the later photograph, D, the Tc $K\alpha$ line is slightly stronger. A third exposure of 195 days following exposure D showed a very faint Tc $K\alpha$ line, but no Mo lines. From these three photographs it is obvious that the source of the Mo x-rays was decaying faster than the source of the Tc x-rays. To explain these two x-rays arising from Tc activities one must assume two activities in Tc of slightly different period. The shorter period decays by K-capture giving Mo x-rays, while the longer period Tc x-rays must result from converted gamma-radiation in an isomeric transition in Tc. The two activities cannot be genetically related since the Mo x-ray intensity dropped below the Tc x-ray intensity in the later photographs and no positrons were observed.

Decay characteristics followed for 900 days show two Tc activities fairly well resolved having half-lives of 95 ± 5 days and 52 ± 3 days (Fig. 8). The activities were produced by deuteron bombardment of Mo and by proton bombardment of Mo. Radiation energies from these two activities obtained by Pb and Al absorption measurements show two groups of soft electrons (Fig. 9), x-rays

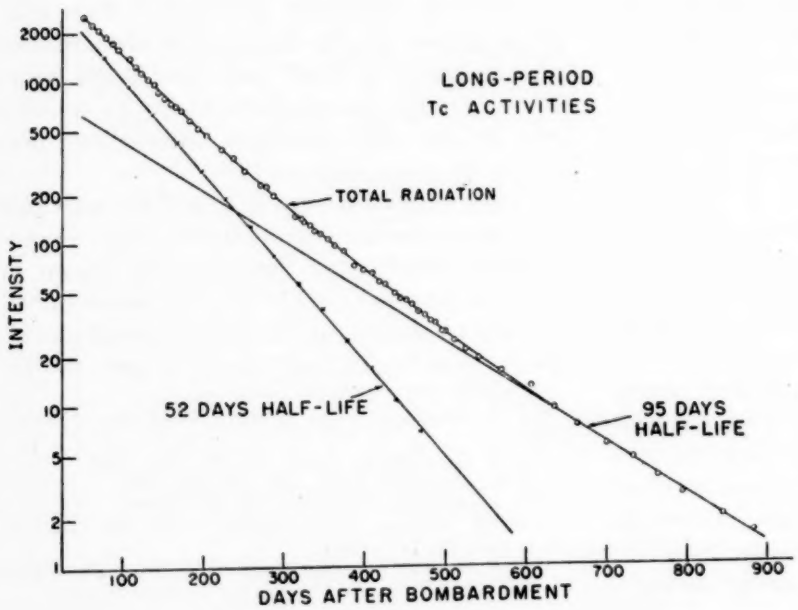

FIG. 8. Decay characteristics of long-period Tc activities.

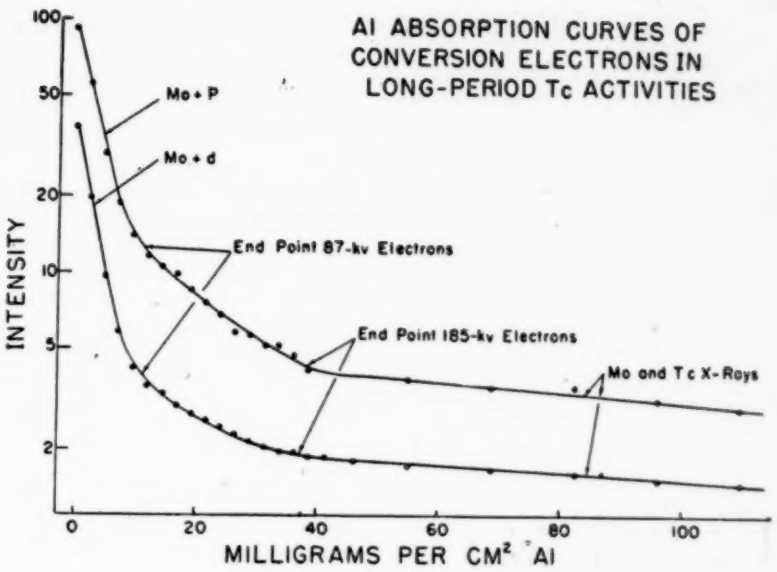

FIG. 9. Thin aluminum absorption of radiations from long-period Tc activities.

characteristic of the Mo–Tc region, and two gamma-rays of energy 0.84 Mev and 0.25 Mev. The soft electron groups are no doubt the conversion electrons previously reported.[15] Since the strong Tc x-rays following the longer 95-day half-life arise from an internally converted gamma-ray, the more intense 87-kv electrons should be associated with this activity. The evidence presented here requires the assignment of the 95-day Tc activity to a metastable state in Tc (Fig. 5). In the isomeric transition which occurs a 0.108-Mev gamma-ray is strongly internally converted giving rise to the Tc x-rays. This interpretation requires the existence of another stable or very long-lived isotope in Tc. Such a long-lived isotope could logically be placed at Tc^{97} permitting the assignment of the 95-day isotope to Tc^{97*} in agreement with previous work.[17]

Observations on the gamma-ray decay characteristics indicate that the hard gamma-rays follow the 52-day half-life. This activity decays by K-capture with associated gamma-rays of 0.84 Mev and 0.25 Mev and is tentatively assigned to Tc^{95} (Fig. 5).

The authors are grateful for the support received from Mr. Julius F. Stone, the Ohio State University Development Fund, and the Ohio State University Research Foundation.

A Class of Exact Solutions of Einstein's Field Equations

SUDHANSU DATTA MAJUMDAR
Palit Laboratory of Physics, University College of Science, Calcutta, India
(Received March 14, 1947)

The work of Weyl on the gravitational field occasioned by an axially symmetric distribution of matter and charge is generalized to the case in which g_{44} and ϕ for an electrostatic field are functionally related, with or without spatial symmetry. It is shown that the most general electrostatic field in which g_{44} and ϕ are related by an equation of the form $g_{44}=\frac{1}{2}(\phi+c)^2$ can be represented by a line element of the form $(ds)^2=-e^{-w}[(dx^1)^2+(dx^2)^2+(dx^3)^2]+e^w(dt)^2$. Certain of the field equations are then identically satisfied while the remaining ones reduce to a single equation for w. The substitution $w=-2\log(1+v)$ transforms this into Laplace's equation for v, so that the solution can be expressed in terms of harmonic function.

1. INTRODUCTION

IN a well-known paper H. Weyl[1] showed that the gravitational field in empty space caused by *any* static axially symmetric distribution of matter and charge can be represented by the line element

$$(ds)^2=-e^u[(dz)^2+(dr)^2]-r^2e^{-w}(d\theta)^2+e^w(dt)^2 \quad (1)$$

with a suitable choice of coordinates. Using these coordinates, which he calls "canonical coordinates," Weyl completely solved the problem of the pure gravitational field with axial symmetry and also obtained a particular class of solutions for an axially symmetric electrostatic field; namely, those involving a functional relation between the electrostatic potential, ϕ, and the component g_{44} of the metric tensor.

In this paper the more general problem of any electrostatic field (with or without spatial symmetry) in which g_{44} and ϕ are functionally related, has been considered. It is found that the *only* type of functional relation that can exist between g_{44} and ϕ is of the form

$$g_{44}=A+B\phi+\tfrac{1}{2}\phi^2, \quad (2)$$

where A and B are arbitrary constants and $\phi/(8\pi)^{\frac{1}{2}}$ is the electrostatic potential in relativistic Lorentz units. If now the constants, A, B, be so chosen that the right-hand side of (2) becomes a perfect square, then the relation (2) reduces to

$$g_{44}=\tfrac{1}{2}(\phi+C)^2. \quad (3)$$

It is then shown that the *most general* electrostatic field in which g_{44} and ϕ are connected by the relation (3) can be represented by the line element

$$(ds)^2=-e^{-w}[(dx^1)^2+(dx^2)^2+(dx^3)^2]+e^w(dt)^2 \quad (4)$$

with a suitable choice of coordinates. Some of the field equations are then identically satisfied, and the remaining ones reduce to a single equation for determining w. The substitution $w=-2\log(1+v)$ transforms this differential equation into Laplace's equation for the function v. The solution can, therefore, be expressed in terms of harmonic functions.

The solution thus obtained is, in a sense, more general than that of Weyl, since in this case there need not be spatial symmetry of the field. In another sense, however, it is less general. For, the functional relation (3) adopted here is a special case of the most general relation (2) adopted by Weyl in the case of axial symmetry.

The solution outlined above is worked out in details in Sections 4 to 6. In Section 5 it has been pointed out that the nature of the solution is such that if the field be due to several charged bodies separated by empty space then to the Newtonian approximation they remain in equilibrium because of their mutual gravitational attraction and electrostatic repulsion.

In Section 7 Weyl's axially symmetric solutions have been examined, and it has been shown that in certain cases no solution of the field equations for empty space exists. A necessary and sufficient condition for the existence of *static* axially symmetric solutions has also been ob-

[1] H. Weyl, Ann. d. Physik [4] **54**, 117 (1917).

tained. It has been proved that static field is possible only when the masses are in equilibrium under the influence of one another. This brings to relief a distinct superiority of the relativistic theory over the older Newtonian theory.

In the last section an attempt has been made to bring out the strong analogy between the old and the new theories by establishing a few simple theorems on the uniqueness of solutions and dependence of solutions on boundary values. The general boundary value problem for any static field is, however, far from being solved.

2. THE FUNDAMENTAL EQUATIONS

As usual we represent the static field by the line element

$$(ds)^2=g_{ab}dx^a dx^b+g_{44}(dt)^2, \quad (a, b=1, 2, 3) \quad (5)$$

the coordinate system so chosen that $g_{14}=g_{24}=g_{34}=0$, and the metric tensor g_{ij} is independent of t. Since no magnetic field is present, the four-potential has the components $(0, 0, 0, \phi/(8\pi)^{\frac{1}{2}})$, where $\phi/(8\pi)^{\frac{1}{2}}$ is the electrostatic potential in relativistic Lorentz units. The only surviving components of the antisymmetrical tensor, F_{ij}, and its associate F^{ij}, representing the electromagnetic field-strengths, are, therefore,

$$(8\pi)^{\frac{1}{2}}F_{4i}=\frac{\partial\phi}{\partial x^i}\equiv\phi_i,$$

$$(8\pi)^{\frac{1}{2}}F^{4i}=e^{-w}g^{ia}\phi_a, \quad (i=1, 2, 3)$$

where e^w has been written for g_{44}. From these the components of the electromagnetic energy tensor E_i^j are calculated by means of the formula

$$E_i^j=-F^{ja}F_{ia}+\tfrac{1}{4}g_i^{\,j}F^{ab}F_{ab}.$$

The gravitational tensor G_{ij} is calculated by the formula

$$G_{ij}=-\frac{\partial}{\partial x^a}\{ij, a\}+\{ia, b\}\{jb, a\}$$
$$+\frac{\partial^2}{\partial x^i\partial x^j}\log(-g)^{\frac{1}{2}}-\{ij, a\}\frac{\partial}{\partial x^a}\log(-g)^{\frac{1}{2}}.$$

The condition for the absence of electric charge and current then comes out to be

$$\frac{\partial}{\partial x^a}(e^{-w}g^{ab}\phi_b(-g)^{\frac{1}{2}})=0, \quad (6)$$

which corresponds to the classical equation $\nabla^2\phi=0$.

In addition we have the seven field equations

$$G_{ij}=-8\pi E_{ij} \quad (i, j=1, 2, 3) \quad (7)$$

$$G_{44}=-8\pi E_{44}, \quad (8)$$

the remaining three equations $G_{i4}=-8\pi E_{i4}$ for $i=1, 2, 3$ having been identically satisfied. The eight equations, (6)–(8) form the set of fundamental equations of the electrostatic field.

3. SOLUTIONS INVOLVING A FUNCTIONAL RELATION BETWEEN g_{44} AND ϕ

In this paper we shall be mainly concerned with those solutions of the field equations in which g_{44} and ϕ are functionally related. First we shall show that the *only* type of functional relation that can exist between them is of the form

$$g_{44}=A+B\phi+\tfrac{1}{2}\phi^2,$$

where A and B are arbitrary constants. In order to prove this we shall require only the two Eqs. (6) and (8).

$$G_{44}=-\frac{\partial}{\partial x^a}\{44, a\}+2\{4a, 4\}\{44, a\}$$
$$-\{44, a\}\frac{\partial}{\partial x^a}\log(-g)^{\frac{1}{2}}$$
$$=\frac{1}{2}\frac{\partial}{\partial x^a}(g^{ab}f_b)-\tfrac{1}{2}\cdot f^{-1}f_a g^{ab}f_b$$
$$+\frac{1}{2}g^{ab}f_b\cdot\frac{\partial}{\partial x^a}\log(-g)^{\frac{1}{2}}, \quad (9)$$

where f is written for g_{44}. Also

$$-8\pi E_{44}=\tfrac{1}{2}g^{ab}\phi_a\phi_b. \quad (10)$$

Therefore, by Eq. (8)

$$\frac{\partial}{\partial x^a}(g^{ab}f_b)-f^{-1}\cdot g^{ab}f_a f_b$$
$$+g^{ab}f_b\cdot\frac{\partial}{\partial x^a}\log(-g)^{\frac{1}{2}}=g^{ab}\phi_a\phi_b.$$

Since f is a function of ϕ, this equation can be

written as

$$\frac{\partial}{\partial x^a}(g^{ab}(-g)^{\frac{1}{2}}\phi_b) = (f')^{-1}(1+f^{-1}f'^2-f'')\cdot g^{ab}(-g)^{\frac{1}{2}}\phi_a\phi_b, \quad (11)$$

where $f'=df/d\phi$ and $f''=d^2f/d\phi^2$. Equation (6) can be written as

$$\frac{\partial}{\partial x^a}(g^{ab}(-g)^{\frac{1}{2}}\cdot\phi_b) = f^{-1}f'\cdot g^{ab}(-g)^{\frac{1}{2}}\phi_a\phi_b. \quad (12)$$

Now Eqs. (11) and (12) can hold simultaneously only if

$$(1+f^{-1}f'^2-f'')/f' = f'/f,$$

that is, if $1-f''=0$. From this it follows that

$$f\equiv g_{44}=A+B\phi+\tfrac{1}{2}\phi^2$$

is the *only* functional relation possible between f and ϕ.

Since any metric approaches that of the special relativity theory at great distances from matter and charge, g_{44} must tend to unity at infinity with the proper choice of the unit of time. And if we choose the arbitrary constant in ϕ so as to make ϕ vanish at infinity, then the above relation may be written in the form

$$g_{44}=1+B\phi+\tfrac{1}{2}\phi^2. \quad (13)$$

From general considerations, solutions of this type are expected to be a bit easier to obtain, since the relation (13) makes the Eqs. (6) and (8) identical, so that there is one equation less to be satisfied. The utmost simplification is expected to result from taking the right-hand side of (13) to be a perfect square. The relation (13) then reduces to

$$g_{44}=\tfrac{1}{2}(\phi\pm\sqrt{2})^2. \quad (14)$$

4. A CLASS OF EXACT SOLUTIONS

It has been possible to find the *most general* solution of (6)–(8) involving the relation (14). The relation (14) itself, however, restricts the generality of the solutions to a great extent.

We proceed to obtain the expressions for the various tensors in terms of g_{ij}, w, and ϕ with the help of the formulas given in Section 2.

$$-8\pi E_{ij}=e^{-w}\phi_i\phi_j-\tfrac{1}{2}e^{-w}g_{ij}g^{ab}\phi_a\phi_b, \quad (i,j=1,2,3), \quad (15)$$

$$-8\pi E_{44}=\tfrac{1}{2}g^{ab}\phi_a\phi_b, \quad (16)$$

$$G_{44}=\frac{1}{2}\frac{\partial}{\partial x^a}(g^{ab}e^w w_b)-\tfrac{1}{2}e^w g^{ab}w_a w_b + \tfrac{1}{2}e^w g^{ab}w_b\frac{\partial}{\partial x^a}\log(-g)^{\frac{1}{2}}. \quad (17)$$

On account of the relation (14), Eqs. (15), (16), and (6) can be written as

$$-8\pi E_{ij}=\tfrac{1}{2}w_i w_j-\tfrac{1}{4}g_{ij}g^{ab}w_a w_b, \quad (i,j=1,2,3) \quad (18)$$

$$-8\pi E_{44}=\tfrac{1}{4}e^w g^{ab}w_a w_b, \quad (19)$$

$$\frac{\partial}{\partial x^a}(e^{-\frac{1}{2}w}g^{ab}w_b(-g)^{\frac{1}{2}})=0. \quad (20)$$

From (8), (17), (19), and (20) we find that the field equations, (6) and (8), become identical on account of the relation (14).

Next we shall show that the relation (14) makes it possible to reduce the general static line element (5) to the isotropic form

$$ds^2=-e^{-w}[(dx^1)^2+(dx^2)^2+(dx^3)^2]+e^w(dt)^2 \quad (21)$$

by suitable transformation of coordinates. In order to do this, we introduce two sets of functions ${}^*g_{ij}$ and $\bar{g}_{ij}$ $(i,j=1,2,3)$ defined by the equations

$$g_{ij}=-{}^*g_{ij}=-e^{-w}\bar{g}_{ij}, \quad (i,j=1,2,3)$$

whence

$$g^{ij}=-{}^*g^{ij}=-e^w\bar{g}^{ij}.$$

${}^*g_{ij}$ is the metric tensor of the three-space in (5) and $\bar{g}_{ij}$ that of an associated three-space *conformal* to it. The contracted Riemann tensors ${}^*G_{ij}$ and $\bar{G}_{ij}$ of these two spaces in conformal correspondence are connected by the equations

$${}^*G_{ij}=\bar{G}_{ij}-\tfrac{1}{2}\bar{w}_{,ij}-\tfrac{1}{4}w_i w_j + \bar{g}_{ij}[-\tfrac{1}{2}\Delta_2 w+\tfrac{1}{4}\Delta_1 w], \quad (22)$$

where

$$\Delta_1 w=\bar{g}^{ab}w_a w_b, \quad \Delta_2 w=\bar{g}^{ab}\bar{w}_{,ab}$$

and $\bar{w}_{,ij}$ is the second co-variant derivative of the scalar function w in the associated space.

The relation between the contracted Riemann tensors G_{ij} $(i,j=1,2,3)$ and ${}^*G_{ij}$ of the four-space and three-space in (5) is

$$G_{ij}={}^*G_{ij}+\tfrac{1}{2}w_{ij}+\tfrac{1}{4}w_iw_j-\tfrac{1}{2}{}^*\{ij,a\}w_a$$
$$={}^*G_{ij}+\tfrac{1}{2}{}^*w_{,ij}+\tfrac{1}{4}w_iw_j. \quad (i,j=1,2,3) \quad (23)$$

Further we have the relations[2]

$${}^*\{ij,k\}={}^{(-)}\{ij,k\}$$
$$+\tfrac{1}{2}[-w_j\delta_i{}^k-w_i\delta_j{}^k+w_a\bar{g}_{ij}\bar{g}^{ak}]$$
$${}^*\{ij,a\}w_a={}^{(-)}\{ij,a\}w_a-w_iw_j+\tfrac{1}{2}\bar{g}_{ij}\Delta_1 w. \quad (24)$$

From Eqs. (22)–(24) we have the relations

$$G_{ij}=\bar{G}_{ij}+\tfrac{1}{2}w_iw_j-\tfrac{1}{2}\bar{g}_{ij}\Delta_2 w. \quad (i,j=1,2,3). \quad (25)$$

Equation (18) can also be written in the form

$$-8\pi E_{ij}=\tfrac{1}{2}w_iw_j-\tfrac{1}{4}\bar{g}_{ij}\Delta_1 w. \quad (i,j=1,2,3) \quad (26)$$

By the use of the expressions (25) and (26) for G_{ij} and E_{ij}, the field equation (7) can now be written as

$$\bar{G}_{ij}-\tfrac{1}{2}\bar{g}_{ij}[\Delta_2 w-\tfrac{1}{2}\Delta_1 w]=0. \quad (i,j=1,2,3) \quad (27)$$

The expression (17) for G_{44} can also be written in a very compact form

$$G_{44}=-\frac{1}{2}\frac{\partial}{\partial x^a}(e^{2w}\bar{g}^{ab}w_b)+\tfrac{1}{2}e^{2w}\Delta_1 w$$
$$-\tfrac{1}{2}e^{2w}\bar{g}^{ab}w_b\frac{\partial}{\partial x^a}\log(-g)^{\frac{1}{2}}$$
$$=-\frac{1}{2}e^{2w}\Big[\bar{g}^{ab}w_{ab}+\frac{\partial\bar{g}^{ab}}{\partial x^a}w_b$$
$$+\bar{g}^{ab}w_b\frac{\partial}{\partial x^a}\log(\bar{g})^{\frac{1}{2}}\Big]. \quad (28)$$

By use of the relations

$$\frac{\partial\bar{g}^{ij}}{\partial x^k}=-{}^{(-)}\{ak,i\}\bar{g}^{aj}-{}^{(-)}\{ak,j\}\bar{g}^{ia},$$

$$\frac{\partial}{\partial x^i}\log(\bar{g})^{\frac{1}{2}}={}^{(-)}\{ia,a\},$$

Eq. (28) can be written as

$$G_{44}=-\tfrac{1}{2}e^{2w}\Delta_2 w. \quad (29)$$

Because of (19) and (29) the field equation (8) now takes the form

$$-\tfrac{1}{2}e^{2w}\Delta_2 w=-\tfrac{1}{4}e^{2w}\Delta_1 w, \quad \text{or} \quad \Delta_2 w=\tfrac{1}{2}\Delta_1 w. \quad (30)$$

From (27) and (30) follows the interesting result

$$\bar{G}_{ij}=0. \quad (i,j=1,2,3). \quad (31)$$

Since in a *three*-dimensional space the vanishing of the contracted Riemann tensor implies the vanishing of the Riemann tensor itself, we arrive at the conclusion that *the associated three-space is Euclidean*. We are, therefore, justified in adopting (21) as the line element of the *most general* static field in which the relation (14) holds. According to (30) the field equations will then reduce to the single equation

$$\nabla^2 w=\tfrac{1}{2}(w_1{}^2+w_2{}^2+w_3{}^2). \quad (32)$$

The substitution,

$$w=-2\log(1+v), \quad (33)$$

transforms it into Laplace's equation

$$\nabla^2 v=0 \quad (34)$$

for the function v.

Also according to (14) and (33) the relation between v and ϕ is

$$v=-\phi/(\phi\pm\sqrt{2}). \quad (35)$$

5. NATURE OF THE SOLUTION OBTAINED

The Newtonian approximation of the above solutions is obtained by neglecting all powers of v higher than the first. We then have

$$g_{44}\equiv e^w=1-2v=1-2\Omega,$$

where Ω is the gravitational potential in gravitational units. Also

$$\phi/(8\pi)^{\frac{1}{2}}=\pm v/2(\pi)^{\frac{1}{2}}.$$

The potential ϕ' in electrostatic units is, therefore,

$$\phi'=\pm v,$$

whence

$$\Omega=\pm\phi'. \quad (36)$$

[2] Editor's note: for typographical reasons the Christoffel symbols associated with the metric coefficients ${}^*g_{ij}$ and $\bar{g}_{ij}$ are indicated with the superposed signs * and $^{(-)}$.

From this we see that if the field be due to several charged bodies separated by empty space, then to the Newtonian approximation they must remain in equilibrium under their mutual interaction. In fact it is because of this interesting property of the solutions that a reduction of the field equations to Laplace's equation has been possible.

6. VANISHING OF THE MATERIAL STRESSES FOR A PROPER CHOICE OF THE INTERNAL FIELD

In the Newtonian theory if the densities of charge and matter bear the same constant proportion everywhere, and if in the above-mentioned units the constant of proportionality is unity, then owing to the exact balancing of the gravitational and electric forces on every piece of matter, the stresses in matter will vanish. It is remarkable that such a result exactly holds in the relativistic theory also. Of course, given an external field in empty space the distribution of matter and charge producing that field is far from being uniquely determined. We shall show below that, corresponding to the external solution obtained above, a particular internal solution can always be constructed so that the stresses in matter may vanish at every point. We choose the internal solution in the following manner.

In the interior of matter: (i) there exists a line element of the form (21), (ii) v is a solution of Poisson's equation, (iii) g_{44} and ϕ are connected by the relation (14), (iv) the first, second (and whatever derivative may be required), of w are continuous at the boundary surface, separating matter from empty space.

The internal field should satisfy the equation

$$G_i^j-\tfrac{1}{2}g_i^jG=-8\pi(M_i^j+E_i^j), \qquad (37)$$

where M_i^j is the material and E_i^j the electromagnetic energy tensor. Since Eqs. (25) and (29) hold for any static field, and Eqs. (19) and (26) follow from the assumption (iii) alone, they continue to hold in this case also. On account of the assumption (i) we can put

$$\bar{G}_{ij}=0, \quad \bar{g}_{ij}=\delta_{ij}, \quad (i, j=1, 2, 3)$$

in (25), (26), (29), and (19) and obtain the expressions

$$\left.\begin{aligned} G_{ij}&=\tfrac{1}{2}w_iw_j-\tfrac{1}{2}\delta_{ij}\nabla^2w \\ -8\pi E_{ij}&=\tfrac{1}{2}w_iw_j-\tfrac{1}{4}\delta_{ij}\Sigma w_a^2 \end{aligned}\right\}, \quad (i, j=1, 2, 3)$$

$$G_{44}=-\tfrac{1}{2}e^{2w}\nabla^2w,$$

$$G=-\tfrac{1}{2}e^w\Sigma w_a^2+e^w\nabla^2w,$$

$$G_i^j-\tfrac{1}{2}g_i^jG=-\tfrac{1}{2}e^ww_iw_j+\tfrac{1}{4}\delta_{ij}e^w\Sigma w_a^2, \quad (i, j=1, 2, 3) \qquad (38)$$

$$-8\pi E_i^j=-\tfrac{1}{2}e^ww_iw_j+\tfrac{1}{4}e^w\delta_{ij}\Sigma w_a^2. \quad (i, j=1, 2, 3) \qquad (39)$$

Combining Eqs. (37)–(39) we arrive at the interesting result

$$M_i^j=0, \quad (i, j=1, 2, 3),$$

that is, the material stresses all vanish at every point. But the situation is quite different in the case of the component M_4^4 which represents the density of matter.

By (19), (29)

$$G_4^4-\tfrac{1}{2}g_4^4G=-e^w\nabla^2w+\tfrac{1}{4}e^w\Sigma w_a^2,$$

$$-8\pi E_4^4=-\tfrac{1}{4}e^w\Sigma w_a^2.$$

Because of Eq. (37) we, therefore, have

$$-8\pi M_4^4=-e^w[\nabla^2w-\tfrac{1}{2}\Sigma w_a^2],$$

whence

$$\nabla^2v=-4\pi(1+v)^3M_4^4.$$

For small v this reduces to Poisson's equation. In empty space $M_4^4=0$, and we get back Laplace's Eq. (34).

7. EXAMINATION OF WEYL'S AXIALLY SYMMETRIC SOLUTIONS

(A) The Case of a Pure Gravitational Field

Weyl has shown that the most general static axially symmetric gravitational field in empty space can be represented by the line element

$$(ds)^2=-e^u[(dz)^2+(dr)^2] -r^2e^{-u}(d\theta)^2+e^w(dt)^2. \qquad (40)$$

Weyl chooses the internal line element also in this form. We then have the following expressions for the components of the material energy

tensor:

$$8\pi T_1{}^1 = -8\pi T_2{}^2 = \tfrac{1}{4}e^{-u}(2u_2/r + 2w_2/r + w_1{}^2 - w_2{}^2), \quad (41)$$

$$-8\pi T_3{}^3 = \tfrac{1}{2}e^{-u}(u_{11}+u_{22}+w_{11}+w_{22}+\tfrac{1}{2}w_1{}^2+\tfrac{1}{2}w_2{}^2),$$

$$-8\pi T_4{}^4 = -\tfrac{1}{2}e^{-u}(w_{11}+w_{22}-u_{11}-u_{22}+2w_2/r-\tfrac{1}{2}w_1{}^2-\tfrac{1}{2}w_2{}^2),$$

$$-8\pi T_1{}^2 = -8\pi T_2{}^1 = -\tfrac{1}{2}e^{-u}(w_1w_2 - w_1/r - u_1/r). \quad (42)$$

Weyl makes the assumption that the stress component $T_3{}^3$ vanishes everywhere. This leads to the two differential equations,

$$\Delta w \equiv w_{11}+w_{22}+w_2/r = 8\pi T_4{}^4 e^u, \quad (43)$$

$$\nabla^2 v \equiv v_{11}+v_{22} = -\tfrac{1}{2}(w_1{}^2+w_2{}^2), \quad (v=u+w) \quad (44)$$

for determining u and w. In empty space $T_4{}^4=0$, and Eq. (43) reduces to Laplace's equation for axial symmetry. This equation is first solved for w and the solution substituted in the right-hand side of (44). The latter equation can then be treated as a two-dimensional Poisson's equation for the function v. The solution for v is made unique by the condition that it vanishes on the axis and at infinity. Thus we see that the two assumptions, $T_3{}^3=0$ and $T_4{}^4=0$, made by Weyl enable us to find any desired solutions for u and w which, when substituted in (41) and (42), will determine the stress components $T_1{}^1$, $T_2{}^2$, and $T_1{}^2$ uniquely. In order that the solutions thus obtained may be the correct solutions for empty space, it is essential that $T_1{}^1$, $T_2{}^2$, and $T_1{}^2$ should vanish in addition to $T_3{}^3$ and $T_4{}^4$. Weyl's method of solution, in many cases, does not lead to the vanishing of these components. In order, therefore, to arrive at the correct solutions for empty space, we set the left-hand sides of Eqs. (41) to (42) equal to zero. The functions w and v then satisfy the equations

$$\Delta w = 0, \quad (45)$$

$$v_1 = rw_1w_2, \quad (46)$$

$$v_2 = \tfrac{1}{2}r(w_2{}^2 - w_1{}^2). \quad (47)$$

As before, we first integrate Eq. (45) by introducing an arbitrary axially symmetric density distribution σ. This solution for w is then substituted in Eqs. (46) and (47). If a solution for v can now be found satisfying Eqs. (46) and (47), then Weyl's Eq. (44) will be automatically satisfied in the empty regions of space. But the converse is not true. A necessary and sufficient condition that a function v may exist satisfying (46) and (47) is that the line integral

$$I = \int (v_1 dz + v_2 dr). \quad (48)$$

(i) along *any* closed curve, A, which lies entirely in empty space should vanish, and (ii) along *any* curve, B, which starts from the axis and terminates on the axis and lies entirely in empty space, should vanish.

First we consider curves of the type A which may surround matter distributed in the shape of a ring. By Stokes' theorem,

$$I = \int\int (v_{12} - v_{21}) dS,$$

where dS is an element of plane area in the $(r-z)$ half-plane enclosed by the curve, and

$$v_{12} = \partial v_1/\partial r, \quad v_{21} = \partial v_2/\partial z.$$

v_1, v_2 are looked upon as two different functions and not as the derivatives of a single function v.

By (46) and (47)

$$v_{12} - v_{21} = rw_1 \cdot \Delta w.$$

If the enclosed area is empty then $\Delta w = 0$ and, therefore, I vanishes. If, however, the area contains matter, then

$$\Delta w = -4\pi\sigma,$$

and

$$I = -4\pi \int\int rw_1 \sigma dS$$

$$= -2\int\int\int rw_1 \sigma dz dr d\theta$$

$$= -2\int\int\int w_1 \sigma d\tau,$$

the last integral having been taken over the entire ring. Now w_1 is the component of force in the z direction acting on the mass element $\sigma d\tau$, and w_1 consists of two parts,

$$w_1 = w_{i,1} + w_{e,1},$$

where $w_{i,1}$ is the internal force attributable to the remaining part of the ring and $w_{e,1}$ is the resultant of external forces acting on the element $\sigma d\tau$. The contribution to the integral I due to $w_{i,1}$ therefore vanishes, and we have

$$I=-2\int\int\int w_{e,1}\sigma d\tau. \tag{49}$$

Thus we obtain as the necessary and sufficient condition for the existence of v that the "resultant force acting on the ring according to classical calculations must vanish."

Next we consider a curve of the type B which starts from a point P on the axis, terminates at a point Q on the axis, and lies entirely in empty space. After going from P to Q along the curve if we go back to P along the axis we complete a circuit, and the above proof can be easily extended to this case also.

From this we conclude that solutions corresponding to two spheres separated by empty space do not exist, whereas solutions corresponding to a sphere at the center of a circular ring do exist.

(B) The Case of an Electrostatic Field

Weyl has shown that the most general axially symmetric electrostatic field in empty space can be represented by the line element (40). He takes the internal line element also in this form and obtains a class of solutions of the type (13). As his solutions may not lead to the vanishing of all the components of stress in empty space, we proceed, as before, to investigate the conditions for existence of solutions for strictly empty space. The field equations in this case are

$$\begin{aligned}
8\pi E_1{}^1 &= -8\pi E_2{}^2=\tfrac{1}{2}e^{-u-w}(\phi_1{}^2-\phi_2{}^2)\\
&=\tfrac{1}{4}e^{-u}(2v_2/r+w_1{}^2-w_2{}^2),\\
-8\pi E_3{}^3 &=\tfrac{1}{2}e^{-u-w}(\phi_1{}^2+\phi_2{}^2)\\
&=\tfrac{1}{2}e^{-u}(\nabla^2 v+\tfrac{1}{2}w_1{}^2+\tfrac{1}{2}w_2{}^2),\\
-8\pi E_4{}^4 &=-\tfrac{1}{2}e^{-u-w}(\phi_1{}^2+\phi_2{}^2)\\
&=-\tfrac{1}{2}e^{-u}(2\Delta w-\nabla^2 v-\tfrac{1}{2}w_1{}^2-\tfrac{1}{2}w_2{}^2),\\
-8\pi E_1{}^2 &=-8\pi E_2{}^1=-e^{-u-w}\phi_1\phi_2,\\
&=-\tfrac{1}{2}e^{-u}(w_1w_2-v_1/r).
\end{aligned}$$

The equations to be satisfied by w and ϕ are, therefore,

$$\Delta w=e^{-w}(\phi_1{}^2+\phi_2{}^2), \tag{50}$$

$$\Delta\phi=w_1\phi_1+w_2\phi_2. \tag{51}$$

We shall consider Weyl's solutions only, which are of the type (13). The two equations, (50) and (51), then become identical. Weyl introduces an auxiliary function χ defined by the equation

$$\chi=\int(1+B\phi+\tfrac{1}{2}\phi^2)^{-1}d\phi. \tag{52}$$

We then have

$$\begin{aligned}
\Delta\chi &= e^{-w}[\Delta\phi-w_1\phi_1-w_2\phi_2]\\
&=(B+\phi)^{-1}[\Delta w-e^{-w}\phi_1{}^2-e^{-w}\phi_2{}^2]. \qquad (53)
\end{aligned}$$

Hence (50) and (51) reduce to Laplace's equation

$$\Delta\chi=0.$$

Inside matter we take the auxiliary function χ to be a solution of Poisson's equation. The equations to be satisfied by v are

$$v_1=rw_1w_2-2e^{-w}\phi_1\phi_2, \tag{54}$$

$$v_2=\tfrac{1}{2}r(w_2{}^2-w_1{}^2)+re^{-w}(\phi_1{}^2-\phi_2{}^2). \tag{55}$$

In this case,

$$\begin{aligned}
v_{12}-v_{21} &= rw_1\Delta w+re^{-w}[w_1\phi_1{}^2-w_1\phi_2{}^2\\
&\quad -2\phi_1\Delta\phi+2w_2\phi_1\phi_2] \qquad \text{by (54) and (55)}\\
&=r[w_1(B+\phi)-2\phi_1]\Delta\chi \qquad \text{by (53)}\\
&=r(B^2-2)\chi_1\cdot\Delta\chi \qquad \text{by (52).}
\end{aligned}$$

Therefore, the line integral

$$I=-2(B^2-2)\int\int\int\chi_{e,1}\sigma d\tau. \tag{56}$$

We therefore arrive at the same condition for existence of solution as before. From (56) we draw the interesting conclusion that *if* $B=\pm\sqrt{2}$, *then a solution always exists irrespective of the distribution of the masses.* This is in agreement with what has been said in Section (5).

8. BOUNDARY VALUE PROBLEMS

If g_{44} and ϕ are functionally related, then every level-surface of g_{44} (thereby meaning a surface

on which g_{44} is constant) is also a level-surface of ϕ. We shall now prove the proposition that if there exists one surface S (either closed or extending to infinity) on which g_{44} and ϕ are both constant, and if one of the two domains into which this surface divides the entire space be completely free from matter and charge, then in this domain, D, every level-surface of g_{44} will also be a level-surface of ϕ, and therefore g_{44} and ϕ will be connected by an equation of the type (13).

To prove this we shall require only Eqs. (6) and (8). Equation (8) can be written as

$$\frac{\partial}{\partial x^a}[f^{-1}(-g)^{\frac{1}{2}}g^{ab}f_b]=f^{-1}(-g)^{\frac{1}{2}}g^{ab}\phi_a\phi_b. \quad (57)$$

Multiplying Eq. (6) by ϕ and subtracting from Eq. (57), we have

$$\frac{\partial}{\partial x^a}[f^{-1}(-g)^{\frac{1}{2}}g^{ab}f_b]-\phi\frac{\partial}{\partial x^a}[f^{-1}(-g)^{\frac{1}{2}}g^{ab}\phi_b]$$
$$-f^{-1}(-g)^{\frac{1}{2}}g^{ab}\phi_a\phi_b=0$$

or

$$\frac{\partial}{\partial x^a}[f^{-1}(-g)^{\frac{1}{2}}g^{ab}(f-\tfrac{1}{2}\phi^2)_b]=0. \quad (58)$$

Equations (6) and (58) are of the form

$$a^{ik}u_{[ik]}+b^iu_{[i]}=0, \quad (59)$$

where

$$a^{ik}=-f^{-1}(-g)^{\frac{1}{2}}g^{ik}, \quad (60)$$

$$b^i=-\frac{\partial}{\partial x^k}[f^{-1}(-g)^{\frac{1}{2}}g^{ik}], \quad (61)$$

$u=\phi-A$, or $f-A$, or $f-\frac{1}{2}\phi^2-B\phi-1$,

$$u_{[i]}=\partial u/\partial x^i, \quad u_{[ik]}=\partial^2u/\partial x^i\partial x^k.$$

We now require the help of a theorem given by Courant and Hilbert[3] on the uniqueness of the solutions of linear elliptic differential equations. The proof, as given by these authors, is for a finite domain only, but the following modification holds for both finite and infinite domains.

We make the substitution

$$u=zv, \quad z=1-e^{-\mu r}, \quad \mu>0$$

with

$$r=[(x^1)^2+(x^2)^2+(x^3)^2]^{\frac{1}{2}}=[\delta_{ij}x^ix^j]^{\frac{1}{2}}.$$

The origin of space-coordinates is chosen to be outside the domain D, so that r is everywhere positive in D. Equation (59) is then transformed into

$$a^{ik}v_{[ik]}+\beta^iv_{[i]}+cv=0, \quad (62)$$

where

$$\beta^i=2z^{-1}a^{ik}z_{[k]}+b^i$$
$$=2z^{-1}\mu e^{-\mu r}(a^{ik}\delta_{kj}x^j/r)+b^i, \quad (63)$$

$$c=z^{-1}(a^{ik}z_{[ik]}+b^iz_{[i]})$$
$$=-z^{-1}e^{-\mu r}\left\{\mu^2\frac{a^{ik}\delta_{ij}\delta_{km}x^jx^m}{r^2}\right.$$
$$\left.-\mu\left[\left(\frac{\delta_{ik}}{r}-\frac{\delta_{ij}\delta_{km}x^jx^m}{r^3}\right)a^{ik}+\frac{b^i\delta_{ij}x^j}{r}\right]\right\}. \quad (64)$$

Now we choose the space coordinates in such a way that the g_{ik}'s approach Galilean values at infinity. We then notice that: (1) the a^{ik}'s tend to δ^{ik} at infinity, and (2) b^i, β^i, c all tend to zero at infinity. Concerning the sign of c, which is very important, we see first of all that the a^{ik}'s form the matrix of a positive definite quadratic form. Therefore, the quantity $a^{ik}\delta_{ij}\delta_{km}x^jx^m/r^2$ in the first term of (64) is everywhere positive in D and approaches the value unity at infinity, and hence possesses a positive lower bound. Similarly the coefficient of μ in the bracketed expression in (64) tends to zero at infinity, and, therefore, its absolute value possesses a positive upper bound. Hence the quantity μ can be chosen so large as to make this expression positive throughout D. Since z is positive throughout D, it follows that c is negative throughout D.

We have thus established the two main requirements for the proof, namely, that a^{ik} should form the matrix of a positive definite quadratic form and that c should be negative. The proof now follows the same course as that given by Courant and Hilbert,[3] and we arrive at the conclusion that if v (and therefore u) vanishes on the boundary of D (and at infinity if the domain be infinite) then v (and therefore u) vanishes throughout D.

[3] R. Courant and D. Hilbert, *Methoden der Mathematischen Physik* (Julius Springer, Berlin, 1937), pp. 274–276.

DEDUCTIONS FROM THE ABOVE THEOREM

(1) First we apply the theorem to the function

$$u=f-\tfrac{1}{2}\phi^2-B\phi-1.$$

If there exists a surface S on which f and ϕ are both constant, then we can always choose the constant, B, so as to make u vanish on S. Hence it follows that if one of the two domains into which the entire space is divided by this surface be empty, then in this domain u vanishes and, therefore, f and ϕ are functionally related. That is, f and ϕ have the same family of level-surfaces in D. This is the theorem stated at the beginning of this section.

(2) Applying the theorem to the function $u=\phi-A$ we draw similar conclusions.

(3) In the *absence* of an electric field we apply the theorem to the function $u=f-A$ and draw similar conclusions. In this case it can be easily shown that space-time is flat in D.

My thanks are due to Professor M. N. Saha, D.Sc., F.R.S., for his constant interest and encouragement during the progress of the work.

Thanks are also due to the authorities of the Council of Scientific and Industrial Research, India, for granting me a scholarship to carry on this work.

The Capture of Negative Mesotrons in Matter

E. FERMI AND E. TELLER
Institute for Nuclear Studies, University of Chicago
(Received May 28, 1947)

A detailed discussion of the energy loss of negative mesotrons in matter is presented. The energy range considered is from +2000 ev to the lowest quantized orbit of the mesotron. The most important mechanism for energy loss is that of electron collisions except very near the nucleus, where radiation losses are important.

The time for the over-all process is of the order of 10^{-12} sec. in condensed matter and 10^{-9} sec. in normal air. In chemical compounds the probability of capture near the various atoms is roughly proportional to their atomic numbers.

1. INTRODUCTION

RECENTLY the significance of experimental results[1] on the capture of negative mesotrons in matter has been discussed from the point of view of the information that it gives concerning the interaction between mesotrons and nucleons. The interaction of slow negative mesotrons with matter has been described as consisting of two steps:[2] first, one in which the mesotron is captured in the Bohr orbit with a radius of the order of 10^{-12} cm near the nucleus; second, a step in which more typically nuclear interactions play a role during which the mesotron is destroyed by its collisions with the nearby nucleons. The present paper will be primarily concerned with the detailed description of the first step.

The chief purpose of a detailed description of the capture process is to make sure that the time required for it is short compared with the natural decay time of the mesotron ($\sim 2\times 10^{-6}$ sec.). We propose to discuss in particular how the physical and chemical state of matter influences the capture process. In this connection we shall investigate also the relative probabilities of the capture of mesotrons near various types of nuclei in case the slowing down material is not a pure element.

Throughout the greater part of the capture process the wave-length of the mesotron is short as compared to the geometric dimensions of the field in which this particle is moving. It is therefore permissible in most of our arguments to consider the motion of the mesotron as purely classical.

[1] M. Conversi, E. Pancini, and O. Piccioni, Phys. Rev. **71**, 209 (1947).
[2] E. Fermi, E. Teller, and V. Weisskopf, Phys. Rev. **71**, 314 (1947).

2. ENERGY LOSS OF ELECTRONS OVER 2000 EV

As long as the energy of the mesotron is more than 2000 ev, the velocity of the mesotron is greater than the velocity of the valence electrons. The slowing down of the mesotrons can then be treated according to the conventional methods applicable to fast heavy particles. In the slowing down of the mesotron the longest time is spent in the state when the mesotron moves with relativistic velocities. The consequences of the decay of the mesotron during this phase of cosmic radiation are well known and will not be discussed here. The time needed to slow a mesotron from the relativistic 10^8 volts to 2000 ev is about 10^{-9} to 10^{-10} second in condensed matter, or 1000 times as long in air. This part of the slowing process is again not our primary concern. It will be found that the time involved is considerably longer than the time needed for the later parts of the capture process. The probability of spontaneous decay during this phase, which corresponds to a range in condensed matter of a few centimeters, is only of the order of 10^{-4}. Consequently a negligible fraction of the decays observed with the ordinary experimental arrangements can be attributed to it.* Most of this time of 10^{-10} second is spent in the phases when the mesotrons still have velocities close to the light velocity. Actually the formula for energy loss per unit time is

$$-\frac{dW}{dt}=\frac{4\pi e^4 NZ}{mV}\ln\left(\frac{b_{\max}}{b_{\min}}\right). \qquad (1)$$

Here W is the energy of the mesotron, V its

* Decays during this phase are completely eliminated if the observations are carried out by delayed coincidence.

velocity, m the electron mass, N is the number of atoms with atomic number Z per cubic centimeter; $b_{\max}$ and $b_{\min}$ are the extreme values of the collision parameters. The logarithmic factor decreases during this interval of time from a value of the order 10 to zero. The latter value is reached when the mesotron velocity becomes equal to the velocity of an electron. Thus the contributions of successive electrons vanish. Finally, the velocity of the mesotron drops below that of the valence electrons. From then on we shall discuss the process of further energy loss in detail.

3. LOSS OF ENERGY TO A DEGENERATE ELECTRON GAS

When the energy of the mesotron has dropped below 2000 ev, and its velocity is therefore less than the velocity of the valence electrons, formula (1) no longer represents a useful approximation, and the loss of energy to electrons can better be approximated in the following way.

We consider the mesotron moving inside a degenerate electron gas with a velocity V much smaller than the maximum velocity v_0 of the electrons. In this case we can estimate the energy loss as follows: in an individual collision between an electron and the mesotron, the change in speed of the electron will be of the order of magnitude V. Indeed for a head-on collision it would be $2V$. Since the electrons belong to a degenerate gas, it is clear that all the collisions for which the final velocity of the electron lies inside the occupied zone of the velocity space will be forbidden on account of the Pauli principle. Only electrons with speeds close to v_0 by amounts of the order of V will, therefore, be capable of colliding. Their number per unit volume is of the order of magnitude

$$n \approx m^3 v_0^2 V/\hbar^3. \tag{2}$$

The collision cross section σ for collisions in which the deflection is appreciable is, on the other hand, of the order of magnitude:

$$\sigma \approx (e^2/mv_0^2)^2. \tag{3}$$

The energy transferred in collisions of this type not forbidden by the Pauli principle will always be positive and of the order of magnitude

$$W \approx mv_0 V. \tag{4}$$

From (2, 3, and 4) we can calculate the order of magnitude of the energy loss per unit time:

$$-(dW/dt) \approx W\sigma n v_0 \approx m^2 e^4 V^2/\hbar^3 \approx m^2 e^4 T/(\mu\hbar^3) \approx T/t_0, \tag{5}$$

where T is the kinetic energy of the mesotron, $t_0 = \mu\hbar^3/m^2e^4 = 4.84\times10^{-15}$ sec., and μ is the mass of the mesotron. We have set $\mu = 200m$.

The difference in the velocity dependence of the energy loss according to (1) and (5) which hold, respectively, for high and low velocities of the mesotron should be noticed. For high velocities the energy loss per unit time is inversely proportional to the velocity of the mesotron; for low velocities it is directly proportional to the square of the velocity. There is, therefore, a maximum in the energy loss which is found near the boundary of validity of the two formulae; namely, for mesotron velocities of the order of the electron velocity v_0. One might wonder why the energy loss (5) is independent of the density of the degenerate electron gas through which the mesotron moves. Actually the collisions occur between the mesotrons and the fastest electrons, and the collision cross section decreases as $1/v_0^4$. This strong dependence on v_0 just suffices to cancel the effect of great electron density, great energy loss per collision, and great relative velocity of the colliding particles. Naturally, if (5) were taken strictly, one would obtain the absurd result that the energy loss remains unchanged even when the density of the electrons becomes extremely small.

Actually there are two reasons that limit the validity of (5) for low electron density. One is expressed by the condition

$$V \ll v_0 \tag{6}$$

that the mesotron should move slowly with respect to the electrons. The second is due to the fact that when a negative mesotron moves through an electron gas, the density of electrons near it is reduced by the electrostatic repulsion. This rarefaction of the electrons near the mesotron effectively neutralizes its charge at distances of the order:

$$(a\hbar/mv_0)^{\frac{1}{2}}, \tag{7}$$

where a is the Bohr radius

$$\hbar^2/me^2. \tag{8}$$

The quantitative treatment of the electron-mesotron collision can be carried out according to the Born approximation method. This is justified if the formula

$$e^2/\hbar v_0 < 1 \tag{9}$$

holds. Now if the Born approximation is applicable, the region in which the relevant collisions take place has dimensions equal to the deBroglie wave-length of the scattered particle. In order that expression (5) be applicable we must demand that this wave-length be less than the length given in (7). It follows that

$$\hbar/mv_0 < (a\hbar/mv_0)^{\frac{1}{2}} \quad \text{or} \quad mv_0/\hbar > 1/a. \tag{10}$$

The left-hand side of the last inequality is approximately equal to the cube root of the density of the electron gas. Condition (10) means, therefore, that the density of the electron gas must be such that, on the average, more than one electron is found in a cube having a side equal to the Bohr radius. Inequalities (9) and (10) are identical in content. It is easy to show that if they are not fulfilled (5) does not apply, and the mesotron loses energy at a much slower rate than the one given by (5). Conditions (6) and (10) are independent, and the more restrictive of the two will apply. Condition (10) is usually fulfilled approximately in condensed matter of not too small density. In the case of gases, however, it will be satisfied only within the atoms, and therefore the energy loss will be confined to these regions.

Quantitatively, the energy loss of a slow mesotron in an ideal degenerate electron gas is expressed by the following integral:

$$\frac{me^4V^2}{8\pi\hbar^3}\int_0^\pi\int_\theta^\pi\int_0^{2\pi} \times\frac{(\cos\theta-\cos\theta')\sin\theta d\theta\sin\theta' d\theta' d\varphi}{\sin^4(\frac{1}{2}\psi)}. \tag{11}$$

The meaning of the integration variables is the following: θ and θ' are the angles between the directions of initial and final electron velocity and the direction of the mesotron velocity; ψ is the angle of deflection for the electron; and φ is given by

$$\cos\psi=\cos\theta\cos\theta'+\sin\theta\sin\theta'\cos\varphi. \tag{12}$$

The integral diverges logarithmically near $\psi=0$. The divergence can be removed by taking into account the fact that collisions involving a small value of ψ occur at large distances where the mesotron charge is screened.

Collisions at a distance greater than (7) will not contribute, and one needs to consider only momentum changes greater than

$$(\hbar mv_0/a)^{\frac{1}{2}}, \tag{13}$$

which is $\hbar$ divided by the length (7). From this one finds that the integration need be carried down only to a value

$$\psi_{\min}=(\hbar mv_0/a)^{\frac{1}{2}}(mv_0)^{-1} =(e^2/\hbar v_0)^{\frac{1}{2}}=(c/137v_0)^{\frac{1}{2}}. \tag{14}$$

One should notice that if (10) is fulfilled, $\psi_{\min}$ is small compared with unity, as it should be. Eliminating the divergence with this prescription, one can evaluate (11) and find finally the following estimate for the rate of energy loss:

$$-\frac{dW}{dt}=\frac{4}{3\pi}\frac{m^2e^4V^2}{\hbar^3}\ln\frac{1}{\psi_{\min}} =\frac{2}{3\pi}\frac{m^2e^4V^2}{\hbar^3}\ln\frac{137v_0}{c}, \tag{15}$$

or finally,

$$-\frac{dW}{dt}=\frac{4}{3\pi}\frac{m^2e^4T}{\mu\hbar^2}\ln\frac{137v_0}{c}. \tag{16}$$

The logarithm will be of a small numerical order of magnitude and will have somewhat larger values in the deep portions of the atom. For estimates of the order of magnitude it will be permissible to use formula (5).

The previous theory will be applicable to those cases in which the electrons in the vicinity of the mesotron can properly be described as a degenerate gas. In particular, the theory will break down within the K shells of the atoms, since the electron density there is less than the value corresponding to the degenerate gas. We shall return to this question in the next section. We shall have to give special consideration to the case of insulators and gases where electrons may be excited only by discontinuous amounts. The case that most nearly approaches the ideal conditions is that of the metals, which we shall now discuss.

4. METALS

In order to calculate the energy loss as a function of the mesotron energy, we have to calculate the average value of the kinetic energy $\bar{T}$ which is to be substituted in formula (5). In calculating average values of T, one makes use of the fact that the probability of finding the mesotron in a given volume element is weighted by the square root of the kinetic energy that the mesotron has at this position. The reason for this weighting is that the volume in the momentum space available to the mesotron is proportional to

$$T^{\frac{1}{2}}dT = T^{\frac{1}{2}}dW. \tag{17}$$

The average kinetic energy is therefore:

$$\bar{T} = \frac{\int (W-U)^{\frac{1}{2}} d\tau}{\int (W-U)^{\frac{1}{2}} d\tau}, \tag{18}$$

where U is the potential energy and $d\tau$ is the volume element.

For high mesotron energy U will be negligible compared with W, and $\bar{T}$ will be equal to W. As the energy approaches zero, namely, that value for which the mesotron can no longer freely pass from one atom to another, the average kinetic energy becomes appreciably larger than W because U is negative. For W negative, the mesotron is bound to a definite atom. For negative values of energy the kinetic energy is of the order of magnitude of the absolute value of W, as will be discussed later.

For positive W values one obtains a low limit for $\bar{T}$ and the energy loss replacing $(W-U)^{\frac{1}{2}}$ by the smaller expression $W^{\frac{1}{2}}+(-U)^{\frac{1}{2}}$ in the numerator of the integral, and replacing $(W-U)^{\frac{1}{2}}$ by the larger expression $W^{\frac{1}{2}}+(-U)^{\frac{1}{2}}$ in the denominator. The error caused by these substitutions is a maximum when W is equal to the absolute value of U, and is then a factor 2. We write thus

$$\bar{T} \approx \frac{\int W^{\frac{1}{2}} d\tau + \int (-U)^{\frac{1}{2}} d\tau}{\int W^{\frac{1}{2}} d\tau + \int (-U)^{\frac{1}{2}} d\tau}. \tag{18a}$$

We shall use the potential obtained from the statistical model

$$U = -\frac{Z^{4/3}e^2}{b}\frac{\varphi(x)}{x}, \tag{19}$$

where we have set for the distance from the nucleus $r = xbZ^{-\frac{1}{3}}$ and the length b is

$$b = (9\pi^2/128)^{\frac{1}{3}} \times \text{Bohr radius} = 0.47 \times 10^{-8} \text{ cm}. \tag{20}$$

The function φ has been tabulated.[3] In some of the following calculations we use the crude approximation**

$$\varphi = 0.4/x. \tag{21}$$

Approximating a lattice cell by a sphere one obtains $\bar{T}$ by integrating (18a) over the cell. The second integral in the numerator can be performed by partial integration using the differential equation[3] for φ. One finds

$$\bar{T} = \frac{N^{-1}W^{\frac{1}{2}} + 4\pi e^3 b^{\frac{1}{2}} Z[1-\varphi(x_0)+x_0\varphi'(x_0)]}{N^{-1}W^{\frac{1}{2}} + 4\pi e b^{5/2} Z^{-\frac{1}{3}} \int_0^{x_0} \varphi^{\frac{1}{2}} x^{\frac{1}{2}} dx}. \tag{22}$$

Here N is the number of atoms per cubic centimeter, and x_0 is the value of x at the edge of the cell. Using (21) we get

$$\bar{T} = \frac{N^{-1}W^{\frac{1}{2}} + 4\pi Z e^3 b^{\frac{1}{2}}(1-0.8/x_0)}{N^{-1}W^{\frac{1}{2}} + 3.96 e b^{5/2} Z^{-\frac{1}{3}} x_0^2}, \tag{23}$$

where x_0 is given by the relation:

$$1/N = 4\pi b^3 x_0^3/3Z. \tag{24}$$

Values of $\bar{T}$ as obtained from (23) are given in Table I for graphite and iron. One finds that $\bar{T}$ has a flat minimum at 7 ev and 20 ev, respectively. This will be, therefore, the value of the energy at which energy is lost at the slowest rate. At higher energies Table I shows that $\bar{T}$ becomes less than W. This is because of the approximation which we made in substituting (18) by (18a). Actually $\bar{T} > W$ always holds, and we underestimate $\bar{T}$ if we use $\bar{T} = W$ for high values of W. From Table I and formula (5), one can calculate, for the two cases in question,

[3] E. Fermi, Zeits. f. Physik **48**, 73 (1928).

** From $x = 0.5$ up to almost $x = 8$ the quantity $x\varphi$ remains between the limits 0.3 and 0.5.

the time needed for the mesotron to lose energy from 2000 ev to zero. One finds 2.6×10^{-14} sec. in graphite and 2.2×10^{-14} sec. in iron. Somewhat longer times would be found in condensed matter of lower density. As a practical average time for crossing the interval from 2000 ev to zero we take for all types of condensed matter about 3×10^{-14} sec.

We proceed now to the question of energy loss when W is negative, when the mesotron can be considered bound to a special atom. If the energy is negative and its absolute value is sufficiently large, it is a sufficient approximation to set the kinetic energy

$$\bar{T}=\alpha|W|, \tag{25}$$

where α is a number of the order of unity. (Actually $\alpha=1$ for a Coulomb field and $\alpha>1$ for the statistical potential.) Expression (25) will lead to a very small loss of energy for small absolute values of W. Actually at $W=0$ the kinetic energy does not vanish, and may be obtained from (23):

$$\bar{T}(0)=\frac{3.2e^2Z^{4/3}}{bx_0^2}(1-0.8/x_0). \tag{26}$$

Since at $W=0$, $\bar{T}$ increases with decreasing W we may use (26) as a lower limit of $\bar{T}$ at negative energies. We shall use for the energy-loss expression (5), and substitute for $\bar{T}$ expression (25) or (26), whichever is the greater. Expression (26) will be relevant from $W=0$ to $-W\approx50$ ev. The time required to cross this energy region is of the order of $t_0=4.84\times10^{-15}$ sec. In the range where $\bar{T}$ is estimated by (25), W as a function of time is given by

$$-W\approx\bar{T}(0)e^{\alpha t/t_0}. \tag{27}$$

This formula is valid as long as the statistical model is permissible, i.e., as long as the mesotron moves outside of the radius of the K-shell. At distances smaller than this radius the actual electron density is less than the density obtained from the statistical model. Nevertheless the energy loss of the mesotron continues to proceed according to the formulas (16), (5), and (27) even when the mesotron is somewhat closer to the nucleus than the radius of the K-shell. The reason for this is that the energy loss of the mesotron does not depend on the electron density, and thus the failure of the statistical model to predict the correct density within the K-shell has no direct effect on the behavior of the mesotron.

TABLE I. Average kinetic energy as a function of the total energy.

W(ev)	$\bar{T}$(ev) Graphite	Iron
0	36	86
5	23	62
10	24	56
20	27	55
30	32	57
50	45	65
100	83	95

When the mesotron moves inside the K-shell it is not permissible, however, to apply the method of deriving formulas (16) and (5) which we have given above. In a collision the energy mv_0V is exchanged, and a time not shorter than $\hbar/mv_0V$ is needed to describe such a collision. During this time the mesotron moves through a distance $\hbar/mv_0$. Our discussion so far has assumed that during a collision the mesotron moves in a straight line. When the mesotron moves along the K-orbit of the atom its path has a radius of curvature equal to $\hbar/mv_0$. For orbits on or within the K-shell it will be a better approximation to consider the time-dependent dipole consisting of the mesotron and a unit positive charge located on the nucleus. One may then calculate, by applying perturbation theory to the statistical model, the energy exchange between the mesotron and the electrons.

If one assumes that the mesotron moves on a circular orbit one may evaluate the rate of energy loss dW/dt. The result of the calculation is identical with (16) provided that the minimum momentum change of the electrons $(\hbar mv_0/a)^{\frac{1}{2}}$ obtained from (7) is greater than the minimum momentum change $\hbar\omega/v_0$ compatible with the requirement that a mesotron with angular velocity ω exchanges energy with the electrons in quanta $\hbar\omega$. At radii somewhat smaller than the radius of the K-shell the inequality $\hbar\omega/v_0>(\hbar mv_0/a)^{\frac{1}{2}}$ holds for not too light atoms. Then (16) must be replaced by

$$-\frac{dW}{dt}=\frac{8e^4m^2T}{3\pi\mu\hbar^3}\ln\left(\frac{mv_0^2}{\hbar\omega}\right). \tag{28}$$

Expression (5) remains a satisfactory approximation as long as the logarithmic factor does not become small compared to unity, i.e., as long as the energy $\hbar\omega$ transferred to the electrons is smaller than the maximum kinetic energy $mv_0^2/2$ of the electrons. For $mv_0^2 \ll \hbar\omega$ the perturbation calculation gives

$$-\frac{dW}{dt}=\frac{2^{5/2}\pi m^{\frac{1}{2}}n_0e^4r^2}{3\hbar^{\frac{1}{2}}}\left(\frac{Ze^2}{\mu r^3}\right)^{\frac{1}{2}}, \qquad (29)$$

where n_0 is the electron density near the nucleus and r is the radius of the circular orbit of the mesotron. Expression (29) agrees with the results of calculations on internal conversion, for the non-relativistic case, provided that the energy of the ejeced electron is great compared with the energy of the K-electrons.[4] It is of interest to note that (28) holds if the radius r of the mesotron orbit is greater than

$$r_1=(m/\mu)^{\frac{1}{2}}r_K=0.171r_K. \qquad (30)$$

Here r_K is the radius of the K-shell. For $r<r_1$ expression (29) is valid.

For very small values of r, energy loss by radiation is faster than energy loss due to interaction with electrons. For circular mesotron orbits one finds by comparing (29) with the radiated energy that radiation becomes predominant for $r<r_2$, where

$$r_2=4^{-1/7}(m/\mu)^{\frac{1}{2}}(\hbar c/e^2)^{3/7}Z^{-5/21}r_c$$
$$=(4.5/Z^{5/21})\times10^{-11}\text{ cm}, \qquad (31)$$

where $r_c=\hbar/mc$ is the Compton wave-length divided by 2π.

From (29) one can calculate the time needed to drop from r_1 to r_2

$$t_{r_1\to r_2}=\frac{1}{6\sqrt{2}}\left(\frac{m}{\mu}\right)^{\frac{1}{2}}\left[\left(\frac{r_K}{r_2}\right)^{9/4}-\left(\frac{r_K}{r_1}\right)^{9/4}\right]t_0$$
$$=\left[\frac{103}{Z^{12/7}}-0.117\right]t_0. \qquad (32)$$

While the classical expression for the radiation by an accelerated charge gives the time spent between r_2 and the lowest quantum orbit $r_0=\hbar^2/Z\mu e^2$,

$$t_{r_2\to r_0}=\frac{\mu^2c^3}{4e^4Z}(r_2^3-r_0^3)$$
$$=\frac{\mu}{4mZ}\left[\left(\frac{r_2}{r_c}\right)^3-\left(\frac{r_0}{r_c}\right)^3\right]t_0$$
$$=\left[\frac{78}{Z^{12/7}}-\frac{16}{Z^4}\right]t_0. \qquad (33)$$

For heavy nuclei r_1 becomes smaller than r_2, and there is no region in which (29) determines the energy loss. Further consequences of high Z-values are that r_0 becomes less than the nuclear radius and that pair production begins to play a role in the last steps of the slowing-down process. All these effects shorten the time the mesotron needs to get close to the nucleus.

For carbon and iron, Table II summarizes the times (measured in units $t_0=4.84\times10^{-15}$ sec.) the mesotron needs to cross the energy regions indicated in the first column of the table.

One sees that the slowing down time is less than 10^{-13} sec. This is very short compared with the lifetime of the mesotron, 2×10^{-6} sec.

TABLE II. Summary of slowing-down times in graphite and iron.

Energy range (ev)	Time: Graphite	Time: Iron
$2000\to0$	$5.4t_0$	$4.5t_0$
$0\to-Ze^2/r_1$	$5.3t_0$	$7.4t_0$
$-Ze^2/r_1\to-Ze^2/r_2$	$4.6t_0$	$0.3t_0$
$-Ze^2/r_2\to-Ze^2/r_0$	$3.6t_0$	$0.3t_0$
$2000\to-Ze^2/r_0$	$18.9t_0$	$12.5t_0$
(total "slow" range)	9.2×10^{-14} sec.	6.1×10^{-14} sec.

5. INSULATORS

The case of insulators differs from that of metals because the amount of energy that may be delivered to electrons in a metal can be arbitrarily small, whereas in an insulator it must be at least as large as the gap between two Brillouin zones. This usually amounts to several volts. The loss of energy to electrons will be thereby reduced in those cases in which energy is transferred in small individual amounts.

In a collision the amount of energy transferred to the electron is of the order of magnitude mv_0V,

[4] See, e.g., Rasetti, *Elements of Nuclear Physics* (Prentice-Hall, New York, 1936), pp. 134–139.

and we can expect that Eq. (5) will hold only if

$$mv_0V>G, \tag{34}$$

where G is the "Brillouin gap," i.e., the minimum energy that the electrons can accept. In case (34) is not fulfilled, the rate of energy loss will be smaller. This limitation will necessitate a change in formula (18) where the integral in the numerator will no longer be extended to all portions of space accessible to the mesotron but only to those for which in addition (34) is fulfilled. For positive W, the effect on dW/dt is most important at and near $W=0$. For $Z\geqslant 6$ actual calculation based on the statistical atom model shows that the rate of energy loss is not changed in this critical region by more than a factor $\frac{1}{2}$. The corresponding increase in the slowing-down time is less than 10^{-14} sec.

For positive energies, regions close to nuclei where (34) is fulfilled will occasionally be visited by the mesotron. For negative energies regions close to the nucleus may be avoided if the mesotron is captured into an almost circular orbit. Therefore the possibility arises of the mesotron spending a long time in such a circular orbit. We shall show that actually the mesotron will spend in a circular orbit a time which is not long compared to the other times we have obtained in the slowing-down process.

Circular orbits of negative energy exist only at a considerable depth within the atom. This can be proved using the statistical potential (19). Circular orbits of negative energy exist only where $x\varphi(x)$ is an increasing function of x.*** The value of $x\varphi(x)$ is zero at $x=0$, increases to a maximum reached at $x=2.25$, and decreases beyond this point. Consequently, circular orbits of negative energy are to be found only within a distance from the nucleus corresponding to $x=2.25$; namely,

$$r=2.25b/Z^{\frac{1}{3}}. \tag{35}$$

For a circular orbit at exactly this radius the energy is equal to zero, and the kinetic energy of the mesotron is equal to

$$0.09e^2Z^{4/3}/b=2.7Z^{4/3}\text{ ev}. \tag{36}$$

*** This statement does not refer to circular orbits outside the core of an atom. In condensed matter there is usually no room available for orbits of such very large radius.

If a mesotron is captured into an orbit which is not circular, its closest approach to the nucleus will be even smaller than the distance given by formula (35), and the maximum kinetic energy will be larger than that given by (36). Applying condition (34), we find that energy loss to the electrons will be possible from at least one part of the orbit if the condition

$$0.09e^2Z^{4/3}/b\text{ ev}>\tfrac{1}{2}(\mu/m)^{\frac{1}{2}}G \tag{37}$$

is fulfilled. If we set for G the fairly large value of 7 volts, we see that relation (37) is fulfilled if Z is 9 or greater. Actually relations (34) and (37) are not to be taken in a quite strict sense because head-on collisions between electrons and mesotrons will give an energy exchange twice as large as assumed in (34). If this is taken into account an additional factor of $\frac{1}{2}$ appears in the right-hand side of (34). If we again assume 7 volts for G the limiting value of Z drops from 9 to 6.

Stable circular orbits of positive energy exist for x values greater than 2.25. The condition of stability for a circular orbit is:

$$\varphi-x\varphi'-x^2\varphi''>0. \tag{38}$$

This condition is fulfilled up to $x=3.3$, or

$$r=3.3bZ^{-\frac{1}{3}}. \tag{39}$$

A mesotron moving on a circular orbit of this radius has a smaller velocity than one moving on the radius given by (35), and one may expect increased difficulties in the energy exchange between mesotron and electron. Actually, in light atoms the greatest stable circular radius (39) differs from (35) by less than the uncertainty due to the spread of the wave function of the mesotron. At the same time the difference in angular momenta between the greatest circular orbit and (35) is small. For $Z=6$ this difference is less than $\hbar$. Thus a mesotron moving in a stable orbit of positive energy will not lose energy at a much smaller rate than will a mesotron whose wave function has its maximum at the radius given by (35).

We can conclude that the circular orbits will hardly ever be too stable. Even in case they should be formed around an element like lithium or beryllium the total time of energy loss will probably be less than the lifetime of a mesotron.

Furthermore, the actual size of the Brillouin gap is affected by the localization of the mesotron

on one lattice atom. Since, at least in the critical cases, the mesotron is captured fairly far inside the atom, the atom is effectively turned into an element with atomic number $(Z-1)$. If we were dealing with an isolated atom, this would lower the ionization energy of the atom and turn it into the much smaller value which usually is called the electron affinity of the atom of charge $(Z-1)$. Actually this electron affinity may even be zero. In the special case of mesotron capture by the hydrogen atom, it is found that when the mesotron approaches the nucleus to a distance of 0.639 Bohr radii, the binding energy of the electron bcomes zero. In the closed shell structures usually found in insulators, an electron affinity of two or three volts is likely to remain. As a consequence of this the mesotron, after it is captured, may lose as a first step an energy smaller than the Brillouin gap. After this loss the atom in which the mesotron is now localized does not have a closed shell, and further excitation may still require less energy than the width of the Brillouin gap. Of course, further ionizations would tend to raise the ionization potential, but the local electron deficiency will be promptly filled by capturing electrons from neighbors.

A special situation arises when the mesotron is captured on a hydrogen atom, as may happen for instance in paraffin. In that case the hydrogen and the mesotron circulating around it form a small neutral system which will move along and will readily permeate to any part of the lattice. As a result one will expect that the mesotron will eventually be caught in the field of a more highly charged nucleus.

After the mesotron has attained negative energies of an absolute value greater than 100 ev, the further energy loss proceeds in insulators as it does in metals.

In conclusion we see that the total time needed for energy loss in insulators is apt to be a little longer than in metals, because of the difficulty in bridging the Brillouin gap. There will be, however, no change in the order of magnitude of the total time which the mesotron needs to reach its lowest orbit.

6. GASES

In gases, as in insulators, electrons cannot accept from the mesotron arbitrarily small amounts of energy. The lowest electronic excitation energy, I, of a gas molecule plays the same role as the Brillouin gap does in insulators.

For positive values of W the energy loss proceeds according to (5) and (18). The upper limit of the integrand in the numerator is determined by the condition

$$mv_0V=I. \tag{40}$$

The integral in the denominator is extended over the whole space. As a result the average value of the energy loss $-dW/dt$ is reduced by the ratio of gas density to insulator density. Under conditions of normal temperature and density the energy loss in a gas is about a thousand times smaller than in a solid insulator. The time needed to slow down the mesotrons from $W=2000$ ev to $W=0$ is approximately 3×10^{-11} seconds.

For negative values of W the mesotron is localized on a specific molecule. As the energy transfer to electrons proceeds, it is likely that enough energy will be given to nuclear motion to cause dissociation of the molecule on which the mesotron is found. Thus we may confine our attention to the atom which carries the mesotron along. The energy loss of the mesotron causes progressive ionization of this atom, and, as a result, the minimum excitation energy I is increased. This may lead to an effective stoppage of the energy loss if the mesotron happens to be moving on a nearly circular orbit. The energy loss may stop when the relation

$$h\omega\approx I \tag{41}$$

is fulfilled. Here ω is the frequency of the mesotron in a circular orbit.

Further energy loss of the mesotron may thus be delayed until the ion carrying the mesotron makes a collision with another molecule. Then a substantial part of the ionic charge will be neutralized, and the energy transfer from the mesotron to the electron cloud will be resumed. We assume that the excitation energy I of the atom which carries the mesotron may be written in the form

$$I=Ki^2, \tag{42}$$

where i is the degree of ionization and K is a constant. The total energy E needed to raise the

ionization from zero to i is

$$E=\tfrac{1}{3}Ki^3. \tag{43}$$

We assume that between two collisions of the mesotron-carrying atom the energy of the mesotron W will change by $E/2$. We have then

$$-\frac{dW}{dt}=\tfrac{1}{2}NE=\tfrac{1}{6}NKi^3, \tag{44}$$

where N is the number of collisions per unit time $\sim 10^{10}\,\mathrm{sec}^{-1}$.

The energy loss of the mesotron will be smallest if the mesotron continues to move on circular orbits. For the radius r of this orbit we write as previously

$$r=xbZ^{-\frac{1}{3}}. \tag{45}$$

Using (19), (21), and (41) we get

$$I=\frac{heZ}{\mu^{\frac{1}{2}}b^{\frac{1}{2}}x^{\frac{1}{2}}}\left[-\frac{d}{dx}\left(\frac{\varphi}{x}\right)\right]^{\frac{1}{2}}=2.06Zx^{-2}\,\mathrm{ev}. \tag{46}$$

From (42), (43), and (44) we now obtain

$$-\frac{dW}{dt}=0.493NK^{-\frac{1}{2}}(eV)^{\frac{1}{2}}Z^{\frac{1}{2}}x^{-3}. \tag{47}$$

If W is calculated for a circular orbit from the statistical model one obtains

$$W=-\frac{Z^{4/3}e^2}{2bx}d(x\varphi)/dx. \tag{48}$$

Here the approximation (21) is not sufficient. In the region where circular orbits of negative energy are possible we may use for the expression $x\varphi$

$$x\varphi=0.489-0.025(x-2.25)^2+0.015(x-2.25)^3. \tag{49}$$

For $x<0.5$, expression (49) is not a good approximation. This region, however, contributes little to the slowing-down time and (49) suffices, therefore, for our purpose.

We calculate the total time by integrating

$$t=\int_{2.25}^{0}\frac{dt}{dx}dx=\int_{0}^{2.25}\left[\frac{dW}{dx}\Big/\left(-\frac{dW}{dt}\right)\right]dx$$

$$=\frac{1}{N}\int_{0}^{2.25}\frac{Z^{4/3}e^2(2b)^{-1}[(0.34/x^2)-0.045]}{0.493Z^{\frac{1}{2}}(eV)^{\frac{1}{2}}K^{-\frac{1}{2}}x^{-3}}dx$$

$$=15.5\left(\frac{K}{eV}\right)^{\frac{1}{2}}\frac{Z^{-1/6}}{N}. \tag{50}$$

A reasonable value of K is 5 ev. This gives

$$t=35\frac{Z^{-1/6}}{N}. \tag{51}$$

The total time needed for the energy-loss process at negative energies will therefore be of the order of 10^{-9} second even if the mesotron continues to move on circular orbits.

7. CHEMICAL COMPOUNDS

It is of interest in experiments on the disappearance of negative mesotrons in chemical compounds to find out with what relative probability the mesotron is captured by the different kinds of atoms. We are led by crude estimates to the conclusion that the capture probability is proportional to the nuclear charge Z. This may be seen as follows.

It is simplest to set the capture probability proportional to the energy loss of the mesotrons near the various atomic species. At low positive mesotron energy, which is the relevant region for our argument, the energy loss is given by an expression whose numerator contains the numerator of (23). For $W=0$ this is proportional to Z. The denominator is a constant integral for all atomic species and does not enter in the evaluation of the ratio of energy losses.

The capture probability will actually be proportional to the rate of energy loss only if the ratio of these rates does not change too rapidly near $W=0$. In particular it is necessary to demand that this ratio should not be strongly altered by the energy change due to a single passage of the mesotron through an atom. For this energy loss δW we may write

$$\delta W=\int[\tfrac{1}{2}\mu(W-U)]^{\frac{1}{2}}ds/t_0. \tag{52}$$

Near $W=0$ we get

$$\delta W=2.3eVZ^{\frac{1}{3}}\ln(x_0/x_{\min}) \tag{53}$$

where $x_{\min}$ corresponds to the distance of minimum approach. The energy given in (53) is small enough so that it does not yet affect significantly the numerator in (23). Thus the ratios of energy losses are hardly affected by δW, and we may

conclude that the ratios of capture probabilities are proportional to Z.

8. CONCLUSION

The over-all conclusions can be summarized as follows. In condensed substances, both conductors and insulators, a negative mesotron is captured in its orbit nearest to the nucleus in about 10^{-13} second. In a gas the corresponding time is a little longer than is indicated by the ratio of densities. In particular, in normal air it is of the order of 10^{-9} sec. In both cases this time is very short compared with the mesotron natural lifetime of 2×10^{-6} sec. so that the mode of ultimate disappearance of the negative mesotron is governed by the balance between natural decay and typically nuclear phenomena leading to mesotron disappearance.

PHYSICAL REVIEW VOLUME 72, NUMBER 5 SEPTEMBER 1, 1947

Spin Dependence of Scattering of Slow Neutrons by Be, Al, and Bi

E. FERMI AND L. MARSHALL
Argonne National Laboratory and University of Chicago, Chicago, Illinois

(Received May 16, 1947)

Some information has been obtained on the spin dependence of scattering of slow neutrons by Be, Al, and Bi by measuring the scattering cross section for filtered neutrons. The result is that in none of these three cases does the sign of the scattering length change when the spin orientation is changed. But in the case of Be and Bi the magnitude of the scattering length for one spin orientation may be up to twice as great as that for the other spin orientation, and in the case of Al the variation may be by a factor of three.

SOME information on the spin dependence of the scattering of slow neutrons can be obtained by measuring the cross sections of some microcrystalline substances for filtered neutrons.[1,2]

When a slow neutron is scattered by an atom having nuclear spin I, two values for the scattering length[2] can be expected according to whether the spin of the neutron is parallel or antiparallel to I; these will be indicated by a_+ and a_-. If these two values are equal, there is no spin dependence of the scattering. In this case interference phenomena are not influenced by the spin, and the neutron waves scattered by the atoms behave as fully coherent. When a_+ and a_- are different, the coherent scattering of the atom is determined by an average scattering length: (see reference 2, formula (6))

$$a=\frac{I}{2I+1}a_-+\frac{I+1}{2I+1}a_+.$$

The remaining scattering behaves as incoherent for interference phenomena.

In order to discuss the significance of coherent and incoherent scattering it is necessary to distinguish between collisions in which the spin orientation is not changed and those in which it changes. The first type of collision is responsible for coherent scattering, the second for incoherent. The reason is that interference takes place only when the scattering is due to the cooperative action of all atoms. This is the case when there is no spin change to indicate which atom has been responsible for the scattering. If there is a spin change, however, the scattering is attributed to the individual action of that atom whose spin has changed.

One can prove by elementary quantum mechanics that the coherent scattering cross section is

$$\sigma_{\text{coherent}}=4\pi\left\{\frac{I}{2I+1}a_-+\frac{I+1}{2I+1}a_+\right\}^2, \quad (1)$$

[1] H. L. Anderson, E. Fermi, and L. Marshall, Phys. Rev. **70**, 815 (1946).
[2] E. Fermi and L. Marshall, Phys. Rev. **71**, 666 (1947).

TABLE I. Scattering cross sections for slow neutrons.

Element	Spin	$\sigma \times 10^{24}$ cm² for unfiltered neutrons $\lambda \sim 1.8$A	$\sigma \times 10^{24}$ cm² for BeO filtered neutrons $\lambda > 4.4$A	$\sigma \times 10^{24}$ cm² for graphite filtered neutrons $\lambda > 6.7$A	Theoretical edge in A	Residual scattering cross section $\times 10^{24}$ cm²	$\sigma_{scattering}$ $\times 10^{24}$ cm²	Limits for value of a_+/a_-
Be	3/2	6.0	0.49	0.64	3.95	0.47	7.5	0.6 to 1.8
Al	3/2	1.7	0.93	1.23	4.67	0.21	1.5	0.25 to 3.3
Bi	9/2	7.2	1.67 to 1.4	0.93	8.00	0.85	8.9	0.5 to 2.1
Pb	—	9.8	4.6 to 1.9	1.61	5.7	0.85	11	—

and the incoherent scattering cross section is

$$\sigma_{\text{incoherent}} = 4\pi \frac{I(I+1)}{(2I+1)^2}(a_+ - a_-)^2. \qquad (2)$$

This last vanishes when a_+ is equal to a_-.

The scattering cross section σ is the sum of (1) and (2).

$$\sigma = 4\pi\left(\frac{I+1}{2I+1}a_+^2 + \frac{I}{2I+1}a_-^2\right). \qquad (3)$$

The scattering of neutrons by micro-crystalline substance is largely due to the Bragg reflections on micro crystals which happen to be oriented in the proper way. Such Bragg reflections are possible only if the wave-length λ is less than $2d$, where d is the maximum lattice spacing of the crystal. Correspondingly, a large drop in the total scattering cross section of micro-crystalline materials is usually observed at this critical wave-length. The cross section usually does not drop to zero, however. The residual scattering is partly caused by the effect of irregularities of the crystal, both permanent and those due to thermal agitation, and partly by the incoherent scattering of Eq. (2), and to the effect of isotopes if they exist.

If the residual cross section could be measured for a substance containing only one isotope and made of perfect crystals at absolute zero, a measurement of the incoherent cross section of Eq. (2) could be obtained. From it one could calculate $|(a_+ - a_-)|$. Practically only an upper limit to this quantity can be obtained on account of the unavoidable irregularities of the sample.

Measurements have been performed on the residual cross section of micro-crystalline Be, Al, Bi, and Pb. A beam of neutrons from the thermal column of the Argonne heavy water pile was passed through a BeO filter (100 g/cm²) or a graphite filter (57 g/cm²). In this beam of filtered neutrons the transmissions of the various elements were measured for samples of increasing thickness. In some cases the cross section decreased appreciably with increasing thickness of the sample. This is due to a further filtering of the neutron beam by the sample, as will be discussed later.

The results of the measurement are summarized in Table I. The cross sections observed for neutrons filtered through BeO and through graphite are given in columns 4 and 5, respectively. For comparison the cross section observed for unfiltered neutrons is given in column 3. These last values, in particular those of Bi and Pb, are appreciably decreased by the fact that the samples had a coarse crystalline structure. Consequently there is extinction of the Bragg reflection within the individual single crystals causing an apparent lowering of the cross section.

The cross sections of columns 4 and 5 are much lower than those of column 3 because the filters have removed a large fraction of the neutrons capable of being Bragg-scattered.

For Be, the theoretical edge ($2d$) is 3.95A. Consequently both filters pass only wave-lengths longer than $2d$ and which cannot be Bragg-scattered. The increase in cross section from column 4 to column 5 is probably due to the Doppler effect resulting from thermal agitation of the Be nuclei. The residual cross section 0.47 given in column 7 has been chosen as the lower of these two values corrected for the small absorption of Be.

In the case of Al, the BeO filter does not completely eliminate all neutrons that may have Bragg reflections. Most of the rise in cross section from column 4 to column 5 is due to increase in the $1/v$ absorption Actually the minimum scattering cross section is observed with the graphite filter. This value of 1.23 is decreased by 1.02

because of absorption of the Al. The residual scattering cross section is therefore taken as 0.21.

For Bi, the theoretical edge $2d$ is 8.0A. Therefore neither filter is able to remove completely neutrons that can be Bragg reflected. For BeO filtered neutrons there is a decrease in cross section with increasing thickness of Bi presumably due to a partial filtering of the neutrons by the sample itself. The graphite filter, because of its larger critical wave-length ($2d$), gives a lower cross section. This last has been decreased by 0.08 because of absorption, and therefore 0.85 has been taken as the upper limit to the residual scattering.

The theoretical edge for Pb is at 5.7A. The BeO filter is therefore inadequate as is apparent from the fact that the cross section varies from 4.6 to 1.9 with increasing thickness of the absorber. As residual scattering cross section we have taken the one measured with the graphite filter corrected by 0.76 for absorption.

The values of the residual scattering cross section so obtained are collected in column 7 of the table. In column 8 are listed the scattering cross sections of the bound atoms obtained by correcting the cross sections of the free atoms by the factor $(A+1/A)^2$ for the reduced mass.

For the elements Be, Al, and Bi, which have only one isotope, the residual scattering cross section is due only to spin dependence of the scattering length and to crystalline irregularities. The assumption that the residual cross section is due entirely to spin dependence leads to an overestimate of the difference between a_+ and a_-. The limits for the ratio a_+/a_- given in column 9 are calculated with this assumption and using the data of columns 7 and 8 together with formulae (2) and (3).

In the three cases investigated it is found that a_+ and a_- have the same sign. This is in accordance with the fact[2] that almost all elements have a positive scattering length. If one is allowed to generalize from these few cases, it would appear that the same is true for the scattering lengths for individual spin orientations. This is quite plausible also on theoretical grounds. On the other hand, differences of as much as a factor of 2 in the two scattering lengths produce a relatively small amount of incoherent scattering. The observation of the residual scattering becomes a sensitive method for investigation of spin dependence only when the difference between the two scattering lengths is quite large. It is quite possible that this difference is much less than the maximum values given, and that the observed residual scattering is due largely to crystal irregularities. An analysis of the data for Pb has not been given because this case is complicated by the presence of several isotopes.

This document is based on work performed under Manhattan Project sponsorship at the Argonne National Laboratory.

The ^5S State of Carbon

A. G. SHENSTONE
Palmer Physical Laboratory, Princeton University, Princeton, New Jersey
(Received May 19, 1947)

The ^5S state of carbon is important in thermo-chemical theory, and its position has been the subject of much speculation. Evidence is here given that it is 33735.2 cm^{-1} above the ground state ^3P and combines with it to emit two lines at λ2965 and 2967.

IN the theory of the chemical binding energies of carbon compounds, the sp^3 ^5S state of the carbon atom plays a large part. Because the tetravalent condition of carbon is ascribed to that state, the excitation energy of ^5S enters intimately into the calculations of the carbon-bond energies derived from observed reaction energies and from band spectra and, perhaps more important, it has been thought to be involved in the derivation of the heat of sublimation of carbon. This whole field has recently been discussed by Long and Norrish[1] in a paper on *The Thermochemistry of Carbon*, from which it is clear that there is serious disagreement on the value of ^5S between various workers in the field.

It is recognized that the well-developed theory of iso-electronic sequences has given quite accurate predictions of the positions of such terms as this ^5S. Using the means so provided, Edlen[2] predicted that ^5S should be about 32900 cm^{-1} above the ground state s^2p^2 ^3P of carbon. Bacher and Goudsmit[3] calculated 35,000 from a wave-mechanical theory, and Ufford,[4] also from the wave-mechanics, predicted 22,000 to 26,000. The value favored by Long and Norrish from the chemical data is in the range given by Ufford's theory and so falls considerably below the theoretical value of Bacher and Goudsmit and the extrapolation of Edlen. There is no doubt that Edlen's value would appeal to most spectroscopists because no radical exceptions have ever been found to the rules of iso-electronic sequences. It appears to have been assumed by spectroscopists, however, that the observations of the spectrum of the carbon arc made by Paschen and Kruger[5] were so complete that there was no hope of finding the absolute value of ^5S by actually observing its spectroscopic combinations.

Before the war when I was working on spectra which extend into the fluorite region, I found that there is in the literature a great lack of data on arc spectra in that region. This is due to the fact that most of the observations have been made with vacuum sources, which are notoriously poor emitters of arc lines. For that reason I had adopted the type of arc source first used by Selwyn,[6] and I had photographed with it the arcs of Cu, Ag, Au, Fe, Ni, Pt, and several other metals in nitrogen for myself and for Dr. Meggers at the Bureau of Standards. In those spectra the nitrogen lines always appeared, and, when carbon electrodes were used, the carbon arc and first

TABLE I.

λ(A)	Int.	ν(cm⁻¹)	Δν	Assignment
1431.597	20	69852.1	24.8	$2s2p^3\ ^5S_2-2s2p^23s\ ^5P_3$
1432.105	15	69827.3	20.7	$^5S_2-\ ^5P_2$
1432.530	10	69806.6		$^5S_2-\ ^5P_1$

TABLE II. Evidence for correctness of assignment in Table I.

	Regular doublet law Δν	$(\Delta\nu)^{\frac{1}{2}}$	Diff.	$(\nu-RN^2 5/36)\times10^{-3}$	Diff.
C *I*	45.5	2.695	.759	54.61	43.36
N *II*	126.6	3.354	.757	97.97	43.40
O *III*	285.6	4.111	.752	141.37	43.55
F *IV*	559.4	4.863		184.92	

[1] L. H. Long and R. G. W. Norrish, Proc. Roy. Soc. **187A**, 337 (1946).
[2] B. Edlen, Nova Acta Regiae Soc. Sc. Upsala IV, **9**, No. 6 (1934).
[3] R. F. Bacher and S. Goudsmit, Phys. Rev. **46**, 948 (1934).
[4] C. W. Ufford, Phys. Rev. **53**, 569 (1938).
[5] F. Paschen and G. Kruger, Ann. d. Physik **5**, 7, 1 (1930).
[6] E. W. H. Selwyn, Proc. Phys. Soc. **41**, 392 (1929); A. G. Shenstone, Trans. Roy. Soc. **A237**, 453 (1938).

TABLE III. Wave-lengths of multiplet at λ1656.

λ(A)	Int.	ν(cm⁻¹)	Δν
1656.255	5	60377.18	
1656.918	3	60353.02	27.08
1656.998	10	60350.10	
1657.368	2	60336.63	
1657.891	4	60317.60	27.11
1658.113	5	60309.52	

TABLE IV. Wave-lengths and assignment of lines.

λ(A)	Int.	ν(cm⁻¹)	Assignment
2964.846	2	33718.74	$2p^3P_1-2p'\,{}^5S_2$
		$\Delta\nu=27.02$	
2967.224	5	33691.72	$2p^3P_2-2p'\,{}^5S_2$
2582.901	5	38704.58	$2p^1S_0-3s^3P_1$

spark lines were observed. In the latter case there was always in addition a group of three lines at λ1432 which definitely associated themselves in character with the carbon lines and yet did not appear in any published wave-length lists. Their separations and position were incompatible with any unknown but predictable transition in C *I* or C *II*, except that from $2s2p^23s\,{}^5P$ down to $2s2p^3\,{}^5S$. Because I had many other spectra in hand and I knew of Professor B. Edlen's interest in the light atoms, I sent him these data in 1939 to use as he wished. He recently published the material given in Table I in Nature[7] and gave the following evidence for the correctness of my assignment of origin in Table II. The data in Tables I and II differ slightly from those originally given to Edlen because more recent measures have been included.

From the comparison with other spectra in the same iso-electronic sequence and from general familiarity with spectral relations, he estimated the position of the $sp^3\,{}^5S$ above the ground state at about 32,700±2 percent cm⁻¹. This prediction was questioned by Long and Norrish on the grounds that the evidence was insufficient and that the value was incompatible with the known thermochemical energy relations of carbon. It therefore seemed important to fix the position of the ⁵S term definitely, by finding, if possible, the lines corresponding to the transition $s^2p^2\,{}^3P-sp^3\,{}^5S$. There should be two such lines with a separation corresponding to the separation $s^2p^2({}^3P_1-{}^3P_2)$, those being the components of ³P with which ⁵S_2 can combine without violation of the ΔJ rule. This separation is given in the literature as 27.5 cm⁻¹ from measurements of unresolved multiplets in the Schumann region. I have recently obtained photographs of the $s^2p^2\,{}^3P-s^2ps^3P$ multiplet at λ1656 completely resolved, and I have made many measurements of the differences. Because of the scarcity of accurate standards, the wave-lengths may be in error by as much as ±0.02A but the differences should be much better, perhaps only ±0.002A. From these measurements I find the intervals to be:

$s^2p^2\,{}^3P_{2,1,0}$ 27.1 and 16.4±0.1 cm⁻¹,
$sp^2s^3P_{2,1,0}$ 40.6 and 19.0±0.1 cm⁻¹.

The wave-lengths are given in Table III. The

1. 2. Hg. 3. 4.

FIG. 1. Carbon arc in argon.
1. C *I* λ2479 $2p^1S_0-3s^1P_1$.
2. C *II* λ2509–12.
3. C *I* λ2583 $2p^1S_0-3s^3P_1$.
4. C *I* λ2964–7 $2p^3P_{1,2}-2p'\,{}^5S_2$.

[7] B. Edlen, Nature 159, 129 (January 1947).

transition from the structure $2s2p^3$ to $2s^22p^2$ is of course an allowed one, being from odd to even, but the intensity of the inter-combination $^3P-{}^5S$ lines is zero in strict Russell-Saunders coupling. However, with a triplet width as large as 43.5 there is a sufficient departure from Russell-Saunders coupling to make one expect lines of intensity about 10^{-3} or 10^{-4} of the allowed lines.

Believing that the past failure to observe the desired transition was probably due to the very dense band spectrum which appears in the ordinary graphite arc, I tried the arc in nitrogen and in argon. Neither of these eliminates the band spectrum at all completely, but they both have the effect of lowering the temperature of the electrodes. The most obvious difference in the spectra is the almost complete disappearance of the ordinary impurities such as Ca and Mg when N_2 or A is used. This may be associated with the fact that the graphite burns away rapidly in air, more slowly in nitrogen, and scarcely at all in argon. The experimental arrangement was a simple enclosure of the arc in a glass bulb with an open neck toward the spectrograph. The gas was purified of oxygen by passage over hot copper turnings and was allowed to escape from the arc enclosure into the open air. The argon undoubtedly contained a percent or two of nitrogen. The arc was operated at about four amperes without any ballast resistance from a constant current source described elsewhere and was focussed on the spectrograph slit by a quartz-water achromatic lens. The potential across the electrodes was about 40–45 V in nitrogen, 55–60 V in argon, and 60–62 V in air, when the gap was about 3 mm. The rods were spectroscopic graphite $\frac{1}{8}$ in. in diameter.

Figure 1 is a 6× enlargement of two sections of an exposure taken on a medium Hilger quartz spectrograph using an Eastman spectrum-analysis No. 1 plate. The shorter wave-length section exhibits the two known C *I* lines at λ2479 and λ2583, which stretch from one electrode to the other, and the C *II* lines at λ2509–11 which are very strong at the negative pole. The other line which stretches across the arc appears only occasionally. It is mercury λ2536. In the longer wave-length section of Fig. 1 the two marked lines have exactly the characteristics of the other C *I* lines and are the only ones observable on the whole plate which do. They can be photographed faintly in less than a second and then appear practically alone in that region of the spectrum. These two lines and λ2583 have been measured on several plates against copper and iron standards. The best values, obtained from a thirty-five minute exposure on a 21-ft. 30000 line grating, are given in Table IV. The lines at a dispersion of 1.25A per mm appear only slightly wider than the

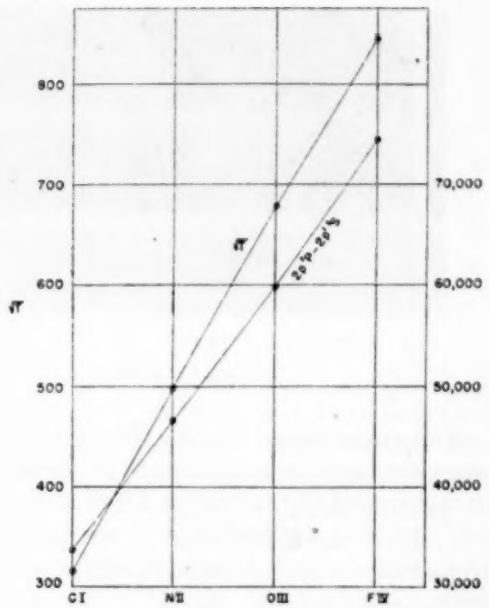

FIG. 2. Plot of $(T)^{\frac{1}{2}}$ and of $2p^3P-2p'^5S$ for iso-electronic sequence C *I* to F *IV*.

TABLE V. Revision of term values.

Electron configuration	Name (Edlen's notation)	Value	
$2s^22p^2$	$2p^3P_0$	90880.5	
			16.4
	$2p^3P_1$	90864.1	
			27.1
	$2p^3P_2$	90837.0	
$2s^22p^2$	$2p^1S_0$	69232.1	
$2s2p^3$	$2p'^5S_2$	57145.3	
$2s^22p3s$	$3s^3P_0$	30546.5	
			19.0
	$3s^3P_1$	30527.5	
			40.6
	$3s^3P_2$	30486.9	
$2s2p^23s$	$3s'^5P_1$	−12661.3	
			20.7
	$3s'^5P_2$	−12682.0	
			24.8
	$3s'^5P_3$	−12706.8	

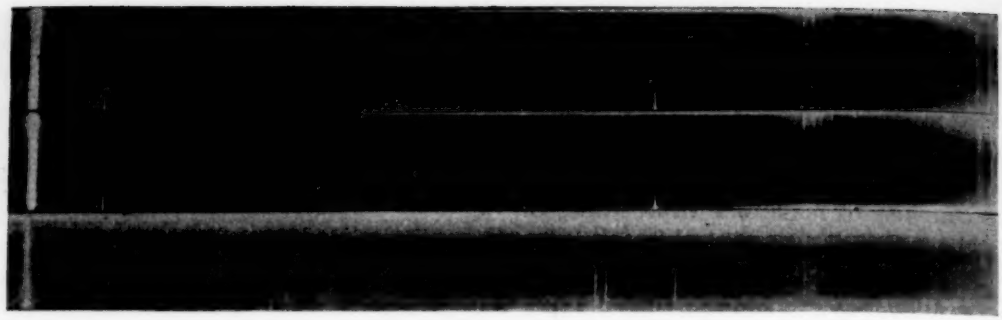

FIG. 3. Carbon arc in (1) argon, (2) nitrogen, and (3) air.

iron comparison lines. The consistency of the measurements indicates an accuracy of ±0.002A.

My assignment of the lines at λ2964 and 2967 as $2p^3P-2p'\ ^5S$ is substantiated by the following positive evidence and a lack of any contrary evidence.

1. The two lines do not correspond to known lines of any element, and they are not band lines.
2. They are very close to the position predicted by Edlen.
3. They have the same character as other C *I* lines and are the only newly observed lines with such a character.
4. They have a wave-number separation which agrees within the small experimental error with the one found from Schumann region multiplets.
5. They have approximately the relative intensities to be expected in such a transition.
6. They have an absolute intensity of a reasonable order of magnitude, roughly 10^{-3} or 10^{-4} of λ2479.322 $2p^1S_0-3s^1P_1$ and of the same order as λ2583.65 $2p^1S-3s^3P_1$, which is the only other known inter-system line.
7. The plot of $(T)^{\frac{1}{2}}$ for ^5S for the iso-electronic sequence is very nearly a straight line, as is also the plot of $2p^3P-2p'\ ^5S$, which illustrates the irregular doublet law. Both plots are given in Fig. 2.

Figure 3 exhibits the difference between arcs in air, nitrogen, and argon, and shows that the identification would have been possible, though with much more difficulty, in an arc in air. The three spectra are of about the same exposure time but the intensity of the air arc is strikingly greater corresponding to its greater visual brilliance. It should be noted that the polar C *II* lines are practically absent in the air arc and that the known C *I* lines are relatively weaker than in the other gases.

The use of the measurements here reported allows the following (Table V) revision of old term values and the addition of the new terms $2p'\ ^5S$ and $3s'\ ^5P$. This places ^5S at 33735.2 cm^{-1} above the ground state. Its excitation requires 4.16 ev or 96.4 kcal. per mole.

If one defines the resonance lines as those due to the transition to the lowest state from the first excited state of opposite parity, then the new lines here discussed are the resonance lines of carbon. It is odd that they are almost the last important lines of C *I* to be discovered. Their existence implies that ^5S can hardly be considered as a metastable state, and should not, therefore, enter in that role into thermochemical theory.

The γ-Instability of Mesons

R. J. FINKELSTEIN*
University of California, Berkeley, California
(Received May 10, 1947)

The following examples of γ-instability are investigated: (a) $M_0 \rightarrow \gamma_1+\gamma_2$, (b) $M_1 \rightarrow \gamma_1+\gamma_2+\gamma_3$, (c) $M_1 \rightarrow M_0+\gamma$, (d) $M_1^{\pm} \rightarrow M_0^{\pm}+\gamma$, where M_0 and M_1 mean a pseudoscalar and a (heavier) vector meson, respectively, and the superscript ± indicates the charge, if there is one. If the coupling constant and meson masses appropriate to the Schwinger mixture are used, the lifetimes are found to be: $\tau_a=1\times10^{-16}$ sec., $\tau_b=2\times10^{-11}$ sec., $\tau_c=1\times10^{-18}$ sec., and $\tau_d=4\times10^{-18}$ sec. In all cases except (b) the calculation leads to logarithmically divergent integrals.

1. INTRODUCTION

ACCORDING to current meson theory both the nucleon and the electron-neutrino carry a virtual meson cloud; conversely, a free meson carries a nucleon cloud and can emit an electron-neutrino pair. The possibility of emitting an electron-neutrino pair permits the β-decay of the free meson, and the nucleon cloud, coupling even a neutral meson to the electromagnetic field, permits γ-decay. Unfortunately, the whole status of meson theory is at present quite uncertain, and our numerical results probably have at most an order of magnitude significance, not only because of uncertainties about the form and numerical constants of the theory, but also because of the dangers of working with a divergent formalism at its limits of validity. Nevertheless the investigation given here may be of interest, since it illustrates a kind of instability common to a class of theories. The following examples of γ-decay, which are probably typical of the more interesting cases, will be considered.

$$\begin{array}{lll} \text{(A)} & M_0 \rightarrow \gamma_1+\gamma_2 & \tau_A=1\times10^{-16} \text{ sec.} \\ \text{(B)} & M_1 \rightarrow \gamma_1+\gamma_2+\gamma_3 & \tau_B=2\times10^{-11} \\ \text{(C)} & M_1 \rightarrow M_0+\gamma & \tau_C=1\times10^{-18} \\ \text{(D)} & M_1^{\pm} \rightarrow M_0^{\pm}+\gamma & \tau_D=4\times10^{-18} \end{array} \qquad (1)$$

where M_0 and M_1 mean pseudoscalar and vector meson, respectively, and the superscript ± indicates a charge, if there is one. Processes of this nature have recently been proposed to explain the soft component of the Auger showers.[1] Process (B) is the simplest mode of decay of a vector meson, since the binary fission is forbidden by Furry's selection rule.[2] Processes like (C) and (D) are logical possibilities in a meson theory such as the Schwinger mixture in which two kinds of mesons of different rest mass are postulated. Another possibility, not described by (C) or (D), is the decay of a heavy meson into a lighter one with a change of charge, e.g., $M_1^+ \rightarrow M_0+e^+$. In fact, Hulthén has proposed a mixture of charged pseudoscalar and neutral scalar fields with different rest masses, and one may ask whether the heavy (neutral) particle decomposes into the lighter one. However, the decay of one meson into a lighter one with the ejection of an electron should not occur; instead the heavy meson should undergo simple β-decay. On the other hand, the processes (A)–(D) are all much faster than β-decay, since they are caused by the coupling of the meson field to the nucleons whose mesonic charge is of the order of e, whereas β-decay arises from coupling of the meson field to the electron and neutrino sources whose meson charge is only of the order of $10^{-8}e$. Whenever there is competition between β- and γ-decay, the latter will win. For example, consider $M_0 \rightarrow e^+ + e^-$; this reaction, whose lifetime is of the order of 10^{-8} sec., should not be expected since (A), with a lifetime of 10^{-16} sec., is much faster.

The lifetimes are given at the right of the corresponding reaction. According to these results a charged vector meson does not disappear through direct β-decay but only as the result of (D) followed by the β-decay of $M_0^{\pm}$. It would also follow from the above scheme that the eventual fate of a neutral vector meson is its

* On leave from Argonne National Laboratory, Chicago, Illinois.

[1] J. R. Oppenheimer, New York Meeting of American Physical Society, January, 1947.

[2] S. Sakata and Y. Tanikawa, Phys. Rev. **57**, 548 (1940).

transmutation into three photons, either directly by (B) or indirectly by (C) and (A). Since, however, (B) and (C) are competing decompositions and (C) is much the faster, (B) should not be expected.

2. HAMILTONIAN AND MATRIX ELEMENTS

The interaction terms in the Hamiltonian responsible for these processes are to the first order in the coupling constants

$$(4\pi)^{\frac{1}{2}}\int \Phi^*\textstyle\sum_\alpha \tau_\alpha\{g_0[U_\alpha\beta\gamma_5] + (f_0/K_0)[\gamma_5\partial_0 U_\alpha+\boldsymbol{\sigma}\mathbf{D}_\alpha U_\alpha]\}\Phi d\mathbf{x}, \quad (2a)$$

$$(4\pi)^{\frac{1}{2}}\int \Phi^*\textstyle\sum_\alpha \tau_\alpha\{g_1[U_{0\alpha}-\mathbf{U}\boldsymbol{\alpha}] + (f_1/K_1)[\mathbf{V}_{0\alpha}\gamma+\mathbf{V}_\alpha\beta\boldsymbol{\sigma}]\}\Phi d\mathbf{x}, \quad (2b)$$

where

α and τ_α = isotopic spin index and matrix,
$(U_0, \mathbf{U})$ = wave function of M_1,
U and Φ = wave function of M_0 and nucleon, respectively,

$$\mathbf{V}=\mathbf{D}\times\mathbf{U} \quad \text{and} \quad \mathbf{V}_0=-\partial_0\mathbf{U}-\mathbf{D}U_0,$$
$$\boldsymbol{\gamma}=-i\beta\boldsymbol{\alpha}, \quad \boldsymbol{\sigma}=\gamma_5\boldsymbol{\alpha}, \quad \gamma_5=-i\alpha_1\alpha_2\alpha_3.$$

f and g have dimensions of charge, and $K=\mu c/\hbar$, $\mathbf{D}_\alpha=\boldsymbol{\nabla}-i(e_\alpha/c)\mathbf{A}$, where $\mathbf{A}$ is the electromagnetic vector potential; $\mathbf{D}=\boldsymbol{\nabla}$ except in case (D). For simplicity we put $g=0$ and consider only the second invariants; in addition, the analysis is limited to transverse mesons. The non-relativistic terms, $\boldsymbol{\sigma}\mathbf{D}U$ and $\mathbf{V}\beta\boldsymbol{\sigma}$, play no role at all in decompositions (A) and (B), since these terms are proportional to the velocity of the meson, and one can assume that the meson is initially at rest. In (C) and (D), however, either the initial or final meson must be moving.

These interaction terms give rise to transitions which have matrix elements with the following absolute values:

M_0:

$$(2\pi/G)^{\frac{1}{2}}(f_0/K_0)\epsilon^{\frac{1}{2}}[u_n^*\gamma_5 u_m + (c\mathbf{p}/\epsilon)(u_n^*\boldsymbol{\sigma}u_m)], \quad (3a)$$

M_1 (transverse):

$$(2\pi/G)^{\frac{1}{2}}f_1\hbar c\epsilon^{-\frac{1}{2}}[(\epsilon/\mu_1c^2)(u_n^*\boldsymbol{\gamma}\mathbf{e}_m u_m) + [(\mathbf{p}/\mu_1 c)\times\mathbf{e}_m](u_n\beta\boldsymbol{\sigma}u_m)], \quad (3b)$$

where $(\mathbf{p}, \epsilon)$ are the momentum and energy of the meson, while its polarization is $\mathbf{e}_m$. When the meson is charged, there are additional terms depending on $\mathbf{A}$; these new terms are not needed before Eq. (28). Matrix elements for the emission and absorption of a photon by a proton are also required:

$$(2\pi/G)^{\frac{1}{2}}e\hbar c\epsilon^{-\frac{1}{2}}(u_n^*\boldsymbol{\alpha}\mathbf{e}u_m). \quad (3c)$$

The functions u represent plane wave solutions of the Dirac equation. These matrix elements correspond to processes in which a nucleon in one state is created while a nucleon in another state is annihilated, and at the same time a meson or photon is created or annihilated. If both nucleon states have positive (or negative) energy, the corresponding process can be described as the emission or absorption of a photon or meson by a nucleon (or antinucleon). If one energy state is positive while the other is negative, the process described is the creation or annihilation of a nucleon pair with the simultaneous emission or absorption of a photon or meson.

Terms of exactly the same form as (2) couple the meson field to the electron-neutrino. The β-decay of a free meson is an illustration of pair creation associated with the matrix elements (3a) or (3b), if u is interpreted as belonging to an electron-neutrino instead of to a proton-neutron. In this process a charged meson disappears, while simultaneously a neutrino in a negative energy state is annihilated, and an electron in a positive energy state is created. Hence the initial charged meson is replaced by an electron and an antineutrino, which is equivalent to a neutrino. One should expect an analogous process with nucleons; instead of $M^+\rightarrow e^+ + n$, one has $M^+\rightarrow P^+ + N$, or if the meson is neutral, $M^0\rightarrow P^+ + P^-$. Since the mass of the meson is less than that of the nucleon, these transitions can take place only virtually; but because the coupling constant is 10^8 times greater for the nucleon, the decomposition into heavy particles is correspondingly more frequent than the decay into light particles. Although such a decomposition cannot lead directly to a final state in which the nucleons separate, it can play an intermediate role in a higher order process which is still very fast, since the virtual decomposition is so frequent.

3. DECOMPOSITION OF A NEUTRAL PSEUDOSCALAR MESON INTO PHOTONS[3]

The lifetime, τ, is given by the usual expression

$$\tau^{-1}=(2\pi/\hbar)\rho|V|^2, \tag{4}$$

where ρ is the density of final states and V is the matrix element for the process. Both photons get the same energies and opposite momenta so that

$$\rho=G4\pi\mu_0^2c/16h^3, \tag{5}$$

where G is the fundamental volume and μ_0 is the mass of the meson.

The decomposition of a neutral meson into two photons requires three steps, e.g., $M_0\rightarrow P^+ +P^-$, $P^+\rightarrow P_1^+ +\gamma_1$, and $P_1^+ +P^-\rightarrow\gamma_2$, where P_1^+ means that the momentum of P^+ has been altered by the emission of γ_1. These three steps can take place in any one of six orders; furthermore, since the theory is symmetrical with respect to nucleons and antinucleons, each of these six possibilities gives rise to another if the roles of the nucleon and antinucleon are interchanged. Hence there are 12 terms in V, the probability amplitude. Further, since the conservation laws do not fix the momentum of the proton pair, there is an infinity of intermediate states, and the probability for the transition from the initial to the final state must be integrated over the momentum space of an intermediate pair particle.

$$V=(G/h^3)\int_0^\infty\int_\omega(\sum N_iD_i^{-1})P^2dPd\omega, \tag{6}$$

where the N_i are products of matrix elements, the D_i are energy denominators, i runs over the 12 possibilities mentioned, and ω is solid angle. In order that (6) be convergent it is necessary that N vanish faster than $1/E$.

It is convenient to expand the ratios N/D in powers of $x=\mu_0/M$:

$$N_iD_i^{-1}=({}^0N_i+{}^1N_ix)({}^0D_i-{}^1D_ix).$$

Writing ${}^0D_i=1/4E^2$, where E is the energy of a pair particle, and anticipating the result that ${}^0N_i=0$, one has to the first order in x

$$\sum N_iD_i^{-1}=x(\sum{}^1N_i)/4E^2. \tag{7}$$

[3] This instability has also been considered in unpublished calculations by Oppenheimer, Christy, and Lewis.

By Eqs. (4)–(7)

$$\tau=512\pi^4(h/\mu_0c^2)(h^3c^3/e^4f_0^2)J^{-2}, \tag{8}$$

where

$$J=\int_1^\infty(\sum\omega_i)(y^2-1)^{\frac{1}{2}}(dy/y), \tag{8a}$$

$${}^1\omega_i=\int{}^1n_id\omega, \tag{8b}$$

$${}^1n_i={}^1N_i/[2e^2f_0h^3(2\pi/G\mu_0)^1], \tag{8c}$$

$$y=E/Mc^2, \tag{8d}$$

n_i, y, and J are dimensionless.

We now calculate the dimensionless numerators n_i. These may be distinguished by three subscripts having the order in which the three intermediate steps occur. For example, by (3),

$$n_{0ij}=\sum(u^-|\gamma_5|u)(u|\alpha\mathbf{e}_i|u_i)(u_i|\alpha\mathbf{e}_j|u^-),$$

where the sum is over the spins of the intermediate states. The quantities u and u^- are plane wave functions having momentum P and energies $+E$ and $-E$, respectively. Similarly u_i corresponds to momentum P_i and energy E_i. To satisfy the conservation of momentum, one must have $\mathbf{P}_i=\mathbf{P}-\mathbf{p}_i$, where $\mathbf{p}_i$ is the momentum of the ith photon. Here $\mathbf{e}_i$ and $\mathbf{e}_j$ are unit polarization vectors of the corresponding photons. Then

$$n_{0ij}=Sp\lambda^-\gamma_5\lambda(\alpha\mathbf{e}_i)\lambda_i(\alpha\mathbf{e}_j), \tag{9}$$

where the λ's are the projection operators defined by

$$\lambda^\pm=\pm\tfrac{1}{2}(\pm1+\alpha(\mathbf{V}/c)+\beta/y), \tag{9a}$$

$$\lambda_i=\lambda(\mathbf{V}_i,E_i). \tag{9b}$$

Evaluation of n_{0ij} gives

$$n_{0ij}=i[\mathbf{e}_i\times\mathbf{e}_j]\{[y^{-1}y_i^{-1}-y^{-2}](\mathbf{V}/c) -y^{-2}(\mathbf{V}_i-\mathbf{V})/c\}.$$

Expansion of E_i and $\mathbf{V}_i$ to the first order in x gives

$$n_{0ij}=(ix/2y^3)[\mathbf{e}_i\times\mathbf{e}_j]\mathbf{k}_i, \tag{10}$$

where $\mathbf{k}_i$ is the unit propagation vector of the ith photon. Since $\mathbf{k}_1=-\mathbf{k}_2$, it follows from (10) that

$$n_{012}=n_{021}.$$

In addition $n_{ij0}=Sp[\lambda^-(\alpha\mathbf{e}_i)\lambda_i(\alpha\mathbf{e}_j)\lambda(\gamma_5)]$. Take

the complex conjugate:

$$n_{ij0}^{*}=Sp[\lambda^{-}\gamma_5\lambda(\alpha\mathbf{e}_j)\lambda_i(\alpha\mathbf{e}_i)]=-n_{0ij},$$
$$\therefore\quad n_{ij0}=n_{0ij}.$$

Hence $n_{012}=n_{021}=n_{120}=n_{210}$. All of these numerators lead to convergent integrals. The situation is quite different if the meson is annihilated in the second step; the corresponding integral is then indeterminate. One rather natural way of evaluating this integral leads to a cancellation and a finite result again equal to n_{012}. We shall tentatively assume this result, but will afterwards return to it. The six n_i values obtained by permutation of 0, 1, and 2 are then equal, and by Furry's theorem are also equal to six others, obtained by interchanging the roles of nucleon and antinucleon. Hence

$$\sum\omega_i=(12)(4\pi)(ix/2y^3)[\mathbf{e}_1\times\mathbf{e}_2]\mathbf{k}_1. \quad (11)$$

After squaring and summing over both polarizations of both photons, one has by (11) and (8)

$$\tau=4\pi^2(\hbar/\mu_0c^2)(\hbar^3c^3/e^4f_0)^2. \quad (12)$$

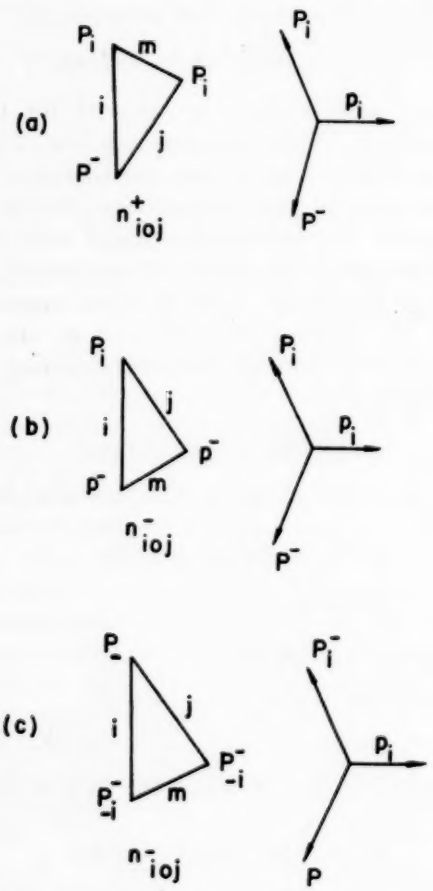

FIG. 1. Transition schemes (on left) and momenta corresponding to n_{i0j}^{+} and n_{i0j}^{-}. On the left the minus superscript means a state of negative energy and on the right it refers to a negatron. P_i means momentun $P-p_i$, while P_{-i} and P_- means momenta $-(P-p_i)$ and $-P$, respectively.

The Elements n_{i0j}

Let n^+ denote the numerator when P^+ absorbs a meson, and let n^- designate the numerator when P^- absorbs a meson. The two transition schemes are shown in Fig. 1a and 1b. Then

$$n_{i0j}^{+}=Sp[\lambda^{-}(\alpha\mathbf{e}_i)\lambda_i\gamma_5\lambda_i(\alpha\mathbf{e}_j)], \quad (13)$$

$$n_{i0j}^{-}=-Sp[\lambda^{-}(\alpha\mathbf{e}_i)\lambda_i(\alpha\mathbf{e}_j)\lambda^{-}\gamma_5]. \quad (13a)$$

The negative sign is introduced in (13a) because two of the vacuum protons are interchanged in the transition to which this equation refers. Evaluation of the spurs gives

$$n_{i0j}^{+}=i[\mathbf{e}_i\times\mathbf{e}_j]\{-[2-y_i^{-2}+y_i^{-1}y^{-1}](\mathbf{V}/c)$$
$$-[1+y_i^{-1}y^{-1}](\mathbf{V}_i-\mathbf{V})/c\},$$

$$n_{i0j}^{-}=i[\mathbf{e}_i\times\mathbf{e}_j]\{[2-y^{-2}+y^{-1}y_i^{-1}](\mathbf{V}/c)$$
$$+[1-y^{-2}](\mathbf{V}_i-\mathbf{V})/c\},$$

and

$$n_{i0j}^{+}+n_{i0j}^{-}=i[\mathbf{e}_i\times\mathbf{e}_j]\{(y_i^{-2}-y^{-2})(\mathbf{V}/c)$$
$$+(-y^{-2}-y_i^{-1}y^{-1})(\mathbf{V}_i-\mathbf{V})/c\}.$$

Both n^+ and n^- contain the logarithmically divergent term $(\mathbf{V}_i-\mathbf{V})/c$ which cancels in the addition. To the first order in x this sum is $2n_{012}$. But according to Furry's theorem n^+ and n^- are of the same absolute value so that they either double or cancel and never give the partial cancellation just described. The reason for this difference is that Furry calculates the n^- by reversing all momenta, energies, and directions of transition. This procedure is equivalent to choosing the momenta as shown in Fig. 1c. Since there is an ultimate integration over solid angle, the relative directions of the protonic momentum in n^+ and n^- should not affect the integral (n^++n^-), if this integral is well defined. But since it is not well defined, its value can be changed by reordering the terms in the integrand. Hence there is an uncertainty in the corresponding lifetimes. The terms in which the meson is annihilated in the second step are similar to

those appearing in the self energy, since one photon is used to create the pair and the other to collapse it. As usual, there is no satisfactory procedure for dealing with this situation.

4. DECAY OF A NEUTRAL VECTOR MESON INTO THREE PHOTONS

According to Furry's theorem a vector meson cannot decompose into two γ-quanta because the n^+ and the n^- cancel.[4] Hence we consider the decomposition into three photons, suggested by Sakata and Tanikawa.[2]

The momenta of the three photons close a triangle. For given $\mathbf{p}_1$ the ergodic surfaces are ellipsoids with foci at the two ends of $\mathbf{p}_1$. The density of final states is determined by the number of states common to the ellipsoidal shell $(E, E+dE)$ and the spherical shell (p_2, p_2+dp_2). The volume of this ring is

$$dR=2\pi yJ\left(\frac{x, y}{p_2, \eta}\right)dp_2d\eta,$$

where (x, y) are Cartesian coordinates in the plane of the moments, and $\eta=p_2+p_3$. Hence

$$\rho=\frac{G^2}{6ch^6}\frac{dR}{d\eta}p_1^2dp_1d\omega_1=2\pi G^2\frac{p_1p_2p_3}{6ch^6}dp_1dp_2d\omega_1. \quad (14)$$

The factor 6 appears in the denominator of ρ because the photons are indistinguishable. The product $p_1p_2p_3$ favors a symmetrical decomposition of the meson, but this initial bias is lost when ρ is combined with V^2. The lifetime now is given by

$$\tau^{-1}=(1/96\pi^5)(\mu_1c^2/\hbar)(e^6f^2/c^4\hbar^4)\times\int_0^1\int_{\frac{1}{2}-f_1}^{\frac{1}{2}}J^2df_1df_2, \quad (15)$$

where

$$8J=\int_1^\infty(\sum\omega_id_i^{-1})(y^2-1)^{\frac{1}{2}}y^{-2}dy, \quad (15a)$$

$$\omega_i=\int n_id\omega, \quad (15b)$$

$$D_i=8E^2d_i, \quad (15c)$$

$$n_i=N_i/[(ehc)^3(f_1hc)(\epsilon_1\epsilon_2\epsilon_3\mu_1c^2)^{-1}(2\pi/G)^2]. \quad (15d)$$

Here $\epsilon_i(=\mu_1c^2f_i)$ is the energy of the ith photon. The n_i and d_i are the dimensionless numerators and energy denominators. It is again convenient to expand in powers of $\mu_1c^2/E(=x/y)$.

$$d_i=1+{}^1d_i(x/y), \quad n_i={}^0n_i+{}^1n_i(x/y).$$

The n_i will now be considered in detail.

The decomposition takes place in four steps of which one is needed to annihilate the meson and three to create the three photons. These four steps may be permuted in 24 ways. Again new possibilities may be realized because of symmetry between nucleons and antinucleons; it is possible to choose three intermediate states of positive (negative) energy and one with negative (positive) energy or two with positive and two with negative energy. Hence there are $24\times3=72$ chains in all. A typical numerator is

$$n_{mijk}=Sp[\lambda^-(\beta\alpha\mathbf{e}_m)\lambda(\alpha\mathbf{e}_i)\lambda_i(\alpha\mathbf{e}_j)\lambda_{ij}(\alpha\mathbf{e}_k)], \quad (16)$$

where

$$\lambda_i=\lambda(v_i), \quad \mathbf{P}_i=\mathbf{P}-\mathbf{p}_i, \quad \mathbf{P}_{ij}=\mathbf{P}-\mathbf{p}_i-\mathbf{p}_j.$$

Equation (16) may be written

$$n_{mijk}=\sum A_{st}=\sum a_{st}Sp(\beta^s\alpha^t).$$

$A_{st}=0$ unless $t=4$ or 6. A_{s4} involves x only through the energy of the virtual proton. But $E/E_i=1+A_ix/y$, where $A_i=f_i\mathbf{V}\mathbf{k}_i/c$ and where $\mathbf{k}_i$ is the unit propagation vector. Hence terms linear in x, being also linear in $\mathbf{V}$, vanish in the angular integration. A similar argument is applicable to the linear portion of A_{s6}, insofar as x appears in the energy. But A_{s6} also has terms linear in x in virtue of

$$\mathbf{V}_i/c=\mathbf{V}/c+f_i[-\mathbf{k}_i+(\mathbf{V}\mathbf{k}_i/c)(\mathbf{V}/c)](x/y).$$

Here the factor of x is even in $\mathbf{V}$, and so are all other factors in the spur except $\mathbf{V}$ itself. Hence the term is odd and may be ignored. In addition

[4] W. H. Furry, Phys. Rev. **51**, 125 (1937). The original statement of this theorem refers primarily to transitory electron-positron pairs interacting with the electromagnetic field. The more general statement of Furry's theorem needed here is the following. Let 0 be any Dirac matrix such that $(k\tau|0|k'\tau')=\pm(-k'-\tau'|0|-k-\tau)$, where k is the momentum and τ is the sign of the energy. The theorem now states that a process is forbidden if it involves an odd number of even matrix elements, where "even" means that the positive sign is correct in the equation just written for 0. The even matrix elements are contained in the vector and antisymmetric tensor interactions; those contained in the scalar, pseudoscalar, and pseudovector combinations are odd.

one has $\sum {}^0\omega_i = 0$ (see Eq. (18)). It follows that

$$\sum \omega_i d_i^{-1} = (x/y) \sum {}^0\omega_i {}^1c_i, \tag{17}$$

where ${}^1c_i$ is the part of ${}^1d_i$ independent of $\mathbf{V}$. It is therefore only necessary to determine the zero-order part of n_i and one can put $\lambda_i = \lambda_{ij} = \lambda$ in all the spurs. The n_i contain terms independent of $\mathbf{V}/c$ and in addition terms of the type $Sp[(\alpha \mathbf{e}_m)(\alpha \mathbf{V}/c)(\alpha \mathbf{e}_i)(\alpha \mathbf{e}_k)(\alpha \mathbf{V}/c)(\alpha \mathbf{e}_j)]$, which are quadratic in $\mathbf{V}/c$ and must be integrated over solid angle. Let

$$\bar{\omega}_i = 2^0\omega_i' + {}^0\omega_i'',$$

where ω' corresponds to those processes in which one intermediate state is positive (negative) and the other three states are negative (positive); and where ω'' refers to those processes in which there are two positive and two negative states.

The results are

$$\bar{\omega}_{mijk} = \{[mijk] + [mjik]\} F(y),$$
$$\bar{\omega}_{imjk} = \{-[mjki] + [mjik]\} F(y),$$

where

$$F(y) = \pi(y^{-3} - y^{-1})$$

and

$$[mijk] = Sp[(\alpha \mathbf{e}_m)(\alpha \mathbf{e}_i)(\alpha \mathbf{e}_j)(\alpha \mathbf{e}_k)],$$
$$[mijk] = [mkji] = 4\{(\mathbf{e}_m \mathbf{e}_i)(\mathbf{e}_j \mathbf{e}_k) + (\mathbf{e}_m \mathbf{e}_k)(\mathbf{e}_i \mathbf{e}_j) - (\mathbf{e}_m \mathbf{e}_j)(\mathbf{e}_i \mathbf{e}_k)\}.$$

The remaining elements can be found from the following relations, which can be established by taking the complex conjugate of (16) and the corresponding equation for ω_{imjk}.

$$\bar{\omega}_{mijk} = -\bar{\omega}_{kjim}, \tag{18a}$$

$$\bar{\omega}_{imjk} = -\bar{\omega}_{kjmi}. \tag{18b}$$

The ${}^1c_i$ are also antisymmetric in the same indices, and

$${}^1c_{mijk} = 1 + (f_k - f_i)/2,$$

$${}^1c_{imjk} = \tfrac{1}{2} + f_k/2 - f_i.$$

Hence

$$\sum_1^{72} {}^0\omega_i {}^1c_i = 16FE, \tag{19a}$$

where

$$E = \sum_{ijk} (\mathbf{e}_m \mathbf{e}_i)(\mathbf{e}_j \mathbf{e}_k)[1 + 2(f_k - f_i)]. \tag{19b}$$

By (15a), (17) and (19)

$$J = -2\pi x E \int_1^\infty (y^2 - 1)^{\frac{1}{2}} y^{-6} dy = -2\pi x E/5$$

and by (15)

$$\tau^{-1} = (1/600\pi^3)(\mu_1/M)^2 (e^2 f_1^2/c^4\hbar^4)(\mu_1 c^2/\hbar) \times \int_0^{\frac{1}{2}} \int_{\frac{1}{2}-f_1}^{\frac{1}{2}} E^2(f_1, f_2) df_1 df_2. \tag{20}$$

An approximate integration of this equation followed by a sum over both directions of polarization of the three photons and by an average over the polarization of the vector meson yields the final result

$$\tau^{-1} = (2.4/600\pi^3)(\mu_1/M)^2 (e^6 f_1^2/c^4\hbar^4)(\mu_1 c^2/\hbar). \tag{21}$$

5. DECAY OF A NEUTRAL VECTOR MESON INTO A NEUTRAL PSEUDOSCALAR MESON AND A PHOTON

The density of states is now

$$\rho = G(4\pi/\hbar^3)(\mu_1^2 c) F_\gamma^3, \tag{22}$$

where the photon carries off the fraction F_γ of the rest energy of the meson. The reciprocal lifetime is now

$$\tau^{-1} = (1/128\pi^4)(\mu_1 c^2/\hbar)(e^2 f_0^2 f_1^2/c^3\hbar^3) \times (M/\mu_0)^2 (F_\gamma^4/1 - F_\gamma) J^2, \tag{23}$$

where

$$J = \int_1^\infty (\sum \omega_i d_i^{-1})[y^2 - 1]^{\frac{1}{2}} y^{-1} dy. \tag{23a}$$

The total process requires three steps; for example, $M_1 \to P^+ + P^-$, $P^+ \to P_i^+ + \gamma_i$, $P_i^+ + P^- \to M_0$. Again there are six permutations, each of which appears twice in the way previously mentioned. This case is slightly different from those already considered, because the pseudoscalar particle is created in a state of motion, and both non-relativistic and relativistic terms in the Hamiltonian must be considered. The relativistic numerator, except for a factor of β, is the same as the numerator appearing in case (A). For example,

$$n_{1\gamma 0} = Sp[\lambda^-(\beta \alpha \mathbf{e}_1)\lambda(\alpha \mathbf{e}_\gamma)\lambda_\gamma(\gamma_5)].$$

One finds

$$n_{1\gamma 0} = i[\mathbf{e}_1 \times \mathbf{e}_\gamma] y^{-1} (\mathbf{V} - \mathbf{V}_\gamma)/c,$$
$$n_{10\gamma} = i[\mathbf{e}_1 \times \mathbf{e}_\gamma] y^{-1} (\mathbf{V} + \mathbf{V}_0)/c,$$
$$n_{01\gamma} = -i[\mathbf{e}_1 \times \mathbf{e}_\gamma](y^{-1} + y_0^{-1})(\mathbf{V}_0/c),$$
$$n_{\gamma 01} = i[\mathbf{e}_1 \times \mathbf{e}_\gamma] y^{-1} (\mathbf{V} + \mathbf{V}_\gamma)/c,$$
$$n_{0\gamma 1} = i[\mathbf{e}_1 \times \mathbf{e}_\gamma] y^{-1} (\mathbf{V} - \mathbf{V}_0)/c,$$
$$n_{\gamma 10} = -i[\mathbf{e}_1 \times \mathbf{e}_\gamma](y^{-1} + y_\gamma^{-1})(\mathbf{V}_\gamma/c).$$

The leading term of $\sum n_i d_i^{-1}$ caused by the relativistic part of n_i is of order $(\mu/M)^2$. Hence we consider only the non-relativistic term which is of the order $(\mu/M)^0$. A typical non-relativistic numerator is

$$n_{1\gamma 0}=Sp[\lambda^-(\beta\boldsymbol{\alpha}\mathbf{e}_1)\lambda(\boldsymbol{\alpha}\mathbf{e}_\gamma)\lambda(\gamma_5\boldsymbol{\alpha}\mathbf{k}_0)].$$

The subscripts on the projection operators have been omitted because only zero-order terms need be calculated. The non-vanishing terms of the spur contain α as a factor three or five times. Those containing α five times are quadratic functions of $\mathbf{V}$ and must be averaged over all directions of $\mathbf{V}$. The results are

$$\omega_{1\gamma 0}=\omega_{01\gamma}=(8\pi i/3)(y^{-3}-y^{-1})[\mathbf{e}_1\times\mathbf{e}_\gamma]\mathbf{k}_0,$$
$$\omega_{10\gamma}=(8\pi i/3)(y^{-3}+2y^{-1})[\mathbf{e}_1\times\mathbf{e}_\gamma]\mathbf{k}_0.$$

Again

$$\omega_{1\gamma 0}=\omega_{0\gamma 1},\quad \omega_{01\gamma}=\omega_{\gamma 10},\quad \omega_{10\gamma}=\omega_{\gamma 01}.$$

Hence

$$\sum_1^{12}\omega_i=(32\pi i/y^3)[\mathbf{e}_1\times\mathbf{e}_\gamma]\mathbf{k}_0. \tag{24}$$

In this case also, logarithmically divergent terms cancel. After squaring J, summing over the two possible polarizations of $\mathbf{e}_\gamma$, and averaging over $\mathbf{e}_1$, one finds by (23) and (24) that the reciprocal lifetime is

$$\tau^{-1}=(16/27\pi^2)(\mu_1c^2/\hbar)(e^2f_0^2f_1^2/c^3\hbar^3)\times(M/\mu_0)^2F_\gamma^4(1-F_\gamma)^{-1}, \tag{25}$$

and by the conservation laws

$$F_\gamma=(1/2)[1-(\mu_0/\mu_1)^2]. \tag{25a}$$

6. DECAY OF A CHARGED VECTOR MESON

The decomposition (D) is very similar to (C). Although the electric charge present in (D) introduces some new complexity, it alters the γ-lifetime only very slightly because the processes permitted by the charge are strongly forbidden by selection rules. Before describing the effects of the charge, however, we consider the decompositions common to both neutral and charged mesons. For example, one such possibility is: $M_1^+\rightarrow P^+ + (N)$, $P^+\rightarrow P_i^+ + \gamma_i$, $P_i^+ + (N)\rightarrow M_0^+$, where (N) means antineutron. There are six permutations and the usual doubling. In the neutral case all of these twelve combinatorial possibilities are realizable, but in the charged case only six of them are permitted because (a) a neutron cannot emit a photon if its magnetic moment is neglected, and (b) reactions of the type $P^+ + M^+\rightarrow P^{++}$ are forbidden. The result is that the matrix element due to these processes for the charged case is only half its value for the neutral case, and the lifetime for either charged meson would be

$$\tau_D=4\tau_C, \tag{26}$$

if the charged and neutral cases were otherwise the same.

However, the charged meson, by interacting directly with the electromagnetic field, can decompose in other ways. It is convenient to divide these new processes which lead to decay into two classes according to whether they require two or three steps. The three-step processes are

(a)	$M_1^+\rightarrow M_1^+ + \gamma$	$M_1^+\rightarrow P^+ + (N)$	$P^+ + (N)\rightarrow M_0^+$
(b)	$M_1^+\rightarrow M_1^+ + \gamma$	$0\rightarrow P^- + N + M_0^+$	$M_1^+ + P^- + N\rightarrow 0$
(c)	$0\rightarrow P^- + N + M_0^+$	$M_0^+\rightarrow M_0^+ + \gamma$	$P^- + M_1^+ + N\rightarrow 0$
(d)	$0\rightarrow P^- + N + M_0^+$	$M_1^+\rightarrow M_1^+ + \gamma$	$P^- + M_1^+ + N\rightarrow 0$
(e)	$0\rightarrow P^- + N + M_0^+$	$P^- + M_1^+ + N\rightarrow 0$	$M_0^+\rightarrow M_0^+ + \gamma$
(f)	$M_1^+\rightarrow P + (N)$	$P + (N)\rightarrow M_0^+$	$M_0^+\rightarrow M_0^+ + \gamma$.

(27)

It will now be shown that all processes (27) are forbidden. The nucleons are involved in only two of the three steps. In (c), (e), and (f) M_1 disappears and M_0 is created in a state of rest. The corresponding spur is $Sp[\lambda^-(\beta\boldsymbol{\alpha}\mathbf{e}_m)\lambda\gamma_5]$. This must be multiplied by the matrix element describing the emission of a photon by M_0^+; but since this spur vanishes, the corresponding process may be ignored. In (a), (b), and (d) both M_0 and M_1 move and the relevant spur is

$$Sp\{\lambda^-[A_0\gamma_5+\mathbf{B}_0\gamma_5\boldsymbol{\alpha}]\lambda_i[\mathbf{A}_1\beta\boldsymbol{\alpha}+\mathbf{B}_1\beta\gamma_5\boldsymbol{\alpha}]\}$$
$$=Sp\{\lambda^-[A_0\gamma_5\lambda_i(\mathbf{A}_1\beta\boldsymbol{\alpha})+(\mathbf{B}_0\gamma_5\boldsymbol{\alpha})\lambda_i(\mathbf{A}_1\beta\boldsymbol{\alpha})$$
$$+A_0\gamma_5\lambda_i(\mathbf{B}_1\beta\gamma_5\boldsymbol{\alpha})+(\mathbf{B}_0\gamma_5\boldsymbol{\alpha})\lambda_i(\mathbf{B}_1\beta\gamma_5\boldsymbol{\alpha})]\},$$

where the A and B coefficients are given in Eq. (3). The first term vanishes identically; the

fourth term vanishes since $\mathbf{B}_0 \perp \mathbf{B}_1$. The second term reduces to a linear function of $V_\perp = [\mathbf{A}_1 \times \mathbf{B}_0]\cdot\mathbf{V}$; and since the energy denominator is an even function of $V_\perp$, this term vanishes after the angular integration. The third term vanishes for a similar reason, and hence all processes (27) are forbidden.

Finally the meson may interact simultaneously with the electromagnetic and mesonic fields in the following ways.

$$\begin{array}{lll} \text{(a)} & 0\rightarrow P^-+N+\gamma+M_0^+ & P^-+N+M_1^+\rightarrow 0 \\ \text{(b)} & M_1^+\rightarrow P^++(N) & P^++(N)\rightarrow M_0^++\gamma \\ \text{(c)} & M_1^+\rightarrow P^++(N)+\gamma & P^++(N)\rightarrow M_0^+ \\ \text{(d)} & 0\rightarrow M_0^++P^-+N & P^-+N+M_1^+\rightarrow\gamma. \end{array} \tag{27}$$

In each case one step involves a pair, a photon, and a meson. The corresponding matrix elements follow from (2), where it is no longer permissible to replace $\mathbf{D}$ by ∇; they are (except for constants which do not concern us)

$$(u_n^*\sigma\mathbf{e}_\gamma u_m), \tag{28a}$$

$$[\mathbf{e}_\gamma\times\mathbf{e}_m](u_n^*\beta\gamma_5\alpha u_m). \tag{28b}$$

The probabilities for the processes (a) and (b) vanish, as one can verify by direct computation or by the following observation. The interchange of the two members of the pair is equivalent to a reflection with respect to the origin of momentum space, since they have equal and opposite momenta. But this interchange reverses the sign of the probability amplitude;[4] hence the probability is an odd function in momentum space and vanishes when integrated over all directions.

In (c) and (d) M_1 is at rest so that it is only necessary to find

$$n_{10}=Sp[\lambda^-(\mathbf{C}_1\beta\gamma_5\alpha)\lambda_\gamma(A_0\gamma_5+\mathbf{B}_0\gamma_5\alpha)],$$

where $\mathbf{C}_1$ is given in (28b). The symbol n_{10} means that M_1 is absorbed before M_0 is emitted. It is also necessary to find n_{01}. The results are

$$n_{10}=A_0\mathbf{C}_1\{[y^{-1}(\mathbf{V}_\gamma/c)+y_\gamma^{-1}(\mathbf{V}/c)] +(c\mathbf{p}_0/\epsilon_0)(y^{-1}-y_\gamma^{-1})\},$$

$$n_{01}=A_0\mathbf{C}_1\{y^{-1}(\mathbf{V}_0/c)+y_0^{-1}(\mathbf{V}/c)] +(c\mathbf{p}_0/\epsilon_0)(y^{-1}-y_0^{-1})\}.$$

On expanding $n_{10}D_{10}^{-1}+n_{01}D_{01}^{-1}$ in powers of y^{-1} one finds that the leading term contains y^{-4}; hence the integral of $\sum n_1 D_1^{-1}$ over momentum space is convergent even though there is only one energy denominator for these processes. Furthermore, the leading term, which is of order $(\mu/M)^2$, can be neglected in agreement with our previous neglect of the relativistic terms, also of the second order in (μ/M), which appear in case (C). Hence the lifetime in case (D) is given by Eq. (26).

7. NUMERICAL RESULTS

The significance of our numerical results is quite uncertain because of doubts concerning the correctness of meson theory and the applicability of quantum theory. For consistency, however, the following parameters were used in all cases: $\mu_1/\mu_0=1.6$, $f_0^2/\hbar c=0.05$, $f_0/\mu_0=f_1/\mu_1$. By Eqs. (12), (21), (25), and (26), the lifetimes given in Eq. (1) were computed. These parameters are given by Jauch and Hu[5] for the Schwinger mixture. The two constants μ_1/μ_0 and f_0 are chosen so as to give the correct ^3S binding energy and the correct ^1S virtual level of the deuteron, while the mass μ_0 is assumed to have the (low) value of 177 electron-masses determined by cosmic ray measurements.

I would like to express my very sincere thanks to Professor J. R. Oppenheimer for having suggested this problem and discussed it with me.

[5] J. M. Jauch and N. Hu, Phys. Rev. 65, 289 (1944).

An Attempt to Verify the Theory of the Long Spark of Loeb and Meek

LEON H. FISHER*
Department of Physics, University of California, Berkeley, California
(Received April 19, 1947)

In an attempt to verify the theory of the long spark of Loeb and Meek, d.c. sparking potentials in a plane parallel gap in air have been measured as a function of plate separation and pressure at and below atmospheric pressure. Below atmospheric pressure, the sparking-potential curve as a function of gap length at constant pressure, displays a peculiar levelling-off at large gap lengths. This has been shown to be due to field distortion of a pressure-dependent type. This field distortion is, in large measure, caused by the walls of the large chamber used in this study. This field distortion prevented the verification of the Loeb-Meek theory. However, there is considerable evidence for believing the results at atmospheric pressure to be valid. Meek's equation represents the data accurately at atmospheric pressure. Water vapor causes a small but definite scattering in sparking potentials.

INTRODUCTION

THE streamer theory of sparking developed by Loeb and Meek[1–3] invokes processes known to occur in discharges at large values of the product of pressure and plate distance. From the theory sparking potentials may be calculated. Other equations are either empirical representations of data such as the one given by Peek[4] or else they are based on mechanisms known to be inoperative at large values of the product of pressure and gap length. Loeb and Meek[2,3] have extended the theory to include the long spark. They postulated that, at a given pressure, above a certain plate distance, δ_0, Meek's equation does not apply. According to Loeb and Meek the slope of the sparking-potential *vs.* gap-length curve should decrease with increasing gap length until δ_0 is reached. At this point the slope should increase and remain constant thereafter. The straight line above δ_0, if extended, should pass through the origin and should lie below the values of the sparking potential for gap lengths less than δ_0. It was also postulated that this inflection in the sparking-potential curve would occur at shorter gap lengths the lower the pressure. On the basis of the only data then or now available, Loeb and Meek calculated δ_0 for air to be 88, 15, and 3.3 cm at 1520, 760, and 380 mm of Hg, respectively. The theory is thus conveniently open to experimental test at pressures of the order of one-half an atmosphere.

The theory of Loeb and Meek as applied to the long spark is admittedly semi-empirical, and the constants are not too well known. While the underlying principles may apply, the quantitative bases of the predictions may be off considerably. The validity of the choice of constants has been discussed recently.[5]

Irrespective of the details of the calculation, which are somewhat in doubt, the very definite predictions require experimental verification, and toward this end, at the suggestion of Professor Loeb, the writer undertook to measure sparking potentials in air at half an atmosphere pressure. Unfortunately, it was just in the region of pressures and gap lengths which should prove of interest that the apparatus failed to function properly because of field distortion. In view, however, of the fact that very consistent sparking-potential data at atmospheric pressure were obtained, and that the instrumental difficulties encountered are of considerable interest, it is believed worth while to report the findings.

APPARATUS AND EXPERIMENTAL PROCEDURE

The chamber used was the one employed by Sanders[6] and Posin[7] for measurements of the

* Now at New York University, University Heights, New York.

[1] J. M. Meek, Phys. Rev. **57**, 722 (1940).

[2] L. B. Loeb and J. M. Meek, J. App. Phys. **11**, 438, 459 (1940).

[3] L. B. Loeb and J. M. Meek, *The Mechanism of the Electric Spark* (Stanford University Press, Stanford, 1941).

[4] F. W. Peek, Jr., *Dielectric Phenomena in High-Voltage Engineering* (McGraw-Hill Book Company, Inc., New York, 1929), p. 73.

[5] L. H. Fisher, Phys. Rev. **69**, 530 (1946).

[6] F. H. Sanders, Phys. Rev. **41**, 667 (1932).

[7] D. Q. Posin, Phys. Rev. **50**, 650 (1936).

first Townsend coefficient of air and nitrogen. This ionization chamber was constructed with the aid of a grant in support of Sanders' research by the National Research Council. A diagram of the chamber as originally used by Sanders (and also for some time by the writer) is given in Fig. 1. For a detailed description of the chamber one may refer to Sanders'[6] original paper. For the purpose of the present discussion it will suffice to recall just a few features of the chamber. The shell consisted of a cylindrical brass casting 45 cm in height and 50 cm in diameter. Both electrodes were 20 cm in diameter. The lower plate was the high voltage electrode and was profiled as shown. This electrode rested on a porcelain insulator, I_1; the insulator in turn rested on a circular metal plate P. The lower insulator, I_2, was made of Pyrex glass and was filled with oil. No mercury was used in the chamber in the present work.

With the arrangement shown in Fig. 1, at half an atmosphere corona from the high voltage electrode occurred at voltages too low to test the Loeb-Meek theory. Figure 2 shows the arrangement finally used. The high voltage electrode of Fig. 1 was replaced by another of equal diameter the edges of which had a radius of two centimeters. In addition, it was necessary to remove the supporting brass plate, P, to the bottom of the chamber. A new hollow porcelain insulator, I_1', was used which reached from the brass plate, P, to the high voltage electrode. This increased the distance from P to the high voltage electrode from 10 to 20 cm. A new oil-filled insulator, I_2', entered the chamber as before, but reached all the way to the lower electrode. With this arrangement, it was possible to reach 60 kv at 380 mm of Hg before corona appeared.

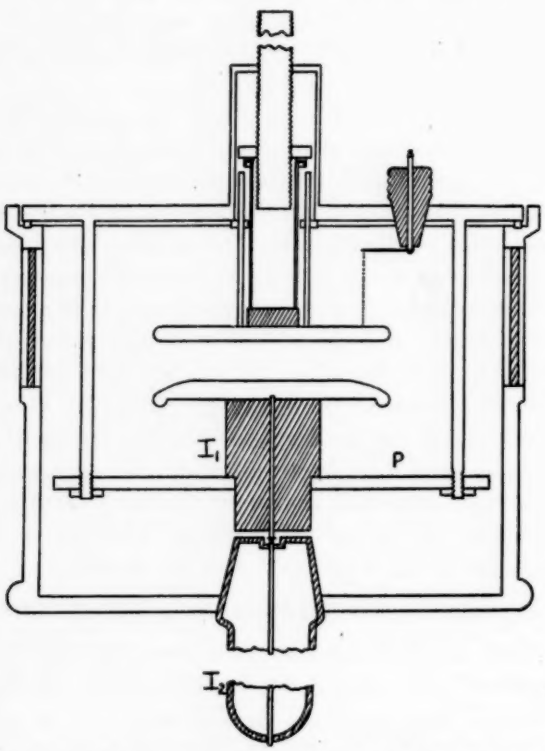

FIG. 1. Ionization chamber as originally used by Sanders.

The plates were levelled to within 0.002 inch outside the chamber by means of a telescopic plug gauge. Whether the plates remained level after the electrode system was lowered is unknown since mechanical stresses are set up. The electrodes were polished with emery paper and rouge, and the chamber surfaces were carefully washed with ethyl alcohol before being closed for a series of measurements. Fiducial marks were placed on both electrodes and gap distances were measured by means of these marks with a cathetometer. Gap separations were read to a few thousandths of a centimeter.

The d.c. potential source was of the same type as the one used by Sanders; it was stabilized by an electronic stabilizer of the saturable-core reactor type. In parallel with the spark gap were wire-wound Taylor resistors of 100 megohms. These resistors are manufactured by Shallcross and carry a one percent accuracy rating when used under the present operating conditions.[8] The voltage was read by potentiometer across 1000 ohms set on a Leeds and Northrup dial box in series with the Taylor resistors. The accuracy of the voltage measurements was therefore determined by the Taylor resistors and is of the order of one percent.

A current-limiting resistor of 0.1 megohm was placed in series with the chamber in order to prevent pitting of the plates and also to avoid excessive production of oxides of nitrogen. The Taylor resistors were placed directly in parallel with the chamber. Leakage across the current-limiting resistor and across the oil-filled insulator

[8] L. S. Taylor, Bur. of Stand. J. Research 5, 609 (1930).

introduced no uncertainty in the measurements. The chamber was grounded during the measurements.

The central portion of the cathode was illuminated by ultraviolet light in order to prevent appreciable time lags, and also to induce the spark to pass in the uniform part of the field. During the entire study, however, ultraviolet light had no effect on the sparking potentials, and in no way influenced the position of the spark. This situation must have been due to the presence of adequate initiating electrons in the chamber at all times.

Air from outside the laboratory was admitted through a capillary, the air passing over two traps of aged liquid air, and one of phosphorus pentoxide. At no time was liquid oxygen observed in the trap. The pressure of the gas was read on a mercury manometer to one millimeter. All pressures have been corrected to 22°C.

To measure a sparking potential, the voltage was raised in steps of 100 volts, the electrodes being in contact with the power supply at all times. After each setting, a 30-second interval elapsed before the voltage was increased again. The time lag was almost always so short that the 30-second wait was unnecessary. The voltage taken as the sparking potential was the reading at the passage of a spark. For a given reading, two measurements were taken with ultraviolet light incident on the cathode, and one was taken with no irradiation of the gap.

Previous observers[9,10] working with air have reported the lowering of sparking potentials because of the formation of oxides of nitrogen. In this study, no such effect was observed, the chamber being large enough to prevent impurities from building up to an appreciable concentration. The current-limiting resistor also helped to reduce the amount of chemical action during a spark.

Sparking potentials in the closed chamber in dry air for any one filling were reproducible to 100 volts regardless of the values of the sparking potential (10 to 60 kv). From one filling to another, the results scattered by about 300 volts. No large spread in individual measurements, as is often reported, was observed. This fact is probably due to the exclusion of dust particles from the chamber, as well as to the presence of adequate initiating electrons. The exclusion of water vapor is believed to have increased the reproducibility of the measurements. On closing the chamber, or even after a new filling, sparks occurred at low voltages, but after five or ten sparks passed, the sparking potential became constant.

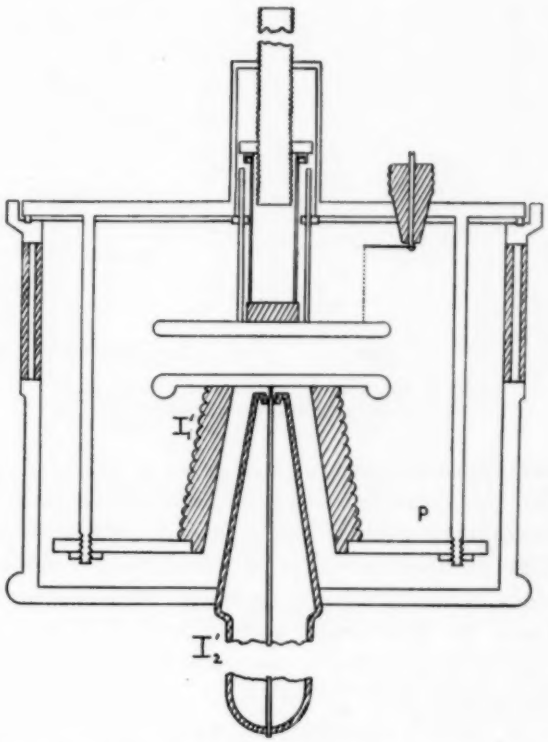

FIG. 2. Ionization chamber as used in the present work.

EXPERIMENTAL RESULTS AND DISCUSSION

Table I represents the results of a run, series I, at atmospheric pressure with varying gap length. The results are plotted in Fig. 3. Series I yields 30.1 kv as the sparking potential for a one-centimeter gap at atmospheric pressure at 22°C.

Table II gives the values quoted by Schumann[11] as a compendium of the results of a large number of workers, and also the careful observations of Spath.[12]

Values for corresponding values of $p\delta$ from series I are also given in Table II. Spath's values

[9] K. S. Fitzsimmons, Phys. Rev. **61**, 175 (1942).
[10] W. R. Haseltine, Phys. Rev. **58**, 188 (1940).
[11] W. O. Schumann, *Elektrische Durchbruchfeldstärke von Gasen* (Julius Springer, Berlin, 1923), p. 26.
[12] Reference 11, p. 173.

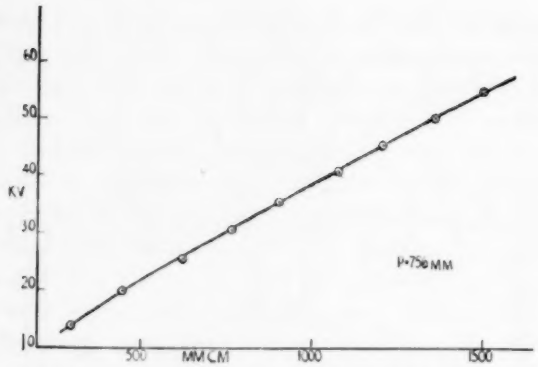

FIG. 3. Sparking potential *vs.* $p\delta$ for series I (near atmospheric pressure).

fall consistently below those given by Schumann, and this difference has been ascribed to Spath's use of ultraviolet light. The present results above 0.60 cm fall below those of Spath, but the agreement below 0.60 cm is excellent. Measurements made by Haseltine[10] give V_s as 15.4 kv at $p_{22}\delta = 324$ mm×cm as compared to 15.5 kv from the present data.

In Meek's equation, a constant, K, appears which is the ratio of the field due to the positive ion space charge to that of the applied field. It is assumed that at the sparking voltage K is a constant independent of pressure and gap length. That K is a constant independent of pressure has been demonstrated for streamer formation in hydrogen in inhomogeneous fields.[13] It is of interest to apply Meek's equation to consistent data in order to evaluate K. As a matter of fact, the reverse procedure may be an extremely valuable method of estimating the consistency of a set of data. As is commonly realized, V_s is an extremely insensitive function of K; therefore, K is an extremely sensitive function of the value taken for V_s. For example, if it is assumed that a one-centimeter gap in air at atmospheric pressure has the sparking potentials given in Table III, the values of K given there result. Thus, for these conditions a range of two kilovolts introduces a change in K of a factor of 1000; a one-kilovolt difference introduces a factor of 30, and a difference of 0.1 kv introduces a change of 20 percent. It is necessary, therefore, to be cautious in interpreting calculated values of K. In Tables I and II are listed values of the natural logarithm of K calculated from series I and from the measurements of Spath. It is seen that the present measurements give values of K constant to within a factor of two, while those of Spath give values of K which vary by a factor of 60. Thus one value of K can be used to represent the data of series I within the limit of experimental error; this is not true for the measurements of Spath. In Tables I and II are also listed calculated values of $\alpha\delta$ at sparking, and it is seen that the condition $\alpha\delta$ = constant represents the data of series I in a satisfactory way. Again this is not true for Spath's measurements.

The small absolute values of K calculated from Spath's and the present data are disturbing, since it is difficult to see how photo-electrons formed in the gas would have much tendency to feed into the positive space charge. Since, however, no great accuracy is claimed for the constants in Meek's equation, errors in this might account for the low value observed.

The fact that series I gives lower values of the sparking potential than are usually reported is in itself not too disturbing. Most of the former

TABLE I. Series I measurements of sparking potential at constant pressure [p(22°C) = 756 mm Hg] and varying gap length.

δ	$p_{22}\delta$	V_s	$\ln_e K$	$\alpha\delta$
1.985 cm	1501 mm×cm	54.7 kv	−7.6	12.3
1.801	1362	50.1	−7.7	12.1
1.606	1214	45.4	−7.2	12.4
1.425	1077	40.7	−7.9	11.6
1.207	912	35.4	−7.2	12.0
1.022	773	30.5	−7.5	11.5
0.831	628	25.5	−7.0	11.5
0.599	453	19.3	−7.0	11.5
0.401	303	13.8	−6.8	11.0

TABLE II. Comparison of present results with those quoted by Schumann** and with those of Spath.***

δ	$p_{22}\delta$	V_s (Schumann)	V_s (Spath)	V_s (This study)	$\ln_e K$ (Spath)	$\alpha\delta$ (Spath)
0.40 cm	306 mm×cm	14.4 kv	13.8 kv	14.1 kv	−7.3	10.8
0.50	382	17.4	16.8	16.9	−6.5	11.6
0.60	459	20.3	19.8	19.6	−5.9	12.4
0.70	536	23.2	22.75	22.3	−5.2	13.2
0.80	612	26.1	25.6	24.9	−4.8	13.8
0.90	688	28.9	28.6	27.5	−3.8	14.9
1.00	765	31.7	31.55	30.1	−3.2	15.6
2.00	1530	59.6		55.7		

[13] L. H. Fisher and G. L. Weissler, Phys. Rev. 66, 95 (1944).

** See reference 11.
*** See reference 12.

TABLE III. Values of the constant K of Meek's equation for various sparking potentials.

Assumed V_s	33.0 kv	32.1	32.0	31.0
K (calculated)	20	0.6	0.5	0.02

work used a.c. potentials. Loeb,[14] among others, has pointed out that a.c. sparking-potential measurements may be expected to be slightly higher than d.c. measurements. The peak value of an a.c. voltage is applied only instantaneously, and because of a statistical time lag, the gap may not break down until a value of the peak voltage is impressed which is somewhat greater than the true sparking potential. Reukema[15] found that the use of ultraviolet light reduced the average observed a.c. sparking potential by 3.5 percent.

Measurements of sparking potentials at half an atmosphere and with varying plate separation, series IV, are plotted in Fig. 4. It is seen there that the sparking-potential curve at half an atmosphere levels off at large values of the plate separation. In order to investigate this levelling-off, runs were made at pressures of 50 and 25 cm. Series V was made at 500 mm, and series VI was made at 261 mm. The results, including those of series I and IV, are plotted in Fig. 5. It is evident from Fig. 5, that for $p\delta > 800$ mm Xcm, Paschen's law is not obeyed, and some kind of field distortion comes into play, at least for pressures below one atmosphere. The data for series IV, V, and VI above $p\delta = 800$ therefore have no significance.

In order to understand the nature of the field distortion, a cylindrical piece of sheet metal was placed in the chamber and was grounded. This cylinder reduced the effective diameter of the chamber by two inches, and measurements were made again at pressures of one atmosphere, 50 cm, 38 cm, and 25 cm. The measurements at atmospheric pressure and at 50-cm pressure did not differ from the values obtained with the original chamber. Therefore, for these high pressures, the effect of reducing the size of the chamber by two inches was unimportant. This, however, was not the case for the lower pressures.

[14] L. B. Loeb, *Fundamental Processes of Electrical Discharge in Gases* (John Wiley and Sons, Inc., New York, 1939), p. 550.

[15] L. E. Reukema, Trans. A.I.E.E. **47**, 38 (1928).

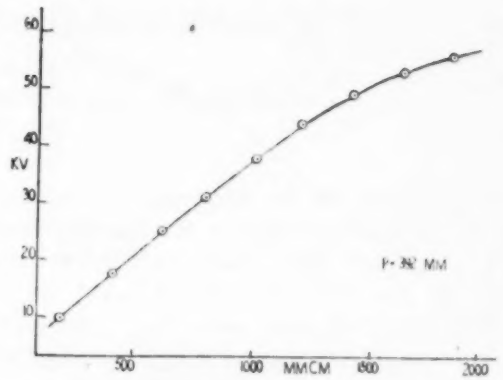

FIG. 4. Sparking potential *vs.* $p\delta$ for series IV (near half an atmosphere pressure).

The data for the 38-cm (series VII) and 25-cm (series VIII) pressure runs with the reduced size of the chamber are plotted. Series IV and VII are plotted in Fig. 6, and series VI and VIII are plotted in Fig. 7. The levelling-off of the sparking potential *vs.* plate-separation curves is more pronounced with the smaller chamber than with the original chamber at pressures in the neighborhood of 380 mm and below. It is clear, therefore, that there is at low pressures and large gap lengths a field distortion imposed by the walls of the chamber, and that the question of the behavior of the sparking potential *vs.* gap-length curve at half an atmosphere must wait until a larger chamber is available. Clearly, a chamber of much greater diameter will be needed in order to study sparking potentials at low pressures and large gap distances.

The question now arises as to the reliability of series I. Below $p\delta = 800$ mm$\times$cm, there seems to be little doubt that the values are reliable.

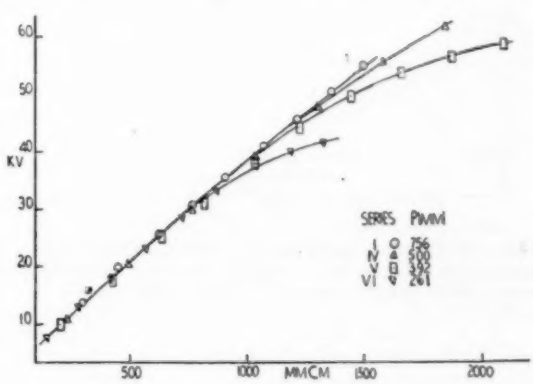

FIG. 5. Sparking potential *vs.* $p\delta$ at four different pressures.

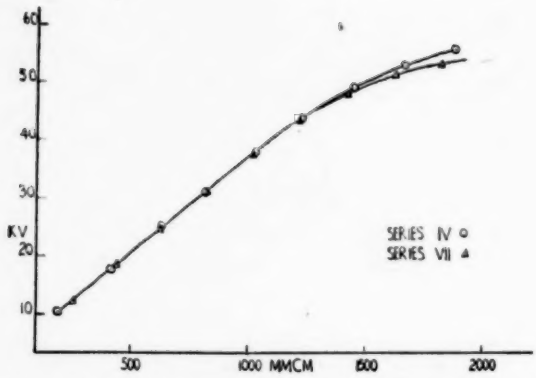

FIG. 6. Sparking potential *vs.* $p\delta$ at half an atmosphere pressure with original chamber (series IV) and with slightly smaller chamber (series VII).

Above this value of $p\delta$, one can only say that consistent values of K are obtained. There is thus some reason for believing series I to be valid in its entirety.

Various other attempts were made to discover in more detail how the geometry of the chamber affected the measurements. The polarity of the electrodes was reversed, and a complete set of measurements was taken at various pressures. The results were, within the experimental error, identical with the values obtained with the usual polarity.

To determine the effect of the small radius of curvature of the grounded electrode, the electrode that was used by Sanders as a cathode (the lower plate in Fig. 1) was inserted as the grounded electrode in the arrangement of Fig. 2. In spite of the decreased curvature of the new electrode, the results were again unchanged. This result indicates that the contour of the low voltage electrode made no contribution to the field distortion. Whether the contour of the high voltage electrode added to the field distortion is at present unknown. A model study is now in progress.

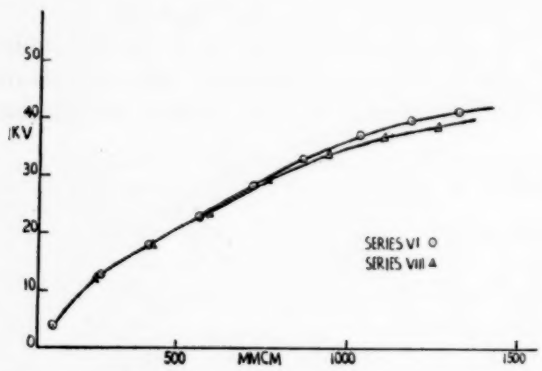

FIG. 7. Sparking potential *vs.* $p\delta$ at one-quarter of an atmosphere pressure with original chamber (series VI) and with slightly smaller chamber (series VIII).

The one fact which seems to require the high voltage plate to have caused some distortion is that the sparking potentials with the reduced chamber at a pressure of 50 cm were the same as for the large chamber at the same pressure, and yet the sparking-potential curves at pressures of 50 cm and 76 cm do not coincide when plotted as a function of $p\delta$.

The electrode system of Fig. 2 was lifted into the open room (the surrounding metal walls were effectively removed) and sparking potentials were determined; the electrode system was then lowered into position so that the electrodes were now surrounded by the metal walls, and measurements were made again. The two sets of observations (at atmospheric pressure) were identical. The complete removal of the walls, just as decreasing the diameter of the chamber, had no influence on the sparking potential at atmospheric pressure over the range of plate separations studied.

In the experiment described in the preceding paragraph it was found that the sparking potentials both in the open and closed system scattered considerably; this probably was caused by the presence of dust or water vapor. The scattering persisted even after considerable sparking and was not removed by ultraviolet light. When clean dry air was admitted in the normal manner, the sparking potentials were again reproducible. Water vapor was then allowed to diffuse into the chamber, and it was found that a small but definite spread of 300 to 500 volts is introduced in the value of the sparking potential.

The author wishes to express his gratitude to Professor Loeb who suggested the problem and under whose direction it was carried out.

The γ-Radiation of Na^{24} and the Energy-Level Scheme of Mg^{24}

M. L. WIEDENBECK
Department of Physics, University of Michigan, Ann Arbor, Michigan
(Received July 23, 1947)

SINCE Na^{24} can be produced easily and because it emits high energy γ-radiation it has long been of interest from the applied standpoint as well as from the standpoint of the structure of the levels giving rise to the radiation. Over the past several years the radiation has been investigated by many workers by various methods and in many cases the results have been inconsistent.

The sodium-β-spectrum has been most accurately studied by Siegbahn[1] and by Lawson[2] and has been found to be simple. Absorption experiments by Langer, Mitchell, and McDaniel[3] in 1939 have shown that the $\beta-\gamma$-coincidence rate is independent of the energy of the β-radiation, thus showing that a single β-transition takes place. The upper limit of the β-spectrum is 1.390 Mev.

The history of the γ-radiation following the β-decay of Na^{24} is somewhat more complex. This has, however, been described in considerable detail by Siegbahn.[1] It would appear that the most accurate results are those obtained by a beta-spectrograph study of the secondary electrons ejected from a body irradiated with the γ-rays in question. Such work has been carried out by Itoh,[4] Elliott, Deutsch and Roberts,[5] Mandeville,[6] and most recently by Siegbahn.[1] Their results all indicate that only two γ-rays are emitted by the Mg^{24} nucleus and these are of "nearly" equal intensity. The values given are 1.38 and 2.76 Mev.

The most simple arrangements of the levels of Mg^{24} would occur if the γ-rays were in cascade. However Guthrie and Sachs[7] have pointed out that such an arrangement would lead to a mass of Na^{24} which is $\sim$1.5 Mev higher than that calculated by Barkas[8] from a study of the fine structure of the mass defect curve. They further pointed out that this difficulty could be eliminated by assuming the level scheme shown in Fig. 1b with a branching ratio of 2:1.

Absorption measurements of the $\gamma-\gamma$-coincidences were carried out by Cook, Jurney, and Langer.[9] These indicate that the 2.8-Mev radiation is involved in the coincidence and hence supports level scheme of Fig. 1a.

Recently Barker[10] has measured the average

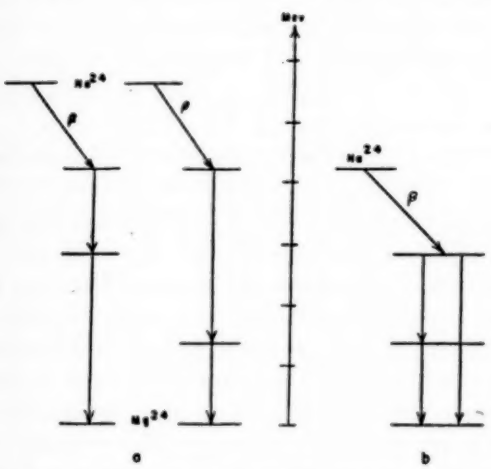

FIG. 1. "a" shows the two possible cascade energy-level diagrams of the decay of Na^{24}. "b" indicates the parallel decay proposed by Sachs.

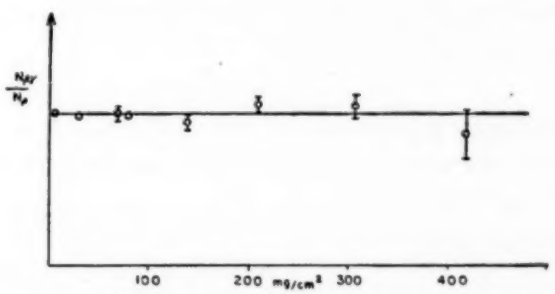

FIG. 2. $\beta-\gamma$-coincidence rate of sodium as a function of β-absorber thickness.

[1] K. Siegbahn, Phys. Rev. **70**, 127 (1946).
[2] J. L. Lawson, Phys. Rev. **56**, 131 (1939).
[3] L. M. Langer, A. C. G. Mitchell, and P. W. McDaniel, Phys. Rev. **56**, 962 (1939).
[4] J. Itoh, Proc. Phys. Math. Soc. Japan **23**, 605 (1941).
[5] L. G. Elliott, M. Deutsch, and A. Roberts, Phys. Rev. **63**, 386 (1943).
[6] C. E. Mandeville, Phys. Rev. **63**, 387 (1943).
[7] A. Guthrie and R. G. Sachs, Phys. Rev. **62**, 8 (1942).
[8] W. H. Barkas, Phys. Rev. **55**, 691 (1939).
[9] C. S. Cook, E. Jurney, and L. M. Langer, Phys. Rev. **70**, 985 (1946).
[10] E. C. Barker, Phys. Rev. **72**, 167(A) (1947), also private communication with E. C. Barker.

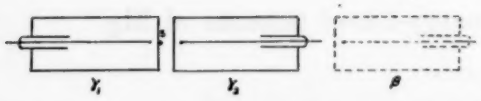

FIG. 3. Counting arrangement used in determining $N_{\gamma_1\gamma_2}$ and $N_{\gamma_1\beta}$. The source, S, is fixed rigidly to counter γ_1.

γ-energy per β-particle for Na^{24} by means of ionization methods. His results give 4.17 Mev (± 10 percent) per β-particle. This would also substantiate the level scheme indicated in Fig. 1a.

To check the simplicity of the Na^{24} β-spectrum, a determination of the $\beta-\gamma$-coincidence rate was made as a function of β-absorber thickness. The minimum thickness of absorber was equivalent to approximately 4 mg/cm^2 of aluminum. The curve, Fig. 2, is seen to be independent of the β-energy and again attests to the simplicity of the β-spectrum.

An additional method which can be used to distinguish between the level schemes of Figs. 1a and 1b lies in the $\gamma-\gamma$- and $\beta-\gamma$-coincidence rates. If we have two counters designated by γ_1 and γ_2 (Fig. 3), each having an efficiency $\epsilon_{1.4}$ for the 1.4-Mev γ-radiation and an efficiency $\epsilon_{2.8}$ for the 2.8-Mev γ-ray, then

$$N_{\gamma_1\gamma_2}=(2\sigma_{\gamma_1}\epsilon_{1.4}\epsilon_{2.8}/\epsilon_{1.4}+\epsilon_{2.8})N_{\gamma_2}, \qquad (1)$$

for level scheme of Fig. 1a. $N_{\gamma_1\gamma_2}$ being the $\gamma-\gamma$-coincidence rate, σ_{γ_1} the fraction of the total radiation intercepted by counter γ_1, and N_{γ_2} the counting rate of counter γ_2. Now if the counter γ_2 is moved farther from the source and converted to a β-counter, the $\beta-\gamma$-coincidence rate for scheme of Fig. 1a is:

$$N_{\beta\gamma_1}=\sigma_{\gamma_1}(\epsilon_{1.4}+\epsilon_{2.8})N_\beta. \qquad (2)$$

Dividing Eq. (1) by Eq. (2), and remembering that the source, S, is fixed rigidly to the counter γ_1, we have:

$$(N_{\gamma_1\gamma_2}/N_{\gamma_2})/(N_{\gamma_1\beta}/N_\beta) = 2\epsilon_{1.4}\epsilon_{2.8}/(\epsilon_{1.4}+\epsilon_{2.8})^2. \qquad (3)$$

Similarly for level scheme of Fig. 1b we obtain

TABLE I. Comparison of $\gamma-\gamma$ and $\beta-\gamma$ coincidence rates.

Radiator	$\frac{N_{\gamma_1\gamma_2}/N_{\gamma_2}}{N_{\gamma_1\beta}/N_\beta}$	Total relative efficiencies (brass = 1)
Brass	0.525	1
Cu	0.525	1
Al	0.51	1.2
Fe	0.502	1.06
Pb	0.517	0.95
Lucite	0.51	1.3

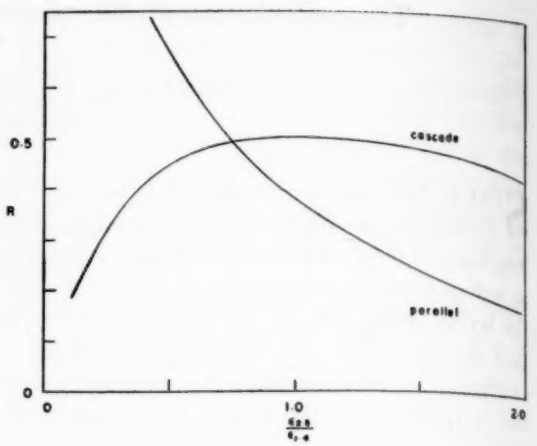

FIG. 4. Ratio, R, of $N_{\gamma_1\gamma_2}/N_{\gamma_2}/N_{\gamma_1\beta}/N_\beta$ as a function of the ratio of the counter efficiencies for the 2.8- and 1.4-Mev γ-rays.

the ratio

$$(N_{\gamma_1\gamma_2}/N_{\gamma_2})/(N_{\gamma_1\beta}/N_\beta) = 3(\epsilon_{1.4})^2/2(\epsilon_{1.4}+\epsilon_{2.8})^2. \qquad (4)$$

It should be noted that these equations are derived on the assumption that the efficiency of the counters is low, actually they are ~one percent efficient.

Equations (3) and (4) are plotted in Fig. 4. It is clear that scheme 1a gives rise to a ratio $(N_{\gamma_1\gamma_2}/N_{\gamma_2})/(N_{\gamma_1\beta}/N_\beta)$ nearly equal to 0.5 over a very wide range of efficiencies while scheme 1b gives a rapid variation in the region of interest.

The counters were of brass construction with a $\frac{1}{2}$-mil Cellophane end window. To convert the counter for γ-counting, a small cylindrical plug was inserted in front of the window.

Table I gives the results of six determinations made with various radiators in front of the thin-windowed counter ($\frac{1}{2}$-mil Cellophane). The total relative γ-efficiencies of the counters are also included in the table. It is seen that over this wide range of radiators the ratio remains essentially constant near the value 0.5. The experiment with the lead radiator was repeated with a greater thickness of lead to shift artificially the efficiency ratio ($\epsilon_{2.8}/\epsilon_{1.4}$) to a higher value. The counting rate with such an arrangement is low but within the statistical error the ratio $(N_{\gamma_1\gamma_2}/N_{\gamma_2})/(N_{\gamma_1\beta}/N_\beta)$ remains in the region of 0.5. It must, therefore, be concluded that the cascade level diagram of Fig. 1a is the correct one.

We wish to express our thanks to Professor Uhlenbeck for his discussions of this problem.

Letters to the Editor

PUBLICATION of brief reports of important discoveries in physics may be secured by addressing them to this department. The closing date for this department is five weeks prior to the date of issue. No proof will be sent to the authors. The Board of Editors does not hold itself responsible for the opinions expressed by the correspondents. Communications should not exceed 600 words in length.

The Yield of Nuclei Formed by Fission

A. J. DEMPSTER
Argonne National Laboratory, Chicago, Illinois
July 9, 1947

THE recently published yield curve[1] for the nuclei formed in fission emphasizes the lack of any explanation for this striking feature of the fission phenomenon. Calculations of the potential energy associated with deformations of the liquid-drop model of the nucleus[2,3] have met with difficulties in attempting to predict any of the details of the fission process. The purpose of this note is to point out that a physical condition is imposed on the fission process by the consideration that, since the pair of fission products are structures of known energy content, they must be formed with a definite potential energy. This condition is automatically satisfied in the liquid-drop model of the nucleus, at least to the extent that this model accounts for the masses of the nuclei, but its formulation as a quantitative physical condition independent of any theoretical interpretation of mass defects is of interest as it suggests a reason why some types of fission are more probable than others.

The curve marked E in Fig. 1 is the kinetic energy acquired by the different pairs of fission products, whose masses are plotted as abscissae. It is computed from the mass changes between uranium and the fission nuclei, using the packing-fraction curve[4] given by the writer in 1938, and allowing 22 Mev for the energy of excitation,[5] and the equivalent energy of eight extra electrons that are in the fission products when formed. E is also the potential energy at the instant of separation of the two fission nuclei.

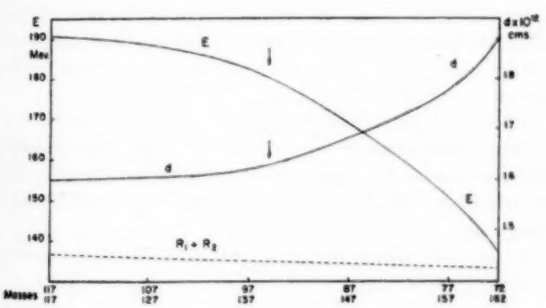

FIG. 1. Curve E gives the kinetic energy of fission products, or the potential energy at separation. Curve d gives the separation of centers of spherical fission products that would account for E. R_1+R_2 gives the theoretical sum of the radii of the fission products.

The most probable type of fission gives the masses 95 and 139, indicated by the arrows, and not two equal masses, even though this latter process would release a greater amount of energy. The curve d is the computed distance between the centers of the fission products, supposed spherical, at which the potential energy, $Z(92-Z)e^2/d$, due to Coulomb repulsion, is equal to E. The value of d comes out to be larger than the sum of the radii R_1+R_2 given by the liquid-drop theory of atomic nuclei, using the formula:[6] $R=r_0A^{\frac{1}{3}}$, with $r_0=1.48\times10^{-13}$ cm. Even smaller values for r_0 have been proposed.[7] The sum of the radii of the two fission products, calculated from this formula, is given by the broken line at the bottom of Fig. 1. There appears to be a difficulty, analogous to the paradox met with in alpha-ray emission, in that the fission particles must have no kinetic energy at a distance between centers (d), greater than the sum of their radii. It may, however, be possible to increase the theoretical values of the radii enough to make the lower curve cut across the curve d.

The curves, however, suggest possible reasons for the different fission yields. For the case of large differences in the masses, d must be large and E small, and only an unusual manner of separation would give the small potential energy permitted. With the fission masses 95 and 139, a normal separation can be considered as leaving the products with the required potential energy. In the case of even division, on the other hand, only unusual separation processes would be able to provide the large potential energy in the fission products required by the curve E.

[1] The Plutonium Project, Rev. Mod. Phys. **18**, 539 (1946).
[2] R. D. Present, F. Reines, and J. K. Knipp, Phys. Rev. **70**, 557 (1946).
[3] N. Bohr and J. A. Wheeler, Phys. Rev. **56**, 426 (1939).
[4] A. J. Dempster, Phys. Rev. **53**, 870 (1938).
[5] K. Way and E. Wigner, Phys. Rev. **70**, 116 (1946).
[6] H. A. Bethe and R. F. Bacher, Rev. Mod. Phys. **8**, 97 (1936).
[7] E. Feenberg, Phys. Rev. **55**, 504 (1937).

Geiger-Mueller Counter Detection of Light Radiation from the Paths of High Energy Particles

PAUL B. WEISZ AND B. L. ANDERSON
Socony-Vacuum Research and Development Department, Paulsboro, New Jersey
July 14, 1947

DETECTION of Čerenkov radiation has been attempted by use of photographic methods[1] and photomultipliers.[2] Furry[3] recently pointed out the possible value of Geiger-Mueller counter tubes of high light sensitivity to cosmic-ray studies.

An experiment was designed in an attempt to detect Čerenkov radiation accompanying the passage of cosmic-ray particles and of radiation from a natural radioactive source by means of light-sensitive Geiger-Mueller counters.

The counters used had been developed in connection with other work[4] and had their spectral response in the ultraviolet, between 2000A and 3000A. They consisted of a cathode cylinder of wire screen of 50 percent coverage, covered with a 0.005-in. thick layer of electroplated gold, and contained in a Corning 9741 glass envelope capable of

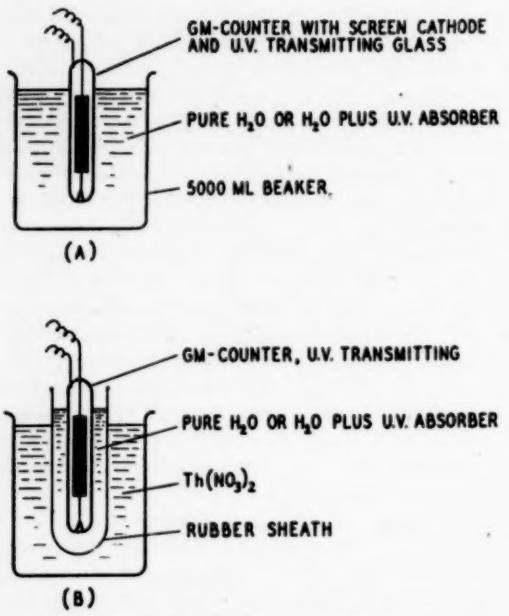

FIG. 1. a. Arrangement of the cosmic-ray experiment. b. Arrangement using thorium-nitrate salt with its decay products.

transmission in that spectral range. The quantum efficiency of the surface can be affected within wide limits by the nature of the degassing process and baking atmosphere before filling.

The experiment is based on an arrangement in which the counter is immersed into a liquid medium which itself is transparent to the light radiation in the 2000–3000A range to which the counter is sensitive. The counting rate N_1 of the counter should then be due to high energy radiation penetrating the counter itself, and in addition to photons emitted by high energy particles in the liquid medium outside of the counter. In the experiment a second counting rate N_0 is obtained after adding a small amount of strongly ultraviolet absorbing chemical, which will neither disturb the geometry nor the density of the liquid by an appreciable amount, but should eliminate those counts obtained from light radiation emitted in the liquid. Effectively, the liquid medium acts to increase the "effective counting volume" of the Geiger counter while the liquid is transparent to the light to which the tube is sensitive.

Figure 1a shows the arrangement of the cosmic-ray experiment (*A*); Fig. 1b for the experiment using thorium-nitrate salt (with its decay products) as emitter (*B*) and (*C*). In the latter experiment it was attempted to stop the beta-radiation from the thorium within the pure water in order to keep the count from direct beta-radiation as low as possible. The liquid medium was always pure water (its transmission was checked to give an optical density of $D=0.005$ at 2500A increasing to $D=0.034$ at 2200A and no measurable absorption between 2650–3000A). The added chemical to make it opaque was 1 percent (by weight) of hydroquinone in (*A*), and a variable amount (as indicated) of potassium-chromate in (*B*) and (*C*).

Table I shows the results of the experiments.

Percentages of chemical are given as weight-percents of chemical added to the pure water. In experiment (*C*), which was done with a smaller quantity of thorium salt, additional amounts of K_2CrO_4 were added to see whether the counting-rate reduction would continue. This was obviously not the case, as had to be expected if light radiation was the source of eliminated counts.

TABLE I. Results of experiments on the detection of Čerenkov radiation from cosmic rays and natural radioactive decay products.

(A) Cosmic rays—counter *K*-5

Run	N_1(counts/min.) pure H_2O	N_0(counts/min.) H_2O +1% hydroquinone
1	232±5	210±5
2	254±5	224±6
3	263±7	224±5
Average	249	219

(B) Thorium nitrate—counter *K*-9

	N_1(counts/sec.) pure H_2O	N_0(counts/sec.) H_2O +0.1% K_2CrO_4
1	247±1	246±1
2	250±1	247±1
3	249±1	243±1
4	247±1	243±1
5	248±1	245±1
Average	248.2	244.8

(C) Thorium nitrate—counter *K*-9

Liquid	N(counts/sec.)	
pure H_2O	148.7±0.8	148.7
H_2O +0.5% K_2CrO_4	146.7±0.8	146.3 (Average)
H_2O +1.0% K_2CrO_4	146.2±0.8	
H_2O +1.5% K_2CrO_4	146.3±0.8	
H_2O +2.0% K_2CrO_4	146.0±0.8	

The counter *K*-5 was unusually sensitive, while *K*-9 had the normal sensitivity which we had been accustomed to obtain from our surface preparations, and which has been estimated from their response to blackbody radiation to be of the order of 2 to 8×10^{-4} counts/quantum.

Calculation shows that the cosmic-ray counting rate experiment could be expected to show a 10 percent effect with a Geiger-Mueller counter quantum efficiency of about 60×10^{-4} counts/quantum. Easy detection of Čerenkov-type light radiation accompanying cosmic-ray particles in an experiment as described is indicated by these calculations at quantum-efficiencies of the order of 5×10^{-3} or better. In the thorium experiment a larger effect might at first be expected due to the large number of primary particles available. However, the very small effective path in emitting Čerenkov radiation before their velocity becomes so low that $Bn>1$ is not satisfied any more, and the smaller sensitivity of counter *K*-9 makes these results appear reasonable.

While such experiments appear relatively simple, it is felt that some attention should be diverted to the possible contribution of electronically excited molecular states in the stopping medium induced by the passage of the high energy particles.

Work using more promising photoelectric surfaces such as zinc is continuing.

[1] P. A. Čerenkov, Phys. Rev. **54**, 499 (1939); G. B. Collins and V. G. Reilling, *ibid.* 499 (1939).
[2] I. A. Getting, Phys. Rev. **71**, 123 (1947); R. H. Dicke, Phys. Rev. **71**, 737 (1947).
[3] W. H. Furry, Phys. Rev. **72**, 171 (A) (1947).
[4] P. B. Weisz, *Electronics*, July 1946.

On Explicit Solutions of the Equations for Steady Compressible Flow

BRUCE L. HICKS
Ballistic Research Laboratories, Aberdeen Proving Ground, Maryland
July 21, 1947

IN classical aerodynamics the steady flow of incompressible, inviscid fluids can often be described explicitly in terms of functions of a complex variable. There are, however, few accurate solutions of the equations for compressible flow that can be obtained in closed form. In view of the importance of obtaining more exact solutions, especially in the transonic region, the following outline of a new method of approach is submitted (see related work of Munk[1]). The flows considered are *adiabatic* but not necessarily isentropic and iso-energetic.

For uniplanar irrotational flow, the compressible flow equations can be written

$$\partial N/\partial\psi=\lambda_1(N)\partial\vartheta/\partial\varphi, \tag{1}$$

$$\partial N/\partial\varphi=-[\lambda_2(N)]^{-1}\partial\vartheta/\partial\psi, \tag{2}$$

where the velocity vector $\mathbf{V}=[g(N)RT]^{\frac{1}{2}}\mathbf{N}$; $|\mathbf{N}|=N=|\mathbf{V}|/[g(N)RT]^{\frac{1}{2}}$; ϑ is the angle of inclination of the vector $\mathbf{V}$ to the x axis; and φ and ψ are potential and stream functions for the vector $\mathbf{N}$, defined by the equations $\mathbf{N}=\nabla\varphi=\nabla\times\mathbf{k}\psi$. To a given choice of the function $g(N)$, there correspond flows with a given physical characteristic, namely, a relation between N and the pressure p on curves normal to the streamlines. Choice of $g(N)$ also fixes the form of the functions λ_1, λ_2 and all other functions of N or $\mathfrak{N}$ which will be introduced subsequently.

Except when $g(N)\propto(1-N^2)^{-1}$, irrotationality of $\mathbf{N}$ requires,[2] if the equation of motion is to be integrable, that (i) the stagnation pressure p_t vary according to the equations

$$\log p_t=\Psi(\psi)=\mathfrak{N}(N)-\Phi(\varphi) \tag{3}$$

(where Φ and Ψ are arbitrary), and is constant (between shocks) on streamlines; (ii) $\nabla^2\varphi\propto\mathfrak{L}(N)\Phi'(\varphi)$. If $g(N)\propto(1-N^2)^{-1}$, the integrability condition yields, instead of (3), the simple result $\nabla p_t=0$. The second of Eqs. (3) can, however, be assumed here also, in order that explicit integration of the flow equations can be achieved for this important case. It is possible, with other choices of $g(N)$, that the detailed analysis may be considerably simplified as it is known to be for diabatic flow.[2]

We now assume that (1) and (2) are integrable; then if $N(\varphi,\psi)$ can be found by some means, ϑ is calculable from

$$\vartheta=-\int_{\varphi,\psi_0}^{\varphi,\psi}\lambda_2(N)\frac{\partial N}{\partial\varphi}d\psi+\int_{\varphi_0,\psi_0}^{\varphi,\psi_0}[\lambda_1(N)]^{-1}\frac{\partial N}{\partial\psi}d\varphi. \tag{4}$$

Equation (3) together with assumed integrability of (1) and (2), demands that the functional-differential equation, involving the functions $\Phi(\varphi)$ and $\Psi(\psi)$, must be satisfied.

$$\mu_2(\mathfrak{N})F'(\Phi)+2\mu_2'(\mathfrak{N})F(\Phi)+\mu_1(\mathfrak{N})P'(\Psi)+2\mu_1'(\mathfrak{N})P(\Psi)=0, \tag{5}$$

where

$$F(\Phi)=(d\Phi/d\varphi)^{-\frac{1}{2}};\quad P(\Psi)=(d\Psi/d\psi)^{-\frac{1}{2}}.$$

After repeated integration with respect to Φ and Ψ, using (3), Eq. (5) can be reduced to a functional equation in $\Phi(\varphi)$ and $\Psi(\psi)$, which we shall schematically represent by

$$\mathfrak{F}[\Phi,\Psi,c_i(\varphi),k_j(\varphi)]=0, \tag{6}$$

in which $c_i(\varphi)$ and $k_j(\varphi)$ are functions introduced in the partial integrations.

If *any* functions $\Phi(\varphi)$ and $\Psi(\psi)$ can be found that reduce (6) to an identity, then (3) and (4) immediately yield explicit, closed expressions for N and ϑ. Further integration would yield x and y as functions of φ and ψ. Simple radial and vortex flows correspond to choosing Ψ and Φ, in turn, to be constant. No other exact solutions of the functional Eqs. (5) and (6) are known at present, although all previously known compressible flows have not been tested for their possible conformity to these equations.

The utility of the method, as compared to others, will, of course, depend on whether exact or approximate solutions of (5) and (6) can be found that yield flow patterns of some physical interest. There are indications that such solutions can be found in the transonic region. It is noted that the description $\mathbf{N}=\nabla\varphi$ applies to fields other than those of constant entropy and stagnation pressure, and may, therefore, make possible investigations of compressible flows down-stream from regions of heating and viscous dissipation.

This investigation was begun at the Cleveland laboratory of the N.A.C.A. in 1945. The assistance of the author's co-workers there, Dr. P. E. Guenther and Mr. R. H. Wasserman, is gratefully acknowledged.

[1] M. M. Munk, Phys. Rev. **72**, 176 (A) (1947).
[2] B. L. Hicks, Phys. Rev. **71**, 476 (A) (1947); B.R.L. Report No. 633, 1947. Also Hicks, Guenther, and Wasserman, Quart. App. Math. (October, 1947).

The Radial Density Variation of Gases and Vapors in a Centrifugal Field*

J. W. BEAMS
University of Virginia, Charlottesville, Virginia
July 21, 1947

IF the equation of state of a gas or vapor is expressed by the well-known relation

$$p=RT\left(\frac{d}{M}+B\frac{d^2}{M^2}+C\frac{d^3}{M^3}+\cdots\right)$$

where p is the pressure, T the absolute temperature, d the density, M the molecular weight, R the gas constant and where B, C, etc., are functions of T and are characteristic of the gas or vapor, then it can be shown theoretically that, under equilibrium conditions in a hollow centrifuge rotor with inside radius r spinning N r.p.s.,

$$\frac{2\pi^2MN^2r^2}{RT}=\log_e\frac{d_r}{d_0}+\frac{2B}{M}(d_r-d_0)+\frac{3C}{2M^2}(d_r^2-d_0^2)+\cdots, \tag{1}$$

where d_r and d_0 are the densities at the radius r and the axis, respectively. Since this latter equation may be used for determining the molecular weight of a gas or vapor, a precise experimental test of the relation has been undertaken. The apparatus consists of an air driven vacuum-type centrifuge which is similar to those previously described.[1] The rotor is a short accurately machined hollow cylinder

(2 cm high and 4.4 cm radius) with flat ends and is supported in the vacuum chamber by a thin flexible hollow shaft. The hollow shaft allows the pressure at the axis of the hollow spinning rotor to be measured at various rotor speeds. Measurements of this axis pressure were made at intervals of 100 r.p.s. up to 1200 r.p.s. with nitrogen, oxygen, and CO_2 gases, respectively. With these data, together with an accurate knowledge of the dimensions of the hollow rotor and auxiliary pressure measuring apparatus, the temperature, and the molecular weights of the respective gases, Eq. (1), could be tested. The results obtained show that this equation holds within the limit of experimental error. When Eq. (1) was used to determine the molecular weights of the nitrogen, oxygen, and CO_2 gases respectively, the values found agreed with the accepted values within considerably less than one percent.

Experiments also were carried out on pure ether vapor in equilibrium with the liquid phase in the periphery of the rotor. Ether was distilled into the evacuated rotor while it was spinning until about a cubic centimeter of the liquid condensed at the periphery. The pressure of the vapor at the axis was then measured as a function of the rotor speed and Eq. (1) was found to hold within the experimental error of roughly one percent. Consequently the molecular weight of a gas or vapor can be measured by the centrifuge method with a precision of about one percent. In the case of a radioactive gas or vapor, the molecular weight may be determined by measuring the amount of radioactivity at the axis of the rotor as a function of the rotor speed. The advantage of this centrifuge method for determining the molecular weights of radioactive gases or vapors is that only an extremely minute amount of the radioactive material is required, especially when the material can be mixed with a gas such as CO_2, nitrogen or helium.

* This work was supported by the Bureau of Ordnance, U. S. Navy under Contract NOrd-7873.

[1] J. W. Beams, Rev. Mod. Phys. **10**, 249 (1938).

The Motion of a Particle in an Electromagnetic and Gravitational Field

H. C. Corben and Mulaika Corben
Carnegie Institute of Technology, Pittsburgh, Pennsylvania
July 21, 1947

FITTING gravitational theory into the framework of special relativity theory is a problem that has proved practically insoluble. At the same time, the incorporation of electromagnetic phenomena into general relativity theory has proved extremely complex. We want to point out that the equations of motion for a particle in an electromagnetic and gravitational field may be derived from a simple Lagrangian which is based on an extended principle of special relativity theory.

We consider the position and velocity space of the particle $q^\alpha=(x^\mu, ilv^\mu)$, $(\alpha=1\cdots8, \mu=1\cdots4)$ where l is a constant of the dimensions of length, and $v^\mu=\dot{x}^\mu$, a dot denoting differentiation with respect to $ds=(dx^\mu dx_\mu)^{\frac{1}{2}}$. For any four-vector $B^4=B_4$, $B^j=-B_j(j=1, 2, 3)$. We now define an 8-invariant Lagrangian

$$L=A_\alpha dq^\alpha/d\tau \quad (\alpha=1\cdots8)$$

where $d\tau=(dq_\alpha dq^\alpha)^{\frac{1}{2}}$ and A_α is an 8-vector describing the interaction between the particle and the field. We write $A_\alpha=(e\kappa_\mu, iml^{-1}\epsilon_\mu)$ where κ_μ, ϵ_μ are two four-vectors and e, m are constants characteristic of the particle. Then

$$\mathfrak{L}=Ld\tau/ds=e\kappa_\mu v^\mu-m\epsilon_\mu v^\mu.$$

Hence we define[1]

$$p_\mu=\frac{\partial\mathfrak{L}}{\partial v^\mu}-\frac{d}{ds}\left(\frac{\partial\mathfrak{L}}{\partial\dot{v}^\mu}\right),$$
$$ilp_{\mu+4}=-P_\mu=\partial\mathfrak{L}/\partial\dot{v}^\mu.$$

The variational principle

$$\delta\int Ld\tau=\delta\int\mathfrak{L}ds=0$$

then yields $\dot{p}_\mu=\partial_\mu\mathfrak{L}$, where $\partial_\mu\equiv\partial/\partial x^\mu$.

In general the A_α may depend upon both the position and velocity coordinates, but we consider here only the special case in which they are functions of the x^μ only. Then

$$p_\mu=m\dot{\epsilon}_\mu+e\kappa_\mu; \quad P_\mu=m\epsilon_\mu;$$
$$\dot{p}_\mu=ev^\nu\partial_\mu\kappa_\nu-mv^\nu\partial_\mu\epsilon_\nu.$$

The Hamiltonian may be defined by

$$H=p_\alpha(dq^\alpha/d\tau)-L=(p_\alpha-A_\alpha)(dq^\alpha/d\tau)$$

so that

$$dq^\alpha/d\tau=\partial H/\partial p_\alpha; \quad dp_\alpha/d\tau=-\partial H/\partial q^\alpha.$$

Using $d/ds\equiv v^\nu\partial_\nu$ for the special case considered here, we may rewrite the equations of motion thus

$$d/ds[v^\nu(\partial_\mu\epsilon_\nu+\partial_\nu\epsilon_\mu)]=(e/m)v^\nu(\partial_\mu\kappa_\nu-\partial_\nu\kappa_\mu)+v^\nu v^\sigma\partial_\mu\partial_\sigma\epsilon_\nu.$$

We now define

$$g_{\mu\nu}=\partial_\mu\epsilon_\nu+\partial_\nu\epsilon_\mu; \quad f_{\mu\nu}=\partial_\mu\kappa_\nu-\partial_\nu\kappa_\mu,$$

so that $g_{\mu\nu}$, $f_{\mu\nu}$ are 4-tensors, respectively symmetrical and antisymmetrical, derivable from the 8-vector A_α. Thus

$$g_{\mu\nu}(dv^\nu/ds)=(e/m)f_{\mu\nu}v^\nu+\tfrac{1}{2}v^\nu v^\sigma(\partial_\mu g_{\nu\sigma}-\partial_\sigma g_{\mu\nu}-\partial_\nu g_{\mu\sigma}),$$

which suggests that we may interpret the $f_{\mu\nu}$ as the electromagnetic field strengths and the $g_{\mu\nu}$ as the gravitational potentials. For the general case in which the A_α involves v^μ explicitly, other types of fields appear in these equations as well.

Alternatively we have

$$\mathfrak{L}+m(d/ds)(\epsilon_\mu v^\mu)=e\kappa_\mu v^\mu+\tfrac{1}{2}mg_{\mu\nu}v^\mu v^\nu$$

from which, clearly, the equations of motion also follow. We also have $\mathfrak{H}=H(d\tau/ds)\equiv\frac{1}{2}mg_{\mu\nu}v^\mu v^\nu$. We note that for $\epsilon_\mu=\frac{1}{2}x_\mu$, $g_{ii}=-1$, $g_{44}=1$, $g_{\mu\nu}=0(\mu\neq\nu)$; then if $\mathcal{P}_\mu=p_\mu+\dot{P}_\mu$, it follows that $\mathcal{P}_\mu=mv_\mu+e\kappa_\mu$, $d\mathcal{P}_\mu/dt=ev^\nu\partial_\mu\kappa_\nu$, the usual electromagnetic equations.

The above results suggest that the equations of motion of a particle are covariant for arbitrary rotations of its position and velocity space. Such rotations are found to relate observers who are spinning or accelerated with respect to each other, and clearly mix the electromagnetic and gravitational components of A_α. Analysis of this group of rotations and of the field equations for A_α will be published soon.

[1] E. T. Whittaker, *Analytical Dynamics* (Dover Press, New York, 1944), p. 266.

X-Rays Associated with U^{234}*

R. L. MACKLIN AND G. B. KNIGHT
Research Laboratories, Carbide and Carbon Chemicals Corporation, Oak Ridge, Tennessee
July 16, 1947

WE should like to report the observation of x-rays associated with U^{234}. L and M x-rays were found to occur spontaneously, the yield of the former, per alpha-particle, being between one-third and two. Detection was accomplished by means of a thin-walled Geiger counter. The efficiency of the tube was between 0.25 and 1 percent, making the quantitative determination of yield uncertain as indicated. Absorption curves in aluminum were measured to determine the energy of the L radiation. Film and counter wall absorption made it impossible to obtain much information on the M x-rays.

The source of the x-rays was a thin film of U_3O_8 containing 0.245 mg of U^{234} plated on a 22 cm^2 disk. Other materials present contributed only 4 percent of the total alpha-activity. The U_3O_8 film was prepared and counted within four hours after the removal of the natural decay products (UX_1, UX_2, UY, UZ). Figure 1, curve A, shows the results of an aluminum absorption experiment run on this source. In addition to the points shown, one millimeter of lead as absorber gave less than three counts per minute above background. The chief component found shows an absorption characteristic of 15.0 ± 0.5 kev x-rays, resembling the L x-rays of thorium or uranium as closely as we were able to determine. The M x-ray has not been identified so decisively but the presence of a soft component with the appropriate absorption coefficient has been shown in this work (Fig. 1, curve A) and in earlier experiments done in cooperation with Mr. L. E. Glendenin of the Monsanto Chemical Company. The absence of detectable K radiation was particularly notable in this work.

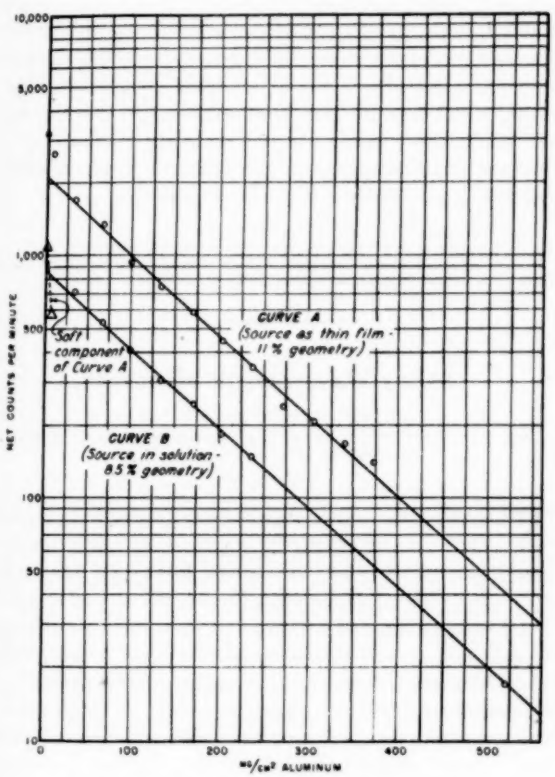

FIG. 1. Absorption of x-rays from U^{234} by aluminum.

A second set of aluminum absorption measurements was made using a solution of the same quantity of uranium as nitrate in 20 ml of solution contained in a shallow dish and of uniform depth, 0.78 cm. These measurements (Fig. 1, curve B) show no change in the absorption characteristics of the radiation. The intensity relative to curve A is 0.54. Calculating the effective intensity for 15-kev radiation from point sources distributed uniformly through the solution gives 0.51. This experiment together with the high yield of x-rays leads us to conclude that we are not dealing with a delta-ray effect.

Our interpretation is that the L and M x-rays observed arise from rearrangement of the electrons in the recoil atoms, after alpha-emission. The energy of these recoils is readily calculated to be about 82 kev by applying the law of conservation of momentum and the measured alpha-energy[1] of 4.76 Mev. This energy is insufficient to excite the K shell electrons (K limit = 100.4 kev),[2] but more than adequate to ionize the L and higher orbital electrons (L_{22} limit = 16.3 kev).[2] An adequate quantum-mechanical treatment of such excitation by recoil has not come to our attention.

Dr. S. DeBenedetti has pointed out the failure of I. Curie and F. Joliot[3] to observe K shell x-rays from polonium, though they did observe L and M x-rays. Other natural alpha-emitters are accompanied by interfering beta- and gamma-radiation to an extent sufficient to make observation of these recoil x-rays improbable.

* "This document is based on work performed under Contract No. W-7405-eng-26 for the Manhattan Project and the information contained therein will appear in Division IV of the Manhattan Project Technical Series as part of the contribution of the Carbide and Carbon Chemicals Corporation."

[1] G. T. Seaborg, Rev. Mod. Phys. **16**, 1 (1944).
[2] Int. Crit. Tab., Vol. VI, p. 39.
[3] I. Curie and F. Joliot, J. de phys. et rad. **7**, 11, 20 (1931).

The Nucleus as a Crystalline Solid

J. G. WINANS
University of Wisconsin, Madison, Wisconsin
June 26, 1947

IN a previous letter,[1] it was pointed out that the relation between mass and charge for stable nuclei was that to be expected on the basis of a crystalline-solid model for the nucleus with the protons on the surface. On the basis of this model, it was proposed that nuclear fission might result from the splitting of a nearly perfect crystal along a cleavage plane by the entrance of a neutron. Davison and Watson[2] have raised an objection to this model and mechanism of fission on the grounds that the unequal mass fragments after fission should be expected to contain a different charge to mass ratio from each other, and from the charge to mass ratio for other elements. They point out that experimental observations of fission fragments

show that these fragments possess the same charge to mass ratio. They therefore conclude that the mechanism of splitting a crystal will not account for fission, and that the charge cannot be considered as residing on the surface of the nucleus.

The objection raised by Davison and Watson on the grounds that fission fragments have equal charge to mass ratio seems not to be valid, since the fragments which are observed after fission are observed a long enough time after the splitting to permit a reorganization of fragments to obtain the charge to mass ratio corresponding to the resulting radioactive isotopes. The rearrangement of fragments may be considered to begin as the fragments start to separate. They can thus contribute their change in mass defect to the kinetic energy of the fragments.

The crystalline-solid model offers a ready explanation for the fact that splitting occurs into fragments of unequal mass. If a nucleus of uranium (235) or plutonium (239) is considered as made up of nuclear particles in spherical close packing, then a crystal so formed can be considered as consisting of a central plane of symmetry with nuclear particles above and below in equal numbers, and with protons above and below the plane as well as in the outside rim of the plane. A model for uranium or plutonium would provide approximately 20 or 22 protons around the edge of the central plane of symmetry.

If such a crystalline solid is split along a cleavage plane, it must be split above or below, but not through the middle of the plane of symmetry. This means that the fragments must have unequal rather than equal masses. The number of protons which would be required to be associated with the fragments is, for uranium (235), 36 and 56 for a clean split just above or below the plane of symmetry. This gives fission fragments krypton and barium. The number of neutrons in these two fragments would be such that the lighter fragment, krypton, would be left in a highly radioactive state and the heavier fragment, barium, would be left in a highly radioactive state after releasing about four neutrons. The various fission fragments observed could be associated with the splitting of the crystal with various parts of different planes going with the separate fragments.

Another aspect or property of nuclei which also indicates that the nucleus may be considered as a crystalline solid is illustrated in Table I. In this table are listed the atomic numbers of the elements which have a given number of stable isotopes. Many elements consist of only a single isotope. All of these elements have an odd atomic number and an odd mass number. The elements of odd atomic number never have more than two stable isotopes, while the elements of even atomic number may have several isotopes. In Table I it is shown that atoms may be arranged in periods, where in some periods the multiplicity of stable isotopes alternates between one and several. In other periods it alternates between two and several. The known stable isotopes then form a periodic system shown in Table I. In this periodic system there are five periods in which, with successively increasing atomic number, the number of stable isotopes alternates between one and several, and these periods are six atomic numbers long. There are four periods, also six atomic numbers long, in which the number of stable isotopes alternates between two and several. There are three periods, each eight atomic numbers long, in which the number of stable isotopes alternates between two and several. All the elements fit into this periodic system except atomic numbers 4, 71, 73, and 83. According to this table it is to be expected that these elements, which are listed as having only one stable isotope,[3] may be expected to have two stable isotopes.

TABLE I. Number of stable isotopes for a given atomic number. s=several—two or more.

1	s	1	s	1	s	1	s	2	s	2	s	1	2	s	2	s	2	s	2	s	1
													1	2	3	4?	5	6	7	8	9
9	10	11	12	13	14	15	16	17	18	19	20	21									
21	22	23	24	25	26	27	28	29	30	31	32	33									
						33	34	35	36	37	38	39									
39	40	41	42	43	44								45	46	47	48	49	50	51	52	53
53	54	55	56	57	58	59	60	61	62	63	64	65									
65	66	67	68	69	70								71?	72	73?	74	75	76	77	78	79
						79	80	81	82	83?											

The periodicity of six in atomic nuclei, as shown in Table I, as well as the existence of elements of odd atomic number with only one or at the most two stable isotopes is readily accounted for on the basis of a crystalline-solid model for the nucleus. We may consider that the plane of symmetry of the nucleus contains an odd number of protons. Those elements which consist of only a single stable isotope may be considered as the ones with perfect symmetry of both mass and charge about the plane of symmetry containing an odd number of particles. Elements which contain several stable isotopes may be considered as those which are not perfectly symmetrical in both mass and charge, and can contain, for a given number of protons, a variable number of neutrons.

[1] J. G. Winans, Phys. Rev. **71**, 379 (1947).
[2] B. Davison and W. H. Watson, Phys. Rev. **71**, 742 (1947).
[3] J. M. Cork, *Radioactivity and Nuclear Physics* (Edwards Brothers Inc., Ann Arbor, Michigan, 1946), Table of Isotopes.

X-Ray Wave-Length Standards

ELIZABETH ARMSTRONG WOOD
American Society for X-Ray and Electron Diffraction, Bell Telephone Laboratories, Murray Hill, New Jersey
July 21, 1947

X-RAY wave-lengths have been expressed in x units. The x unit is defined in terms of the calcite spacing and is nearly 10^{-11} cm, but is now known to differ from 10^{-11} cm by about 0.2 percent. During the last twenty-five years x-ray diffraction workers have expressed x-ray wave-lengths and crystal dimensions in terms of a unit which was $1000x$ units, but instead of calling it $1000x$ units have erroneously called it an Ångström unit. In recent years, the x-ray diffraction groups have agreed to use the term kilo x unit (abbreviated kx) in place of the incorrectly used Ångström unit, until agreement was reached on the

best conversion factor to use for converting from *kx* to Ångström units. Agreement on the factor has now been reached.

As secretary of the American Society for x-ray and Electron Diffraction, I have been instructed to call the attention of American x-ray workers to the following announcement which appeared in the January, 1947, issue of the Journal of Scientific Instruments. Because of its importance it is here reproduced in its entirety.

The Conversion Factor for kx Units to Angström Units

At the annual conference of the X-ray Analysis Group of the Institute of Physics in July 1946 it was announced that agreement had been reached concerning the factor for converting measurements in kx units to Ångström units. The factor agreed upon, after consultation with the American Society for X-ray and Electron Diffraction and Professor Siegbahn was 1.00202. This factor is probably correct to 0.003 percent. Since wave-lengths in *X*-units have been measured to an accuracy of 0.001 percent, the wave-lengths in Ångström units can be taken as accurate to 0.004 percent in general.

The following is a list of values of wave-lengths in Ångström units of certain emission lines and absorption edges in common use. The column headed $K\alpha$ gives the mean value of $K\alpha_1$ and $K\alpha_2$, $K\alpha_1$ being allowed twice the weight of $K\alpha_2$.

Current values of the physical constants, such as those quoted by Birge in the 1941 volume of the Physical Society's *Reports on Progress in Physics*, should be used in conjunction with these wave-lengths. In particular density ρ is given by the equation

$$\rho = 1.66020 \Sigma A / V,$$

where ΣA is the sum of the atomic weights of the atoms in the unit cell, and V is the volume of the unit cell in A^3.

	$K\alpha_1$	$K\alpha_2$	$K\alpha$	$K\beta_1$	Absorption edge
Cr	2.28962	2.29352	2.2909	2.08479	2.0701
Mn	2.10174	2.10570	2.1031	1.91016	1.8954
Fe	1.93597	1.93991	1.9373	1.75654	1.7429
Co	1.78890	1.79279	1.7902	1.62073	1.6072
Ni	1.65783	1.66168	1.6591	1.50008	1.4869
Cu	1.54050	1.54434	1.5418	1.39217	1.3802
Zn	1.43510	1.43894	1.4364	1.29520	1.2831
Mo	0.70926	0.71354	0.7107	0.63225	0.6197
Rh	0.61326	0.61762	0.6147	0.54559	0.5341
Pd	0.58545	0.58982	0.5869	0.52052	0.5090
Ag	0.55941	0.56381	0.5609	0.49701	0.4855

It is recommended that in any published work the values of the wave-lengths used should be explicitly stated.

W. L. BRAGG
Chairman, X-Ray Analysis Group of
the Institute of Physics (England)